# INTEGRATING CONNECTED ARRAYS AS ISOLATION ENHANCEMENT STRUCTURES IN MIMO ANTENNA SYSTEMS

BY

**MUHAMMAD IKRAM**

A Thesis Presented to the

DEANSHIP OF GRADUATE STUDIES

**KING FAHD UNIVERSITY OF PETROLEUM & MINERALS**

DHAHRAN, SAUDI ARABIA

In Partial Fulfillment of the
Requirements for the Degree of

# MASTER OF SCIENCE

In

**ELECTRICAL ENGINEERING**

**JANUARY 2017**

KING FAHD UNIVERSITY OF PETROLEUM & MINERALS
DHAHRAN 31261, SAUDI ARABIA

DEANSHIP OF GRADUATE STUDIES

This thesis, written by **MUHAMMAD IKRAM** under the direction of his thesis adviser and approved by his thesis committee, has been presented to and accepted by the Dean of Graduate Studies, in partial fulfillment of the requirements for the degree of **MASTER OF SCIENCE IN ELECTRICAL ENGINEERING**.

**Thesis Committee**

Prof. Mohammad S. Sharawi (Adviser)

Dr. Khurram K. Qureshi (Member)

Dr. Sheikh S. Iqbal (Member)

Dr. Ali A. Al-Shaikhi
Department Chairman

Prof. Salam A. Zummo
Dean of Graduate Studies

12/1/17
Date

*To my parents, To my adviser, To my brothers and sister*
*To my country*

# ACKNOWLEDGMENTS

In the name of My Dear Allah, the Most merciful and the Most forgiving Alhamdu-LILLAH, all praises to Allah for the strengths and his blessing in completing this thesis. First of all, I would like to express my special thanks to my supervisor, Prof. Dr. Mohammad S. Sharawi, for his supervision support and guidance. His precious help of beneficial comments and suggestions throughout the experimental and thesis works have contributed to the success of my research. It was an excellent experience for me to be a part of his research group, the Antenna and Microwave Structure Design Lab (AMSDL).

I would like to extend my thanks to AMSDL group members specially Dr. Rifaqat Hussain who helped me in designing and measuring antenna systems in AMSDL.

Not forgotten, special thanks to my thesis committee members Dr. Khurram K. Qureshi and Dr. Sheikh S. Iqbal for their valuable comments.

I would like to express my thanks to KFUPM for its funding support in the fabrication and testing of different antennas from outside the kingdom.

Sincere thanks to all my friends and my beloved parents for their gentleness and support during my graduation.

# TABLE OF CONTENTS

**ACKNOWLEDGEMENT** **iv**

**LIST OF TABLES** **ix**

**LIST OF FIGURES** **x**

**ABSTRACT (ENGLISH)** **xv**

**ABSTRACT (ARABIC)** **xvii**

**CHAPTER 1 INTRODUCTION** **1**

1.1 4G (LTE) and 5G . . . . . 2

1.2 MIMO Systems . . . . . 3

1.3 Connected Antenna Arrays (CAAs) . . . . . 5

1.4 Thesis Motivation . . . . . 6

1.5 Thesis Contributions . . . . . 7

1.6 Thesis Organization . . . . . 8

**CHAPTER 2 THEORETICAL BACKGROUND** **10**

2.1 Printed Inverted-F Antennas (PIFA) . . . . . 10

2.2 Printed Monopole Antennas . . . . . 11

2.3 MIMO Antenna System Performance Metrics . . . . . 13

2.3.1 Total Active Reflection Coefficient (TARC) . . . . . 13

2.3.2 Isolation . . . 14
2.3.3 Envelope Correlation Coefficient (ECC) . . . 14
2.3.4 Diversity Gain (DG) . . . 15
2.4 Isolation Enhancement Techniques . . . 15
2.5 Connected Antenna Arrays (CAAs) . . . 16
2.5.1 Connected Antenna Array Principles . . . 18
2.5.2 Feeding Techniques in CAA . . . 20
2.5.3 Applications of CAA . . . 23
2.6 Summary . . . 23

**CHAPTER 3 LITERATURE REVIEW 25**

3.1 Isolation enhancement Techniques . . . 25
3.1.1 Antenna Orientation and Placement . . . 25
3.1.2 Decoupling Networks . . . 27
3.1.3 Parasitic elements . . . 28
3.1.4 Defected Ground-Plane Structures(DGS) . . . 29
3.1.5 Neutralization Lines . . . 30
3.1.6 Metamaterials . . . 31
3.2 PIFA MIMO antenna Systems . . . 33
3.3 Monopole MIMO based antenna Systems . . . 37
3.4 Connected Antenna Arrays (CAAs) . . . 40
3.5 Summary . . . 42

**CHAPTER 4 4G MIMO ANTENNA SYSTEMS 43**

4.1 Printed Inverted-F Antenna (PIFA) MIMO Antenna System . . . 43
4.1.1 Current Distributions . . . 45
4.1.2 S-Parameters . . . 47
4.1.3 Radiation Patterns . . . 50
4.2 4-Element L-Shaped Monopole MIMO antenna System . . . 51

4.2.1 S-Parameters . . . . . 54
4.2.2 Current Distributions . . . . . 56
4.2.3 Radiation patterns . . . . . 57
4.3 6-Element Monopole based MIMO antenna System . . . . . 60
4.3.1 S-Parameters . . . . . 63
4.3.2 Current Distributions . . . . . 67
4.3.3 Radiation Patterns . . . . . 69
4.3.4 Envelope Correlation coefficient (ECC) Values . . . . . 72
4.3.5 Summary . . . . . 72

**CHAPTER 5 4G/5G INTEGRATED ANTENNA SYSTEMS WITH CONNECTED ANTENNA ARRAYS 74**

5.1 L-shaped Monopole with Connected antenna array . . . . . 75
5.1.1 S-parameters . . . . . 76
5.1.2 Current Distributions . . . . . 77
5.1.3 Radiation Patterns . . . . . 79
5.2 A 4G/5G Antenna System with Dual Function Connected Antenna Array (CAA) . . . . . 80
5.2.1 Design of the integrated 4G/5G antenna system . . . . . 80
5.2.2 MIMO Antenna System . . . . . 81
5.2.3 DGS and CAA . . . . . 82
5.2.4 Port Parameters . . . . . 86
5.2.5 Radiation Patterns . . . . . 92
5.2.6 MIMO Performance . . . . . 97
5.3 Summary . . . . . 98

**CHAPTER 6 CONCLUSIONS & FUTURE WORK 99**

6.1 Conclusions . . . . . 99
6.2 Future Work . . . . . 100

**VITAE** **113**

**PUBLICATIONS** **113**

# LIST OF TABLES


3.1 Summary of literature review based on isolation enhancement techniques. . . 33

3.2 Comparison between proposed and previous work based on size and no. of antenna elements. . . . . 37

3.3 Comparison between proposed and previous work based on monopole. . . . . 40

3.4 Comparison between proposed and previous work based on connected array . 42

4.1 Measured envelop correlation coefficient (ECC). . . . . 60

4.2 Measured envelop correlation coefficient (ECC) . . . . . 72

4.3 Comparison between proposed 4G designs. . . . . 73

5.1 Comparison of 4G/5G integrated designs based on spacing between feed lines of 5G bands. . . . . 83

5.2 Measured envelope correlation coefficient (ECC) values . . . . . 98

# LIST OF FIGURES


1.1 Current Vs. Forecasted cellular data traffic requirements (ExaBytes)[3]. . . 3
1.2 MIMO system block diagram . . . . . 4
1.3 Currents distribution (a) Unconnected array of dipoles (b) CAA of dipoles [8] 6
1.4 Flow chart . . . . . 8

2.1 PIFA geometry [9]. . . . . 12
2.2 Monopole antenna shapes [9]. . . . . 12
2.3 Connected antenna array of TEM horn antenna [10]. . . . . 17
2.4 Linear connected antenna array [10]. . . . . 17
2.5 A prototype of connected dipole array [13]. . . . . 19
2.6 $10\lambda$ wire current distributions with feed at $\lambda/4$ separation [12]. . . . . 20
2.7 Feeding network for connected dipoles (a) Loop shaped transformer [14] (b) Circular/Radial feed design [15]. . . . . 22
2.8 Feeding network for connected slots (a) Planar slots fed with connected dipoles [16] (b) Linear slot fed with reactively matched transmission lines [17]. . . . 23

3.1 8-element PIFA based MIMO system[45]. . . . . 35
3.2 4-element monopole MIMO system [59]. . . . . 39

4.1 Geometry of PIFA Antenna. . . . . 44
4.2 Proposed 4-element PIFA based MIMO antenna system (a) Top view (b) Bottom view- all dimensions are in mm. . . . . 46

4.3 Proposed 4 element PIFA based MIMO antenna with DGS: Fabricated Model (a) Top view (b) Bottom view - All dimensions are in millimeters (mm). . . 46
4.4 Current distributions: (a) P1 is activated at 2.1 Without DGS (b) P1 is activated at 2.1 GHz With DGS (c) P2 is activated at 2.1 GHz With DGS. . 47
4.5 S-parameters curves (a) $|s_{ii}|$-Simulated and measured without DGS (b) $|s_{ii}|$-Simulated with DGS. . . . . 48
4.6 Isolation curves (a) $|s_{ij}|$-Simulated without DGS (b) $|s_{ij}|$-Simulated with DGS. 49
4.7 S-parameters curves (a) $|s_{ii}|$-Measured with DGS (b) $|s_{ij}|$-measured with DGS. 49
4.8 Simulated 2-D Radiation patterns of $E_{total}$, $\phi - cuts$ at $\theta = 90^o$ (a) Ant-1 (b) Ant-2 (c) Ant-3 (d) Ant-4. . . . . 50
4.9 Geometry of monopole Antenna. . . . . 51
4.10 Propsed L-shaped MIMO antenna (a) Top view (b) Bottom view- All dimensions are in millimeters (mm). . . . . 53
4.11 Fabricated models: (a) Without DGS (b) With DGS- all dimensions are in mm. 53
4.12 Measurement setup in a Satimo star Lab chamber. . . . . 54
4.13 S-parameters curves (a) $|\mathbf{s}_{ii}|$-Simulated and measured without DGS (b) $|\mathbf{s}_{ij}|$-Simulated and measured without DGS. . . . . 55
4.14 S-parameters curves (a) $|\mathbf{s}_{ii}|$-Simulated and measured with DGS (b) $|\mathbf{s}_{ij}|$-Simulated and measured with DGS. . . . . 56
4.15 Current distributions on proposed 4 element monopole MIMO antenna system at 2.1 GHz (a) Without DGS (b) With DGS. . . . . 57
4.16 Measured 2-D Radiation patterns of $E_{total}$ (a) $\theta - cuts$ for Ant-1 at $\phi = 154^o$ and Ant-2 at $\phi = 133^o$ (b) $\phi - cuts$ for Ant-1 and Ant-2 at $\theta = 90^o$ (c) $\theta - cuts$ for Ant-3 at $\phi = 26^o$ and Ant-4 at $\phi = 74^o$ (d) $\phi - cuts$ for Ant-3 and Ant-4 at $\theta = 90^o$. . . . . 58
4.17 Measured gain and efficiency curves (a) Ant-1 (b) Ant-2 (c) Ant-3(d) Ant-4 59
4.18 Geometry of loop shaped monopole Antenna. . . . . 61

4.19 Propsed 6-element MIMO antenna system (a) Top view (b) Bottom view - All dimensions are in millimeter (mm). . . . . 62
4.20 Proposed Fabricated model of MIMO antenna system (a) Top view (b) Bottom view - All dimensions are in millimeter (mm). . . . . 63
4.21 Measurement setup in a Satimo star Lab chamber. . . . . 64
4.22 S-parameters curves (a) $|s_{ii}|$-Simulated without DGS (b) $|s_{ii}|$-Measured without DGS. . . . . 65
4.23 Isolation curves (a) $|s_{ij}|$-Simulated without DGS (b) $|s_{ij}|$-Measured without DGS. . . . . 65
4.24 S-parameters curves (a) $|s_{ii}|$-Simulated with DGS (b) $|s_{ii}|$-Measured with DGS. . . . . 66
4.25 Isolation curves (a) $|s_{ij}|$-Simulated with DGS (b) $|s_{ij}|$-Measured with DGS. . 66
4.26 Current distribution on proposed 6 element monopole MIMO antenna at 2GHz (a) P1 is activated Without DGS (b) P2 is activated without DGS (c) P6 is activated without DGS (d) P1 is activated with DGS (e) P2 is activated with DGS (f) P6 is activated with DGS. . . . . 68
4.27 Measured and simulated 2-D radiation patterns (a) $(\theta - cuts)$ Ant-1 at $\phi = 10^o$ and Ant-2 at $\phi = 110^o$ (b) $(\phi - cuts)$ Ant-1 and Ant-2 at $\theta = 90^o$ (c) $(\theta - cuts)$ Ant-3 at $\phi = 166$ and Ant-4 at $\phi = 4$ (d) $(\phi - cuts)$ Ant-3 and Ant-4 at $\theta = 90^o$ (e) $(\theta - cuts)$ Ant-5 at $\phi = 4$ and Ant-6 $\phi = 78$ (f) $(\phi - cuts)$ Ant-5 and Ant-6 at $\theta = 90^o$. . . . . 70
4.28 Measured gain and efficiency (a) Ant-1 (b) Ant-2 (c) Ant-3 (d) Ant-4 (e) Ant-5 (f) Ant-6. . . . . 71

5.1 Integrated MIMO antenna system (a) Top view (b) Bottom view - All dimensions are in millimeter (mm). . . . . 76
5.2 S-parameters curves (a) $|s_{ii}|$-Simulated (only for CAA) with DGS (b) $|s_{ij}|$-Simulated with DGS. . . . . 77

5.3 Current distributions on proposed MIMO antenna (a) Without DGS (b) With DGS and CAA at 2.1 GHz. . . . . 78
5.4 Current distributions on CAA at 4GHz. . . . . 78
5.5 Simulated 3-D gain patterns (a) Ant-1 (b) Ant-2(c) Ant-3 at 2.1 GHz (d) CAA at 4 GHz. . . . . 79
5.6 Proposed integrated design (a) Top view (b) Bottom view - All dimensions are in millimeters (mm). . . . . 81
5.7 Feed network geometry of CAA. All dimensions are in mm. . . . . 83
5.8 Transmission coefficient curves of the PCA feed network alone (a) $|s_{ij}|$-Simulated magnitude (b) $|s_{ij}|$-Simulated phase. . . . . 84
5.9 Current distributions on the proposed 4G/5G integrated design (a) P1 of MIMO antenna system at 2.1 GHz is activated (b) P1 of MIMO antenna system is activated with a CAA at 2.1 GHz (d) P2 of MIMO antenna system is activated with a CAA at 2.1 GHz (e) CAA (P5) is activated at 12.5 GHz. 86
5.10 The Proposed 4G/5G Integrated antenna design in the measurement setup in a Satimo star Lab. . . . . 87
5.11 Fabricated model of the MIMO antenna system without CAA (a) Top view (b) Bottom view - All dimensions are in millimeters (mm). . . . . 88
5.12 Fabricated model of the integrated 4G/5G antenna design (a) Top view (b) Bottom view - All dimensions are in millimeters (mm). . . . . 88
5.13 S-parameters curves without DGS (a) $|s_{ii}|$-Simulated (b) $|s_{ii}|$-Measured (c) $|s_{ij}|$-Simulated (d) $|s_{ij}|$-Measured, {simulated (sim.), measured(meas.)}. . . . 89
5.14 S-parameters curves of the integrated 4G/5G design only for the MIMO antenna system (a) $|s_{ii}|$-Simulated (b) $|s_{ii}|$-Measured (c) $|s_{ij}|$-Simulated (d) $|s_{ij}|$-Measured, {simulated (sim.), measured(meas.)}. . . . . 91
5.15 S-parameters curves of the integrated 4G/5G design only for the CAA (a) $|s_{ii}|$-Simulated and measured (b) $|s_{ij}|$-Measured, {simulated (sim.), measured(meas.)}. . . . . 92

5.16 Normalized measured and simulated radiation patterns ($E_{total}$) (a) ($\theta - cuts$) Ant-1 and Ant-2 at $\phi = 90^o$ (b) ($\phi - cuts$) Ant-1 and Ant-2 at $\theta = 60^o$ (c) ($\theta - cuts$) Ant-3 and Ant-4 at $\phi = 90^o$ (d) ($\phi - cuts$) Ant-3 and Ant-4 at $\theta = 60^o$ (e) ($\theta - cuts$) CAA at $\phi = 0^o$ (f) ($\phi - cuts$) CAA at $\theta = 90^o$. . . . . 94
5.17 3-D simulated gain patterns (a) Ant-1 (b) Ant-2 (c) Ant-3 (d) CAA. . . . . 95
5.18 Measured maximum gain and efficiency curves (a) Ant-1 (b) Ant-2 (c) Ant-3 (d) Ant-4. . . . . 96
5.19 Measured and simulated maximum gain and efficiency curves for CAA. . . . 97

# THESIS ABSTRACT

**NAME:** Muhammad Ikram

**TITLE OF STUDY:** Integrating Connected Arrays as Isolation Enhancement Structures in MIMO Antenna Systems

**MAJOR FIELD:** Electrical Engineering

**DATE OF DEGREE:** January 2017

*Multiple-input multiple-output (MIMO) antennas are currently used in 4G and will be also used in 5G communication systems. To implement such MIMO antenna systems on the base station side does not pose many challenges due to the excess space available, but when it comes to the mobile terminal, it is a very serious issue for the designer because of the size constraints. When we place MIMO antenna systems in the mobile, due to small spacing between the antennas, they exhibit mutual coupling which degrade their performance.*

*In this work, a planar printed PIFA and monopole antennas are designed with MIMO antenna configurations. Two MIMO antenna systems consist of 4-elements operating at 2.1 GHz frequency band for 4G LTE applications with board dimensions of 100×60×0.8 $mm^3$. Another MIMO configuration with 6 elements based on new monopole like antenna is also presented. It is operating at 2 GHz. The board dimensions for this configuration are 115×65×0.8 $mm^3$.*

*The proposed designs are compact, low profile and planar antenna structures versatile for smart mobile phones and wireless handheld devices.*

*Moreover, we introduce isolation enhancement structures between closely packed 4G MIMO antenna systems and have them also act as radiating antenna arrays based on the concept of Linearly connected antenna arrays (CAA) for 5G applications. This dual function operation of CAA is unique and has never been done before. Such arrays will provide radiation operation at 12.5 GHz with wide-band characteristics. Finally, a 4G/5G integrated antenna system is designed on RO4350 substrate with dimensions of 100×60×0.76 $mm^3$ and it is covering 5G band from 12.17 to 12.75 GHz with the bandwidth of more than 500 MHz, gain of 8dBi and efficiency of 80%.*

## ملخص الرسالة

**الاسم:** محمد إكرام

**عنوان الدراسة:** دمج المصفوفات المتصلة كتراكيب تحسين العزل في أنظمة هوائيات الـMIMO

**التخصص:** الهندسة الكهربائية

**تاريخ الدرجة العلمية :** كانون الثاني 2017

هوائيات متعددة-المدخلات-متعددة-المخرجات (MIMO) تستخدم الآن في في الجيل الرابع (4G) وسوف تستخدم أيضاً في أنظمة اتصالات الجيل الخامس (5G). لتحقيق أنظمة هوائيات MIMO على جهة أبراج الاتصالات لا يوجد أي تحديات بسبب توفر المساحة الزائدة، لكن في جهة الموبايل، هي معضلة حقيقية بسبب قيود الحجم. عندما نضع أنظمة هوائيات MIMO في الموبايل، بسبب صغر المسافة بين الهوائيات، يظهر اقتران متبادل بينهم مما يُضعف من أدائهم.

في هذا العمل، هوائيات PIFA مستوٍ وأحادي القطب تم تصميمهم وفق ترتيب هوائيات MIMO. اثنان من أنظمة هوائيات MIMO تحتوي على 4-عناصر تعمل على نطاق تردد 2.1 جيجاهيرتز لتطبيقات الجيل الرابع 4G LTE بلوح أبعاده 100×60×0.8 مليميتر مكعب. التصاميم المقترحة هي مضغوطة الحجم، وذات تركيب هوائيات مستوٍ متعددة الاستخدامات في هواتف الموبايل الذكية والأجهزة اللاسلكية المحمولة.

علاوة على ذلك، قدمنا تراكيب تحسين العزل بين أنظمة هوائيات MIMO مضبوبة على نحوٍ متراص وجعلهم أيضاً يعملون كمصفوفة هوائيات مبنية على مفهوم مصفوفات الهوائيات المتصلة خطياً (CAA) لتطبيقات الجيل الخامس (5G). هذا التشغيل مزدوج الوظائف لـCAA منفرد ولم يتم إنجازه من قبل مطلقاً. هذه المصفوفات توفر عملية إشعاع على تردد 12.5 جيجاهيرتز مع خصائص واسعة النطاق. أخيراً، نظام هوائيات 4G/5G المدمج تم تصميمه على مادة RO4350 بأبعاد 100×60×0.76 مليميتر مكعب وهي تغطي نطاق 5G من 12.17 إلى 12.75 جيجاهيرتز بنطاق عرضه أكثر من 500 ميجاهيرتز، قوة توجيهية بمقدار 8 ديسيبل وبكفاءة 80%.

# CHAPTER 1

# INTRODUCTION

The $21^{st}$ century has seen a rapid advancement in wireless communication technology. Since antennas form a core part of communications, specially in mobile phones. A myriad of antenna systems have been developed through the years to meet this rapid advancement. The Multiple-Input Multiple-Output(MIMO) technology and its MIMO antenna systems have played an essential role in the development of emerging wireless communication technologies such as LTE, WiMAX, and WLANs. Most of these emerging technologies along with the existing systems such as GSM/UMTS/WLAN are integrated into future LTE/4G/5G devices to create heterogeneous systems with complementary coverage, enhanced capacity and performance [1]. MIMO systems allow the communication system to have an increased data rate within the bandwidth and power constraints by increasing the number of antennas [2]. In this chapter, we will go over the concepts of forth generation (4G), fifth generation (5G), MIMO antenna systems and connected antenna arrays (CAA).

## 1.1 4G (LTE) and 5G

MIMO antenna systems are used in 4G networks to enhance the data rate and MIMO will be used in emerging systems like 5G as well. LTE is considered the fourth generation (4G) in mobile communications. It is internet protocol (IP) based and provides higher data rates and utilize wider bandwidth. It supports a data rate of 1Gbps and 100Mbps for stationary and mobile users, respectively. Miniaturization techniques are needed for the deployment of multiple antennas in an ever decreasing mobile phone sizes, therefore presenting challenging research problem since the proximity between tiny antennas for small mobile phones for 4G applications in a crucial performance factor in MIMO antenna systems [2].

The wireless data explosion is real and will continue [3] as shown in Figure 1.1. There is a statistics in the literature that IP based data has increased by 100 times, from under 3 exabytes in 2010, to over 190 exabytes by 2018, and will continue growing to 500 exabytes by 2020. To meet these requirements, researchers are working on fifth generation (5G) communication systems. 5G will be highly integrative with 4G and WiFi so that it can provide high data coverage to users. A possible spectrum utilization will be in this way, a high frequency will be used for small cells and low frequency will be used for wide range coverage and mobility support. Studies are ongoing within the international telecommunication unit (ITU) and some other organizations along with major operators, indicating that several potential frequency bands for 5G will be above 6 GHz [4]-[7] as long as the available bandwidth is at least 500 MHz.

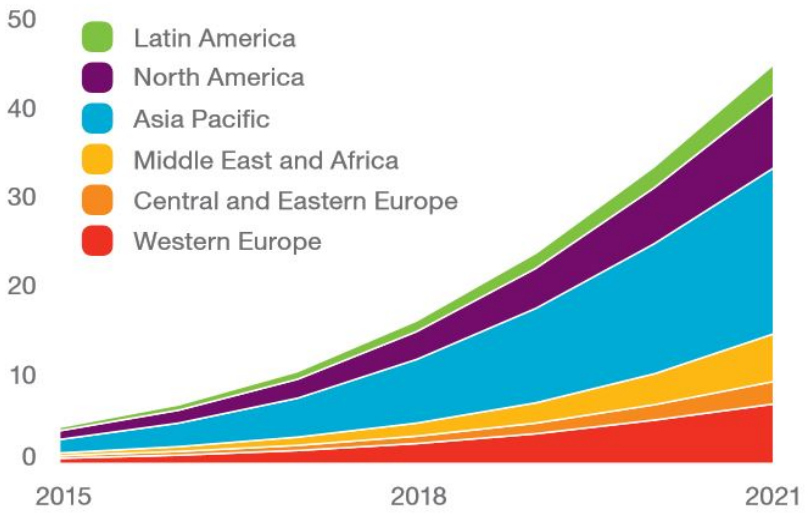


Figure 1.1: Current Vs. Forecasted cellular data traffic requirements (ExaBytes)[3].

## 1.2 MIMO Systems

The requirements for future technologies are high data rate, efficient spectrum utilization, wide band and compact size devices. Data rates were limited in conventional antenna systems so these systems are not suitable to handle modern requirements. MIMO systems were introduced to suite nowadays requirements. They use multiple antennas both at the transmitter and receiver ends to increase the channel capacity and achieve higher data rates in multipath channels. The channel capacity is directly proportional to the number of antennas. As number of antennas increase, capacity will increase. The simplified channel capacity of an isotropic environment is given by [2],

$$C = B \times \log_2(1 + M \times N \times SNR) \tag{1.1}$$

Where, C is the channel capacity (bps), B is the bandwidth (Hz), and M and N are the number of transmitter antennas and receiver antennas, respectively, and SNR is the signal-to-noise ratio (absolute value). From the above equation 1.1, we can see that the capacity can also be increased by enhancing the bandwidth. The bandwidth can be increased using connected antenna arrays (CAAs). We will discuss CAAs in the following section.

In MIMO systems, data is transmitted through different channels and also received from different channels to enhance the space diversity. The block diagram of a MIMO system is shown in Figure 1.2.

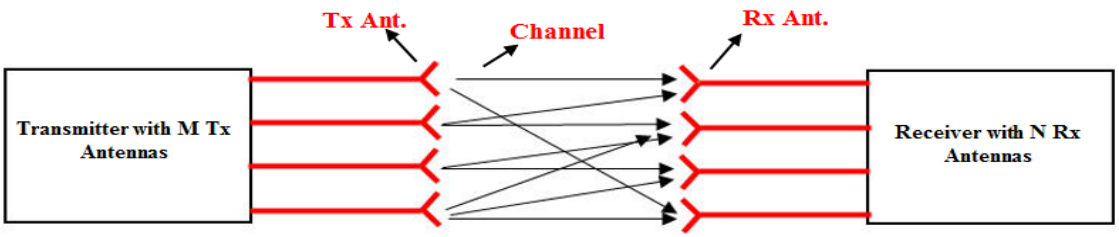


Figure 1.2: MIMO system block diagram

Printed antennas are good candidates for MIMO systems. They have several features such as easy fabrication, low profile, compact size and can easily integrate within mobile phones and other hand-held devices. The port isolation and channel correlation should be high and low, receptively, for the MIMO antennas to give the anticipated enhancement in the system performance [2].

## 1.3 Connected Antenna Arrays (CAAs)

An ordinary array consist of 2 or more antenna elements to give more directive patterns. In this type of arrays, high mutual coupling is a drawback and there is a trend to make it as small as possible because high mutual coupling can lead to narrow bandwidth and low efficiency. Unlike ordinary arrays, nowadays there is a new approach to connect antenna elements electrically so that mutual coupling increases. This is called a connected antenna array (CAA). A CAA is an array of slots or dipoles that are electrically connected with each other. When all elements are connected, they look like a single antenna instead of different antenna elements of an array. Current distributions on the ordinary array and CAA are shown in Figure 1.3(a) and Figure 1.3(b), respectively. As can be seen, currents on ordinary arrays are sinusoidal (Figure 1.3(a)) but on CAA, remains constant (Figure 1.3(b)) with the frequency which yields wide-band characteristics. Another feature of CAA is that they can provide low cross polarization [8]. The principle of operation of such arrays will be discussed in the following chapter.

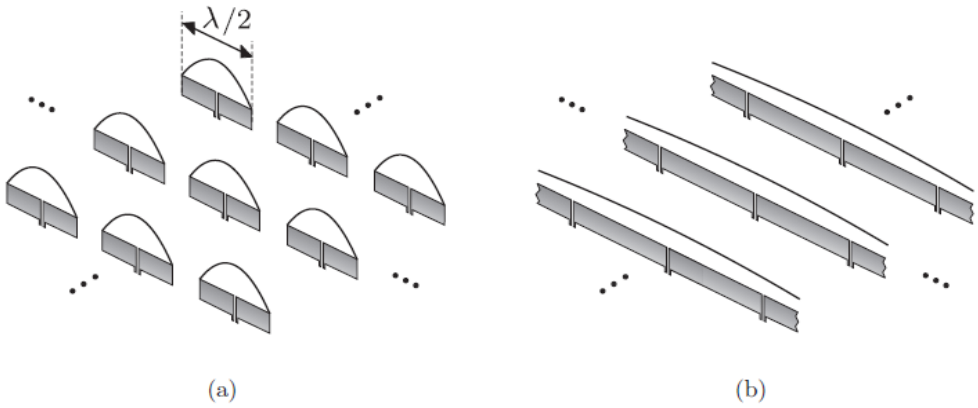


Figure 1.3: Currents distribution (a) Unconnected array of dipoles (b) CAA of dipoles [8]

## 1.4 Thesis Motivation

In this work, we are targeting to integrate MIMO antenna systems within a mobile phone with enhanced isolation for 4G LTE applications. We focus on two type of antennas as the basic building elements of the MIMO antenna system, monopole and PIFA. These types of antennas have several features as compared to other antennas like patch and dipole. They can exhibit wideband operation, compact in size, easy to fabricate, easy to integrate within mobile phones and have relatively low backward radiations towards the head of mobile user. Another aim of this work to integrate 4G MIMO antenna systems and 5G antenna system together within a same geometry. The isolation enhancement structure is introduced with dual functionality. It acts like a isolation enhancement structure within the 4G MIMO system at 2.1 GHz and also acts like a radiating connected antenna array for 5G frequency at 12.5 GHz. Initially, connected antenna arrays were used for phased array application [10],

after that people used them for radar and astronomy applications but the size was big [12]. We are the first to implement isolation enhancement structures as a connected antenna array for smart mobile phones and wireless handheld devices.

## 1.5 Thesis Contributions

The thesis contribution are listed below:

1. Two 4-element printed low profile MIMO antenna systems operating around 2.1GHz, with two antenna element types (i.e. PIFA and monopole), with at least 80MHz bandwidth for 4G wireless terminals.

2. The design of a 6-element based MIMO antenna system based on modified monopole antennas to fit within a smart phone size backplane of 110×65 $mm^2$, and covering the 4G band of 2GHz with 60 MHz bandwidth.

3. Integration of defected ground structures (DGS) in all MIMO antenna designs (4 and 6 antenna elements) to enhance the port isolation between some of the antenna elements within the MIMO antenna design.

4. Application of the concept of connected antenna array to have a dual function isolation enhancement DGS as well as an integrated radiating connected antenna array operating at 12.5 GHz for potential 5G applications.

   The flow chart is shown in Figure 1.4 to describe the step-by-step procedure.

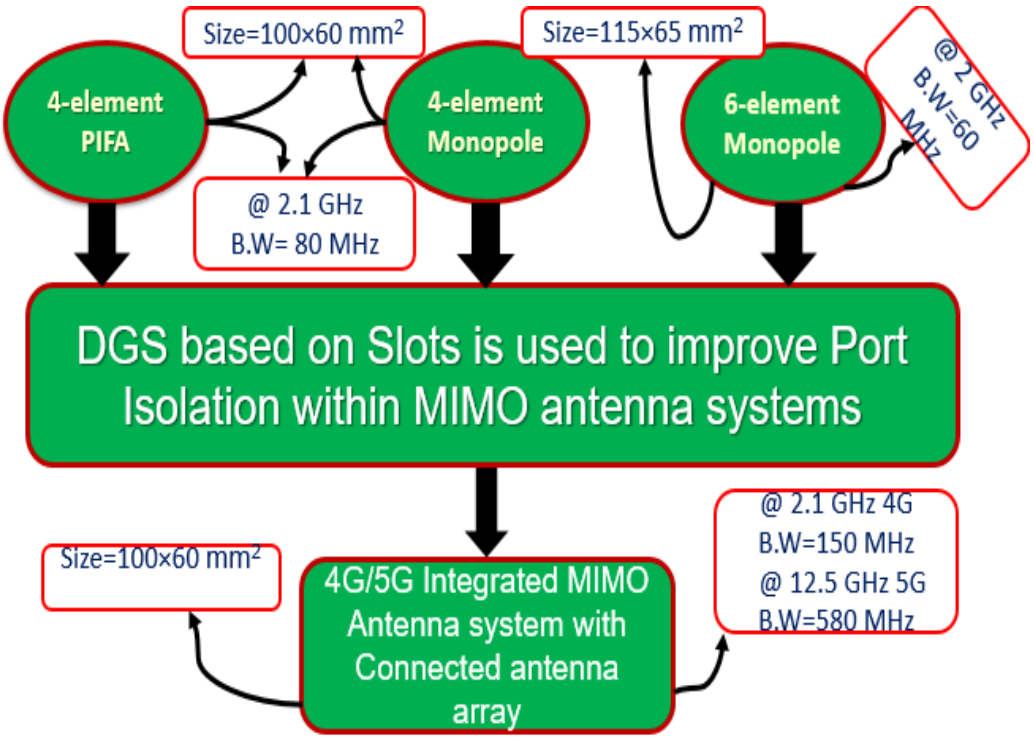


Figure 1.4: Flow chart

## 1.6 Thesis Organization

The thesis begins with a general introduction, the motivation and objectives. This is followed by a brief theoretical background on MIMO antenna systems. In this chapter, we focus on printed inverted-F antennas and their characteristics. This is followed by monopole antenna systems with details about their shapes and radiation patterns. Subsequently, we define MIMO performance metrics and their acceptable values. At the end of the chapter theoretical background of connected antenna arrays (CAA) is discussed. In chapter 3, a brief literature review is covered. We divide it into 4 sections based on isolation enhancement techniques

within MIMO antenna system to improve the port isolation, PIFA MIMO antenna system, Monopole MIMO antenna system and CAA. Chapter 4 covers our proposed 4G MIMO antenna systems at 2 and 2.1 GHz frequency bands. Three designs are discussed with 4 and 6 antenna element configurations. Their simulated and measured results are discussed. Chapter 5 starts with implementation of CAA within MIMO antenna system to enhance the isolation at 4G band and a radiator at 5G band. Then, it show the practical integrated 4G/5G MIMO antenna system. It operates at two bands 2.1 and 12.5 GHz for 4G and 5G applications, respectively. The thesis ends with some conclusions and future work.

# CHAPTER 2

# THEORETICAL BACKGROUND

In this chapter, we will discuss PIFA and monopole antennas and their features with some examples from the literature. We will also present some MIMO performance metrics like, total active reflection coefficient (TARC), envelope correlation coefficient (ECC),port isolation and diversity gain. The theory about isolation enhancement techniques also will be briefly discussed and finally, we will discuss the background and working principle of connected antenna arrays.

## 2.1 Printed Inverted-F Antennas (PIFA)

PIFAs are the most used antennas for mobile phones. These antennas consist of four main parts: 1) feed, 2) shorting pin, 3) radiating element, 4) ground plane. PIFAs are also famous because of their compact design, easy fabrication, and low backward radiation towards the head of the mobile user. It can also give multiband characteristics using more shorting pins in the design. Impedance bandwidth can be increased by modifying the ground plane or

increasing the height of the PIFA from the ground plane. The overall dimension of a PIFA is approximately $\lambda/4$ and it can be calculated using the following formula [2],

$$L + W = \frac{\lambda}{4\sqrt{\epsilon_r}} \tag{2.1}$$

Where L and W are the lengths and width of the PIFA antenna and $\epsilon_r$ is the dielectric constant of the material. Figure 2.1 shows the geometry of a PIFA antenna.

## 2.2 Printed Monopole Antennas

A monopole antenna consists of a radiating part and a ground plane as shown in Figure 2.2. The length of the radiating part is approximately $\lambda/4$ which is very small as compared to other antennas thus they can be easily integrated in mobile phones. This type of antenna has several features such as easy fabrication, compact size and wide impedance bandwidth. Moreover, this type of antenna can be modified to support dual band operations. The radiation pattern of a monopole antenna is omni-directional but it can be modified to become directive for some applications.

There are many shapes of monopole antennas that were reported in the literature like rectangular, spiral, circular, L-shape and folded monopoles. Figure 2.2 shows the most common shapes of monopole antennas.

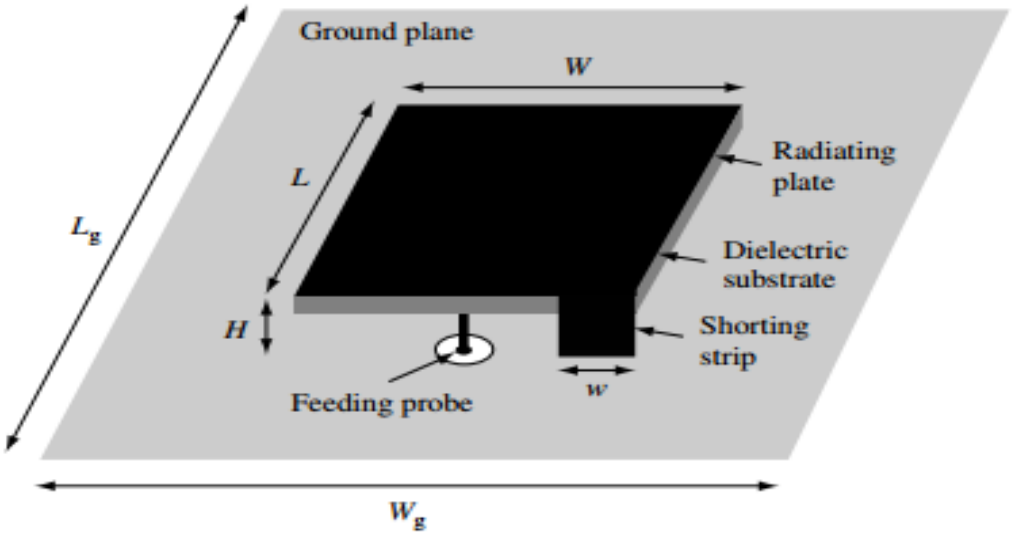


Figure 2.1: PIFA geometry [9].

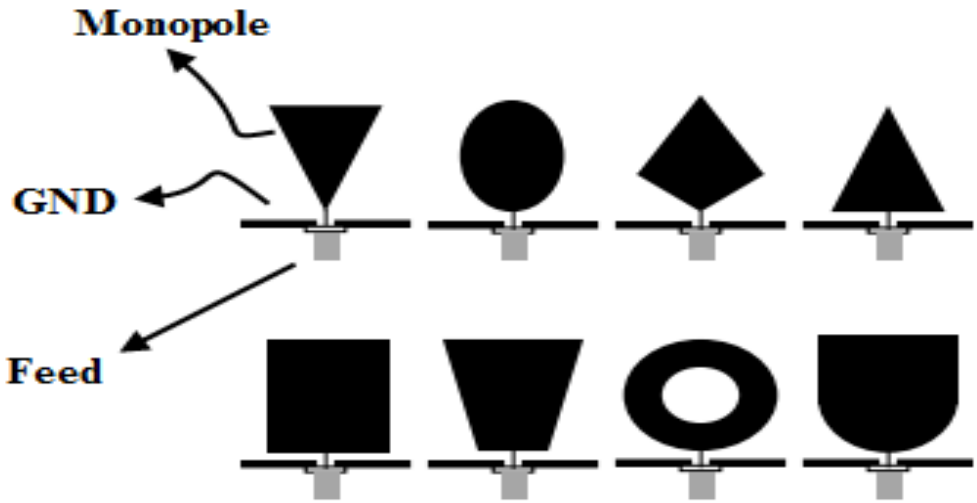


Figure 2.2: Monopole antenna shapes [9].

## 2.3 MIMO Antenna System Performance Metrics

MIMO antenna systems have several performance matrices but we will discuss four of them which are the Total Active Reflection Coefficient (TARC), Envelope Correlation Coefficient (ECC), Isolation and Diversity Gain in the following subsections because other MIMO performance metrics such as diversity gain, mean effective gain and branch power ratio are not in the scope of this thesis.

### 2.3.1 Total Active Reflection Coefficient (TARC)

The total active correlation coefficient is used to characterize the efficiency and Bandwidth of a MIMO antenna system. TARC is defined as the ratio of the square root of the total reflected power to the square root of the total incident power in a multi-point system [2]. TARC is presented in dB and is in a range from 0 to 1. Where TARC of 1 and 0 indicates all power reflected or all power radiated respectively.

For a two part MIMO antenna system, TARC calculated using S-parameters from the formula [2],

$$\Gamma_a^t = \frac{\sqrt{|S_{11} + S_{21}e^{j\theta}|^2 + |S_{21} + S_{22}e^{j\theta}|^2}}{\sqrt{2}} \tag{2.2}$$

Where $\theta$ is the input phase, $S_{xx}$ is the reflection coefficient of the port and $S_{xy}$ is the coupling between the two ports associated with the antenna structure.

### 2.3.2 Isolation

Isolation measures how much power is coupled between adjacent ports within a multi antenna system. Port Isolation is measured using the s-parameters. Some factors that affect the antenna-to-antenna isolation are physical inter-antenna separation and the polarization of antennas. More than 10dB is an acceptable value of isolation for mobile application [2]. No equation exist in the literature to measure isolation. we usually use S-parameter curves ($S_{ij}$) from simulation and measurements to show the isolation value.

### 2.3.3 Envelope Correlation Coefficient (ECC)

The correlation coefficient gives a measure of how much channels in a communication system are isolated or correlated with each other. The envelope correlation coefficient is calculated as the square of the correlation coefficient of a MIMO antenna system and it is given by [2],

$$\rho_e = \frac{|\iint_0^{4\pi}[\vec{F_1}(\theta,\phi) \times \vec{F_2}(\theta,\phi)]d\Omega|^2}{\iint_0^{4\pi}|\vec{F_1}(\theta,\phi)|^2 d\Omega \iint_0^{4\pi}|\vec{F_2}(\theta,\phi)|^2 d\Omega} \tag{2.3}$$

where, $\vec{F_i}(\theta,\phi)$ is 3D field radiation of the antenna and $\Omega$ is the solid angle.

When the antenna elements are very efficient then s-parameters based equation can be used which is given by,

$$|\rho_{eij}|^2 \cong \rho_{eij} = \left| \frac{|S_{ii}^* S_{ij} + S_{ji}^* S_{jj}|}{\sqrt{(1-|S_{ii}^2| - |S_{ji}^2|)(1-|S_{jj}^2| - |S_{ij}^2|)}} \right|^2 \tag{2.4}$$

where, $\rho_{eij}$ is the correlation between antenna i and j. $S_{ij}$ is the s parameters between

antenna i and j (coupling). Eq. 2.3 should be used as Eq 2.4 under estimates ECC. The ECC value of 0.5 has been set as an acceptable value for 4G wireless systems.

### 2.3.4 Diversity Gain (DG)

Diversity gain shows the effect of diversity performance on communication channel. It can be calculated using Eq. 2.5 [2].

$$DG = \left[\frac{\gamma_c}{SNR_c} - \frac{\gamma_1}{SNR_1}\right]_{p(\gamma_c<\gamma_s/SNR)} \tag{2.5}$$

Where, $\gamma_c$ and $SNR_c$ are the instantaneous and mean SNR for the diversity system, respectively, whereas $\gamma_1$ and $SNR_1$ are the instantaneous and mean SNR for the single input system. $\gamma_s/SNR$ is the reference point.

## 2.4 Isolation Enhancement Techniques

The Performance of MIMO antenna systems depend on multiple antennas. If these antennas have low port isolation among them, most of the power will go through the adjacent ports instead of being radiated thus degrading the performance and efficiency of the system.
To Improve port isolation between the antennas within a MIMO system, several major techniques have been used in literature. Such as the ones mentioned in [2],

1. Antenna orientation.

2. Use of decoupling Networks.

3. Use of parasitic elements.

4. Use of defected ground plane structures.

5. Use of neutralization lines.

6. Use of metamaterials.

## 2.5 Connected Antenna Arrays (CAAs)

An array of 2 or more antennas which are electrically connected is called a connected antenna array (CAA). CAAs were invented by Buan in 1970 [10]. He used TEM horn antennas for such a configuration. He mentioned that it is a timed array radiating a short pulse along the array in an end-fire direction. Figure 2.3 shows the TEM horn antenna CAA.

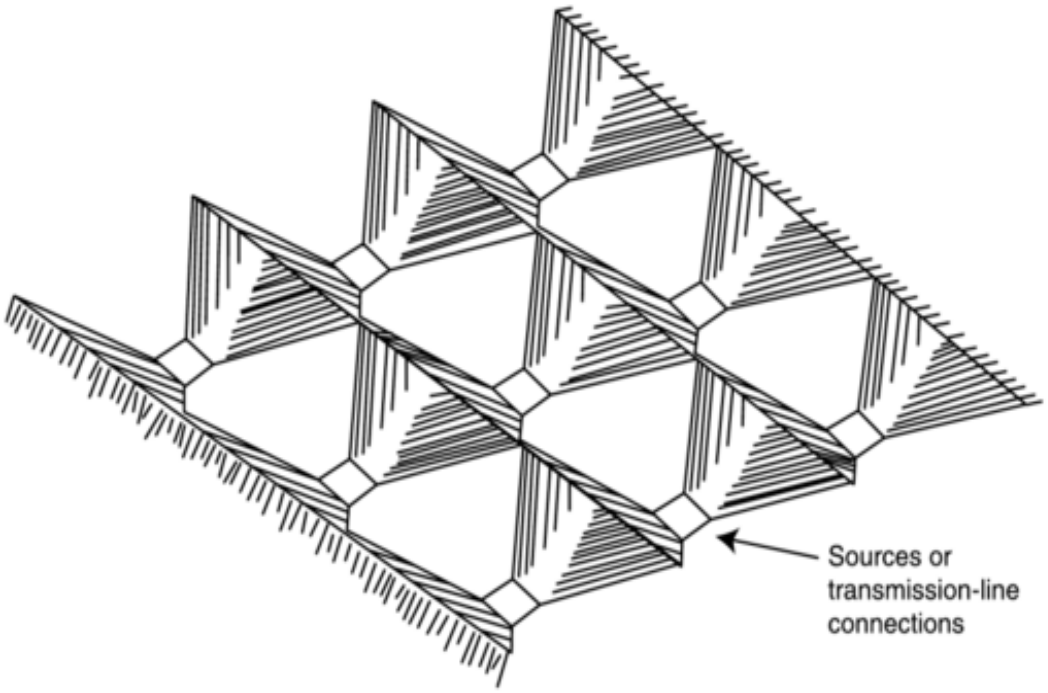


Figure 2.3: Connected antenna array of TEM horn antenna [10].

In 1979, Inagaki invented the self-complimentary antenna. Figure 2.4 shows a bowtie type linear CAA. Inagaki showed that the input impedance of this antenna is $60\pi$ $\Omega$ which is one half of the free space impedance [10].

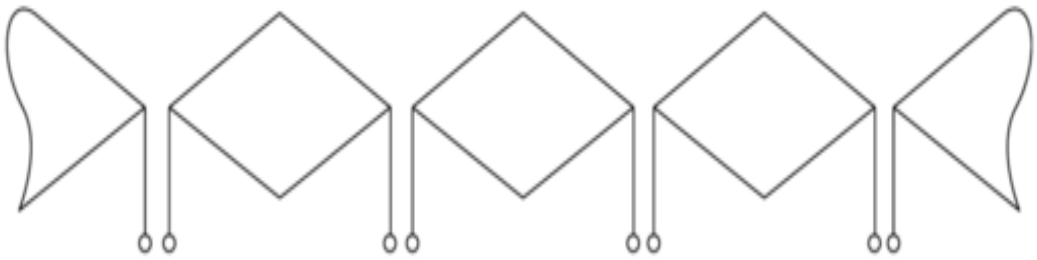

Figure 2.4: Linear connected antenna array [10].

### 2.5.1 Connected Antenna Array Principles

The dipole antenna resonate at an electrical length of $l \sim \lambda/2$. The impedance bandwidth of an ordinary planar array of dipoles is limited because, below dipole resonance the impedance becomes highly reactive and the real part becomes small. When the dipoles are arranged in a collinear configuration and their ends are connected with each other, the array will no longer be but a single antenna with many feed lines. These feed lines are applied after continuous intervals corresponding to the antenna under consideration electrical length.
In this configuration, the impedance changes become very small. When the entire length of the array becomes on the order of $\lambda/4$, this causes a higher bandwidth of operation. For a wide range of frequencies, the input impedance of a planar CAA of dipoles will be $60\pi$ $\Omega$ [10].

For the CAA that consists of slots, the impedance can be adjusted by changing the following:

- Width of the source
- Width of the slots
- Thickness of the substrate

The value of impedance for 2D slots in free space is given by [11]. From equation 2.5, one can see that the impedance is not frequency dependent which leads to a broader bandwidth of operation.

$$Z_{in} \approx \frac{dy}{dx}\frac{\zeta_o}{2}\frac{\cos\theta}{1-\sin^2\theta\sin^2\theta} \tag{2.6}$$

$Z_{in}$ is the input impedance of connected slot array, $\zeta_o$ is impedance of the free space, $\theta$ is a scan angle, dy and dx are the single element dimensions in x and y directions, respectively. The center frequency of an ordinary planar array of dipoles is at $l = \lambda/2$ but for a CAA the central frequency is shifted to $l = \lambda/4$ for each CAA element. Moreover, the usable frequency will double which gives extraordinary performance in terms of the bandwidth. A CAA of dipoles is shown in Figure 2.5.

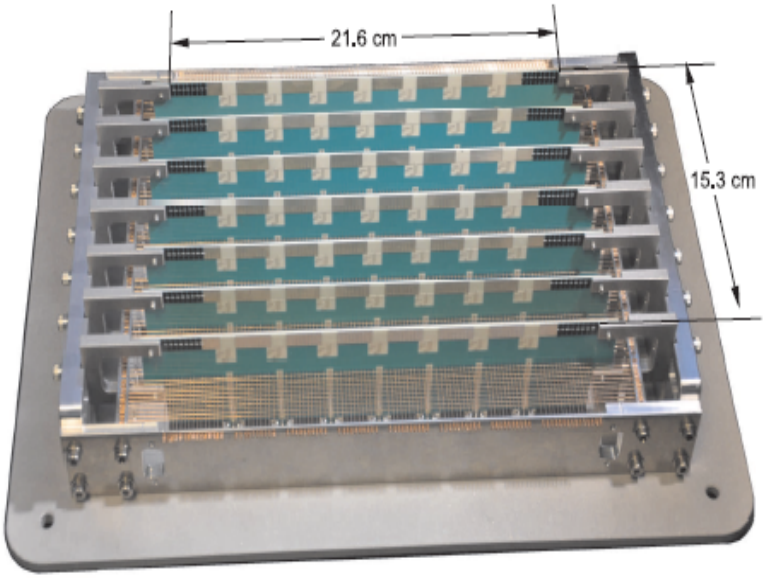


Figure 2.5: A prototype of connected dipole array [13].

The current distribution of connected dipoles is shown in Figure 2.6. In the Figure, the x-axis shows the segments of the CAA and y-axis shows the amplitude of the current. For an array with dipole length around $\lambda/4$ or less, the current distribution remains constant over a wide range of frequency. CAA made of dipoles produce a forced resonance in the currents. To connect dipoles with a reactance would make them perform better. At half wave feed spacing, the ideal reactance would be infinite but for small spacing the ideal reactance would

be small and allows the continuity of the current [12].

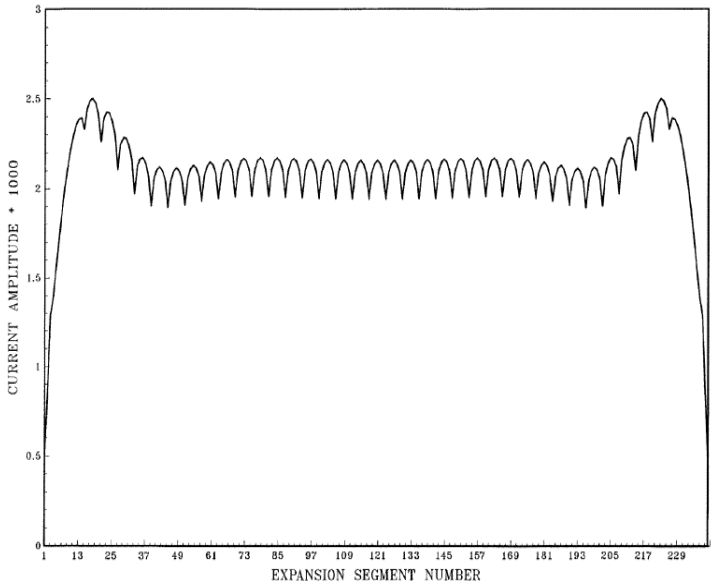


Figure 2.6: $10\lambda$ wire current distributions with feed at $\lambda/4$ separation [12].

### 2.5.2 Feeding Techniques in CAA

There are two type of resonances that occur in CAA; common and differential mode resonances. When we connect a dipole directly to the coaxial cable, it creates unbalanced current called common mode resonance current. This current flow on the outer conductor of the coaxial cable yields unwanted monopole type radiations. To suppress this type of current, a feeding network with a balun is used. A balun can suppress the common mode current as well as transfer the impedance for matching purposes. Usually differential mode resonance is preferred for CAA because it provides wide band characteristics and low cross polarization [13].

The basic type of antenna elements used in the literature for CAA are long slots, tapered

slots, dipoles and spirals. In the following parts, we will discuss the feeding methods for connected dipoles and long slots.

**Connected dipole arrays:**

Dipole based CAA are the most used type of CAA because of their ease of fabrication, providing wideband performances and polarization purity. In [14], a loop shaped transformer was used to feed the dipoles. This transformer was used to suppress the common mode currents and generate differential mode currents to make it wide band. Another feature of this transformer was to transform the impedance from 350 Ω to 100 Ω. Figure 2.7(a) shows the loop shaped transformer.

Another feeding network was studied recently in [15]. They used radial/circular stubs to design a feed network. It was used to reduce common mode currents in connected dipoles. It was covering 400-1600 MHz band. Figure 2.7(b) shows the layout of the feeding network.

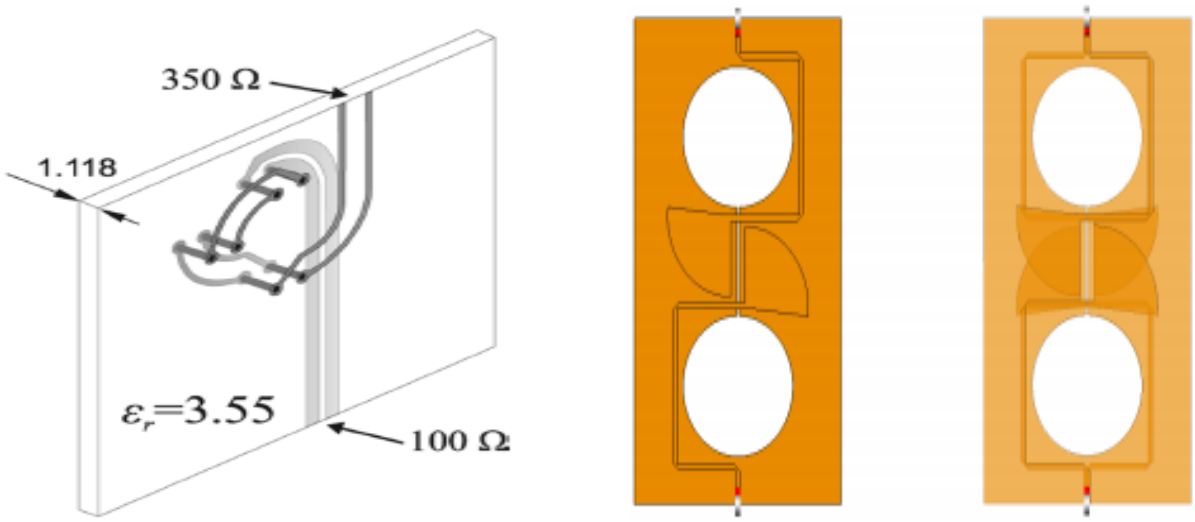


(a) (b)

Figure 2.7: Feeding network for connected dipoles (a) Loop shaped transformer [14] (b) Circular/Radial feed design [15].

**Long slot arrays:**

Feeding of a long slot is much easier than connected dipoles because slots are printed on the ground plane. Slots can be fed through microstrip lines and will not degrade the impedance performance. A planar long slot array above the ground plane fed by an array of feed elements was presented in [16] and it is shown in Figure 2.8(a). Another single long slot fed by reactively matched microstrip lines was presented in [17] as shown in Figure 2.8(b).

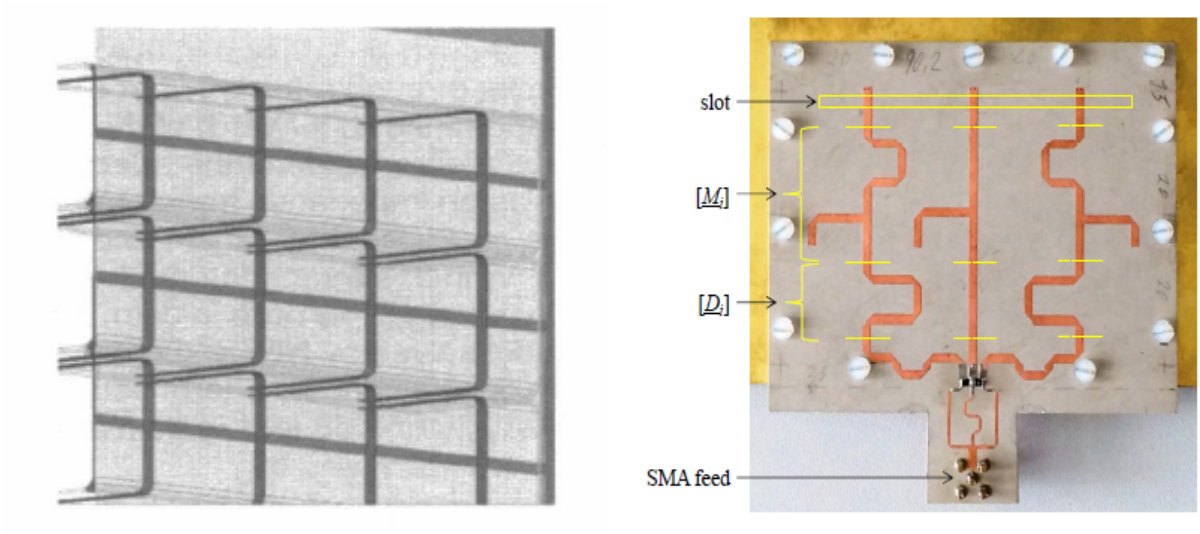


(a) (b)

Figure 2.8: Feeding network for connected slots (a) Planar slots fed with connected dipoles [16] (b) Linear slot fed with reactively matched transmission lines [17].

### 2.5.3 Applications of CAA

Some applications of CAA are:

- In-flight entertainments.
- Wideband and Multiband Radars.
- Radio Astronomy : The square Kilometer Array.
- Mobile communications.

## 2.6 Summary

In this chapter, the operating principles of PIFA and monopole antennas were discussed.

Such types of antennas are suitable for MIMO systems because of their compact size and wide bandwidth. MIMO performance metrics used to characterize multi-antenna systems were also discussed. The underlying principles of CAA were introduced with some historical background. Feeding techniques for the connected dipoles and long slots were also reported while regular dipole require an electric length of $\lambda/2$, CAA requires $\lambda/4$ length for similar band dipoles.

# CHAPTER 3

# LITERATURE REVIEW

This chapter will provide a brief literature review about isolation enhancement techniques, PIFA based MIMO antenna systems, Monopole based MIMO systems and CAA.

## 3.1 Isolation enhancement Techniques

There are several techniques available in the literature to enhance the isolation between closely placed antennas in a MIMO configuration.

### 3.1.1 Antenna Orientation and Placement

Antenna configuration or orientation is very important in MIMO systems because it can be used to enhance the isolation between adjacent antennas. If the MIMO antenna system is working at high frequency bands (>1GHz) then the radiating elements are usually placed far away from each other. This will enhance the isolation. Current distribution phase and polarization orthogonality can also be used to enhance the isolation in antenna configura-

tions. If the MIMO system is working at low frequency bands (<1GHz) then relying on antenna orientation and placement can not be used for isolation enhancement because at low frequencies the ground plane usually becomes a part of radiating element and enhances the coupling between adjacent MIMO elements. So at lower frequencies this technique can not be used.

In [18], the effect of placement of planar inverted-F antennas(PIFA) was studied. The PIFAs were placed in collinear, parallel and orthogonal modes. The spacing was ranging from $0.1\lambda$ to $0.9\lambda$. It operated at 2.45 GHz. It was found that if the antennas are placed in collinear arrangements then minimum mutual coupling can be achieved which means that isolation was improved. In the parallel configuration, the same results were obtained. In the orthogonal arrangement, both antennas were placed at $90^o$ to each other. This configuration resulted in the minimum isolation because currents were opposite to each other.

In [19], the position of an IFA MIMO antenna array of two radiating elements was studied. In this study, two antenna elements were working together just like an array at 3 GHz. The size was $100\times50\times0.8mm^3$ as a possible solution for mobiles and other hand held devices. It was found that due to different configurations or antenna placements within MIMO system. Improvement in the isolation as well as the diversity of the system can be achieved. Five different configurations were discussed. In each configuration the distance between the elements was different that resulted with different isolation. The conclusion of this study was that large distance between the antenna elements will provide better isolation.

In [20], antenna orientation was also studied. The MIMO antenna was dual band and con-

sisted of two different antennas. One was IFA which was working at 2.45 GHz and the second was loop antenna which was working at 5 GHz. In this work when antennas were placed orthogonal to each other, they provided the best results with high isolation.

### 3.1.2 Decoupling Networks

Decoupling networks can be used to reduce the coupling between the antenna elements. These networks can enhance the port isolation of the MIMO system. Due to these networks, the reflection coefficient $S_{ii}$ might also be affected but these parameters can be corrected using separate matching networks at every port of antenna system.

In [21], a decoupling network technique was studied for enhancing the isolation between two closely spaced ports. Two transmission lines were used at the ports. These lines converted the complex impedance to a pure imaginary impedance and then a shunt reactance was used to cancel out the effect of this imaginary component. This circuit was used for impedance matching. Before placing this network, isolation was 5dB. After placing this, it became 35dB. The antenna system was working at 2.45 GHz. In [22], a dual element MIMO antenna system working at 710 MHz was studied for LTE applications. It consisted of two meander line Monopole antennas. The separation was $\lambda/45$ between the elements from edge-to-edge. Antennas were printed on FR-4 material and overall size was $50 \times 87mm^2$. An LC-Based branch-line for a hybrid coupler was used to remove the coupling between the ports and enhance the isolation more than 10 dB throughout the band.

### 3.1.3 Parasitic elements

The isolation of a MIMO antenna system can be enhanced using proper parasitic element coupling usage. Using these elements, we can also increase the port efficiency of the system. Parasitic elements generate a opposite current fields which cancel out the original fields that cause the mutual coupling between the radiating elements. Placement should be such that it generates a $180^o$ out of phase current on the other radiating element to cancel out the coupling current that yields high isolation. This mechanism is similar to neutralization line but there is no physical link between radiating elements of the MIMO system in this case.

In [23], Parasitic elements were used to enhance the isolation of a MIMO system. Two monopoles have been used as parasitic elements. The printed dual slot Antennas were working at 1920-2170MHz in UMTS band. Two monopoles were introduced between these slot antennas. They provided extra path for the current so that the coupling current can be reduced. Through this method isolation was enhanced. Before providing this technique isolation was below 20dB and after this, it was above 25dB.

In [24], 4-channel MIMO antenna system consisting of 4 Patch antennas working at 5GHZ for WLAN band applications was studied. Isolation was provided through parasitic elements. It was improved by at least 10dB. In this study different horizontal and vertical transmission lines were introduced as parasitic elements and the isolation was calculated. The best results were achieved from the combination of horizontal and vertical transmission lines.

In [25], a dual Planar Inverted-F MIMO antenna was studied for WLAN applications. It was working in the 2.4-2.484GHz band. Isolation was improved by the use of a folded resonator. It

was introduced in the antenna structure like a parasitic element which canceled the mutual coupling between the antenna elements and enhance the isolation. Without this element isolation was 10-13dB. After Using this, it was within the range from 15 to 35dB in the band.

### 3.1.4 Defected Ground-Plane Structures(DGS)

In printed MIMO antenna systems, all antennas use a common ground that is the major cause of generating coupling currents in the system and degrade the port isolation. At low frequencies the ground plane becomes a part of the radiating element. Defected ground-plane structures(DGS) are widely used to eliminate ground based coupling issues. DGS acts like a band reject filter and minimize the mutual coupling between the radiating elements.

In [26], The DGS was applied between two PIFA antennas to enhance the isolation. The DGS was a dumbell shaped structure. Before applying DGS, Isolation at 7.5 GHz was 23dB. After using DGS, It was about 40dB. In this reference , there were different types of DGS studied like split ground, metallic wall but the best result was attained through dumbbell shaped DGS.

A four element MIMO antenna working at 2.4GHz for WLAN applications was presented in [27]. It consisted of two proximity coupled fed micrstrip square ring patch antennas and two $\lambda/4$ slot antennas. These two types of antennas were printed on the two sides of a substrate. This configuration provided reduction in mutual coupling. Another technique was introduced to enhance isolation which was introduction of slits in ground plane. Isolation achieved was

more than 25dB. The total size of the MIMO antenna system was $0.64\lambda \times 0.48\lambda$.

Isolation was improved in [28] using three slots in ground plane of two rectangular patch antennas. Patch antennas were resonating at 9.1GHz. In this study, they tried with different arrangements of DGS and the isolation was calculated. After several parametric studies about 16.5dB isolation improvement was achieved using DGS.

In [29], a DGS was introduced not only for isolation enhancements but also for improvement in impedance bandwidth. This impedance bandwidth improvement was significant at the higher frequency as compared to the lower one. The band of interest was ranging between 2.4 to 6.5GHz. This antenna system consisted of two edge-to-edge monopoles with separation of $0.083\lambda_o$ at 2.5GHz. To reduce coupling between the monopoles, the authors introduced slits in the ground plane. These slits capture the coupling currents and enhance the isolation of the system.

### 3.1.5 Neutralization Lines

Another technique to enhance the isolation between the close antenna elements within a MIMO system is called Neutralization line(NL). This technique is just like a parasitic element because it is also used to cancel out the coupling current between the radiating elements. A NL takes the current from a specific area of the radiating element and inverts this current through its length and places this current to the neighboring radiating element and due to phase reversal it reduces the coupling currents thus enhancing isolation. The selection of this specific high coupling current location is very important when using NL. It should have

high current and low impedance because the effective bandwidth of NL technique depends on the impedance. A stable impedance area can be used as starting point through out the band.

In [30], a NL technique was used for isolation enhancement. Two monopole based MIMO antenna was presented and working at WLAN applications ranging from 2.4 to 2.48GHz. A NL was connected between two monopoles near the feeding point. This point was determined based on the two conditions mentioned earlier. By applying the NL, isolation was improved from 19 to 40dB within the band.

A NL is used to enhance the isolation as well as efficiency of the system in [31]. The MIMO system consisted of two patch antennas working at 5.75GHz. As discused in the previous paragraph, a NL was connected between the ports of two antennas. The isolation was improved from 9dB to 20dB. In this work current distribution was also presented which demonstrated, how NL cancel out the coupling current and enhance the port isolation.

In [32], two monopoles making a MIMO system were presented. Isolation was provided through the use of a NL. Antenna elements were resonating at frequency range from 2.4 to 2.497GHz for WLAN applications. Isolation was improved from 13dB to 30dB using this method.

### 3.1.6 Metamaterials

Metamaterials are man-made structures. They have negative permeability and permittivity or both. Due to the band gap in their frequency response, they can be used as band reject

filters and reduce mutual coupling between the radiating elements of a MIMO antenna system. Metamaterials consist of basic building blocks of Unit Element (UE) or unit cell (UC). These UEs contain the characteristics of Metamaterials when arranged in a periodic manner. There are two important types of metametrials which have been seen in the literature [2],

- Split-ring resonators (SRRs)
- Capacitive loaded loops (CLLs)

A MIMO antenna system was presented in [33] that consisted of two antenna elements resonating in WiMax band ranging from 3.4 to 3.6GHz. This antenna system consisted of multi-layers. Two FR4 ($\epsilon_r = 4.4$) substrates have been used. One was 0.8mm thick and the other was 1.6mm thick. Antenna elements were printed on the top of the 0.8mm material and the bottom was working as a ground. SRRs were used to enhance the isolation in this MIMO system. It was etched on the 1.6mm thick substrate. Isolation was improved from 13dB to 35dB. Total volume of the MIMO system was $50mm \times 90mm \times 2.4mm$.

In [34], a new technique was used to enhance the isolation between two loop antennas. This antenna system was working on 2.45GHz. An absorber cell was used in this system which have negative permittivity and permeability at 2.45GHz. There were three cells which have been used between tha antenna elements to enhance the isolation. Total antenna volume was $51mm \times 24mm \times 2mm$ with spacing between antenna elements was $0.23\lambda_o$.

Table 3.1 shows a comparison between the brief literature review of isolation enhancement structures. A lot of work has been done to enhance the isolation between closely packed antennas. Our target is to use DGS based isolation enhancement structure, because it is

simple to implement and can be modified into connected antenna arrays.

Table 3.1: Summary of literature review based on isolation enhancement techniques.

| MIMO Isolation structure | Single Band | Multi Band |
|---|---|---|
| Antenna Placement | [18], [19] | [20] |
| Decoupling Network | [21], [22], [35] | |
| Parasitic Elements | [23], [24], [25] | [37] |
| Defected Ground-Plane Structures (DGS) | [26], [28] | [27], [29], [36], [38] |
| Neutralization Lines | [30], [31], [32] | |
| Meta-Materials | [33], [34], [39] | [40] |

## 3.2 PIFA MIMO antenna Systems

In [41], a box folded PIFA MIMO antenna system was developed for LTE (1.84-2.69 GHz) applications. The MIMO antenna system consisted of 4 antenna elements. MIMO performance matrices were discussed. Isolation was 14.2 dB. The envelope correlation coefficient (ECC) obtained was 0.3. The overall size of the MIMO system was $136 \times 68.8 \times 6mm^3$ and single element size was $10 \times 10 \times 5mm^3$.

In [42], a 4-element PIFA MIMO antenna system was proposed for WLAN(2.45 GHz) applications with 73% efficiency. Two substrates used were Roger 3035. The height of both substrates was 0.75mm and $\epsilon_r$ was 3.5. The air gap between these substrates was 5mm. The

overall size of the MIMO system was $105 \times 55mm^2$. Each antenna had a volume of 0.455 $cm^3$.

In[43], a MIMO system for LTE 13-band applications was presented. It was covering from 746 MHz to 787 MHz frequency band. The MIMO system consisted of 2 antenna elements. For the MIMO performance, Isolation and ECC were 17dB and 0.05 respectively. FR4 was used as a substrate with $\epsilon_r = 4.4$. The size of the MIMO system was $60 \times 90 \times 1mm^3$ .

A 2 element modified PIFA for MIMO terminals was reported in [44]. It was operating at 2.5 GHz. The separation between the elements was less than $\lambda/2$ (20mm). It was 3D elevated design with high isolation of 28 dB. ECC and gain were measured with values of 0.01 and 9.3 dB, respectively. An FR4 substrate was used. The overall size of the MIMO system was $100 \times 40mm^2$.

In [45], A MIMO antenna array of 8-elements was reported. It was targeting two bands from 2.6-2.8GHz and 3.4-3.6 GHz. The MIMO system consisted of 4 U-slits etched PIFAs and 4 L-slits etched PIFAs. These two sets were placed orthogonal to each other to improve the isolation. They were using different ground planes. Isolation reported was above 20dB. ECC and efficiency were 0.01 and 70%, respectively. The size of the MIMO system was $140 \times 70 \times 9.55mm^3$. The geometry of the model is shown in Figure 3.1

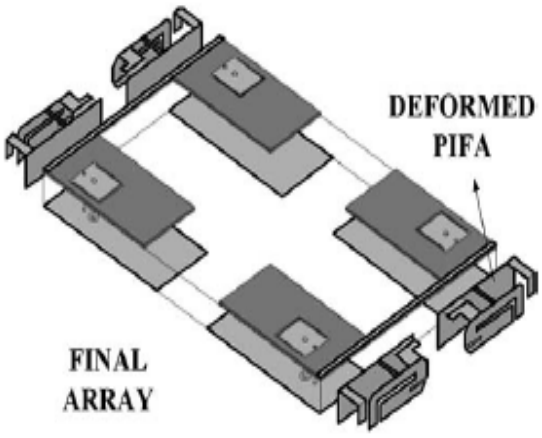


Figure 3.1: 8-element PIFA based MIMO system[45].

In [46], a 4-elements elevated design for MIMO terminals was presented. It was covering 2.4-2.8 GHz band for WLAN applications. MIMO performance matrices were discussed. Mean effective gain, TARC, ECC and channel capacity were -3.5dB, -7dB, 0.5 and 22bits/sec/Hz, respectively. Antennas were fabricated on FR4. Height and dielectric constant of the FR4 were 1.6mm and 4.4, respectively. Each antenna size was $30 \times 30 \times 16.4 mm^3$. Size of the substrate was $120 \times 120 mm^2$. The separation between antennas was $0.43\lambda$.

In [47], S(2.2-2.4 GHz) and C(4.4-5GHz) bands unidirectional PIFA antennas for MIMO terminals were developed. It consisted of bend ground plane on the cylindrical conducting surface with height and radius of 55mm and 45mm, respectively. Separation between antennas was around $1\lambda$. ECC for low and high band was 0.005 and 0.03, respectively.

In [48], a miniatured meanderline MIMO-PIFA was presented. It consisted of 4-elements operating at 2.45 GHz for WLAN applications.The size of the MIMO system was $105 \times 55 mm^2$. Isolation was investigated using different placements of the antenna elements. The maximum

effective diversity gain reported was 16.31dB.

In [49], a dual miniatured PIFA was presented. It was an elevated design and consisted of two antenna elements. The operating frequency was 2.1 GHz. They placed the antennas with different orientations to see the effect of mutual coupling. The minimum coupling was 19dB. The size of the MIMO system was $100 \times 50 \times 0.8mm^3$.The air gap between antenna and ground plane was 5mm. Size of single element was $15 \times 8mm^2$.

In [50], a multi-band and multi antenna system was presented. Multiband characteristics were achieved using different slots in the geometry of the PIFA. The whole system was operating at 1.8, 1.92-2.7, 2.17-2.22, 2.3-2.36, 5.15-5.35 and 5.47-5.825 GHz bands. Isolation was achieved using ground slots in the ground plane. The size of the whole system was $75 \times 50mm^2$ and height of the PIFA was 8mm.

Table 3.2 shows the comparison of the proposed design (details in chapter 4) and previous work with respect to frequency band, size of the board and number of antennas. In [45], 8 element based MIMO system was presented but they have used separate ground planes which is not practical for MIMO system and size is also quite large. In [52], another configuration of 8-element MIMO system was reported but they have presented at 3.5 GHz and only simulated results were presented. From this discussion, we have concluded that our design is more suitable for mobile applications at 2.1 GHz.

Table 3.2: Comparison between proposed and previous work based on size and no. of antenna elements.

| Ref. | No. Ant. | Freq(GHz) | board size(mm) | Min. Isolation | B.W(MHz) |
|---|---|---|---|---|---|
| [41] | 4 | 1.84-2.69 | 68.8×136×6 | 14 | 850 |
| [42] | 4 | 2.45 | 55×105×6.5 | 10 | |
| [51] | 5 | 3.4-3.6 | 40×60×0.8 | 6 | 200 |
| [45] | 8 | 2.6-2.8, 3.4-3.6 | 70×140×9.55 | 20 | 200, 200 |
| [52] | 8 | 3.5 | 40×100×5 | 6 | |
| Pro. Design | 4 | 2.072-2.210 | 60×100×0.8 | 20 | 138 |

## 3.3 Monopole MIMO based antenna Systems

In [53], two monopoles with meander-line parasitic elements were presented for 1.92-2.17, 2.3-2.5, 2.4 and 3.2-10.6 GHz frequency bands. Isolation was enhanced using parasitic elements and it was 20dB. The size of the MIMO system was $55 \times 86.5mm^2$. FR4 substrate was used with h=0.8mm, $\epsilon_r = 4.4$.

In [54] , a MIMO system consisting of 3 different types of antennas was reported. They used two PIFAs with Minkowski and Koch monopoles. The substrate which have been used was having $\epsilon_r = 3.384$ and loss tangent=0.0027. The size of the ground plane was $46.6 \times 88.7mm^2$. It was a dual band antenna system and operating at 2.4 and 5.2 GHz bands.

In [55], printed C-shaped monopole antenna array was presented. It was dual band MIMO system. A NL was used between the two antenna elements to enhance the isolation between them. The gain at 2.4 GHz was 2.91 and at 5.2 was 2.82 dB. Size of the MIMO system was $32 \times 44\ mm^2$. FR4 was used as a substrate with $\epsilon_r = 4.4$.

In [56], a new folded monopole antenna was presented for mobile phones. It was a multiband diversity antenna which was suitable for MIMO applications. It consisted of two elements.It was covering 890 MHz and 6 GHz frequency bands. It was an elevated 3D design and fabricated on the FR4 substrate with dimensions $105 \times 55 \times 1.5mm^3$. Dielectric constant was 4.4. Antenna size was $7 \times 15 \times 7.5mm^3$. The antenna conducting surface supported by another substrate with $\epsilon_r$ 4.4 and thickness of 1mm.

In [57], A printed MIMO system was reported.It consisted of two monopoles and neutralization line(NL). This NL was used to decouple the mutual current between the antenna elements. Isolation was reported to be 19dB. The purposed design was operating at 2.45 GHz for USB-dongle applications.The size of the board was $65 \times 30 \times 1mm^3$.

In [58], 4-element monopole based MIMO antenna system was presented. It was operating at 2GHz. It used two different shapes for monopoles. It had 11.2dB isolation and -5dB mean effective gain. The overall system size was $95 \times 60mm$.

In [59], four element MIMO system was presented. It was a multiband system covering 1.95, 2.39, 2.64 and 3.27 GHz frequency bands with impedance bandwidhts of 2.66, 6.57, 8.8 and 4.09%, respectively. Different ground planes were used for each element which led to an enhancement of the isolation up to 20dB. The measured ECC was less than 0.01.

The dimension of single element was $50 \times 50mm^2$ and the size of the 4-element MIMO was $110 \times 110mm^2$. FR4 was used as a substrate with thickness of 0.8mm and dielectric constant of 4.2. The geometry of the design is shown in Figure 3.2.

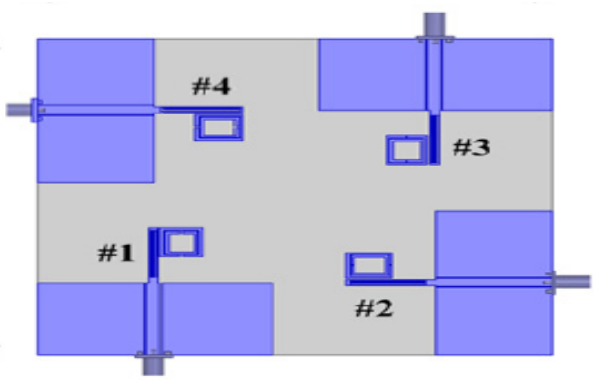


Figure 3.2: 4-element monopole MIMO system [59].

From the above discussion, 2-element based MIMO antenna systems were presented in [53]-[57], and 4-element MIMO antenna systems were reported in [58]-[60]. One can see all MIMO system have big size and there were no configurations of MIMO antenna systems in the literature based on monopole antennas which have more than 4 antennas. Table 3.3 can show a comparison summary between the proposed designs (details in chapter 4) and previous work with respect to size of the board, frequency band and number of antenna elements. For the monopole based MIMO antenna systems, our proposed design (section 4.3) is the first to place 6-elements within a smart phone size operating at 2 Ghz with good characteristics.

Table 3.3: Comparison between proposed and previous work based on monopole.

| Ref. | No. Ant. | Freq(GHz) | board size(mm) | Min. Isolation | BW(MHz) |
|---|---|---|---|---|---|
| [53] | 2 | 1.92-2.17, 2.3-2.5, 3.2-10.6 | 55×100×0.8 | 17.2 | 250, 200, 7400 |
| [56] | 2 | 0.89 | 55×105×9 | 12 | 200 |
| [57] | 2 | 2.45 | 30×65×1 | 20 | 100 |
| [54] | 4 | 2.4 | 46.6×108.7×1.6 | | 200 |
| [58] | 4 | 1.88-2.20 | 60×95×0.8 | 11.5 | 320 |
| [59] | 4 | 1.95, 2.39, 2.64, 3.27 | 110×110×0.8 | 20 | 50, 60, 150, 60 |
| [60] | 4 | 0.69,1.7,2.3, 3.5 | 150×150×0.8 | 20 | 99, 300, 100 |
| Pro. Design1 | 4 | 1.997-2.190 | 60×100×0.8 | 15 | 193 |
| Pro. Design2 | 6 | 1.999-2.060 | 65×115×0.8 | 15 | 61 |

## 3.4 Connected Antenna Arrays (CAAs)

A connected slot array was reported in [11] for ultrawide-band applications. They developed green functions to study the single and 2D connected slots. They mentioned that currents were continuous on the entire slot and impedance of the slots remain constant with respect to frequency which lead to a wide bandwidth. It was also stated that one can change the input impedance of the slots by changing the width of the slot and the source and thickness of the substrate.

A wide-band CAA of dipoles from 3 to 5 GHz was reported in [14]. A $7 \times 7$ prototype of the CAA was reported. The total size of the array was 15.2×21.6 $cm^2$. A loop shaped transformer was used for matching and feeding purposes. It transformed 350 Ω to 100 Ω impedance. Wide-band and low cross polarization characteristics in CAAs were studied.

In [15], CAA of dipoles was presented with a feeding network to suppress common mode resonance. It was covering 450-1450 MHz frequency band. The feed network consisted of two back to back wide-band microstrip slot-line transitions. The array was placed 75mm above the ground plane. The spacing between the elements was 80mm.

In [17], a linear CAA of a long slot was reported and they claimed that it can be used for broadband cellular communications. A long slot fed from three points using a reactively matched feeding structure and operated at 1.74, 2.55 and 3.4 GHz bands. The total size of the board was 235×118 $mm^2$ with a slot size of 1.8×71 $mm^2$. It was fabricated on roger 6002 with dielectric constant of 2.94 and thickness of 0.762 mm.

A long slot based CAA was presented in [61] for phased array applications. It covered 0.4-2 GHz band. It consisted of 15×15 elements. Every slot had a 15 elements. A balance feed network was used to match the impedance with 50 Ω. Total thickness of the array was 8.1cm.

In [62], scanning properties of wideband CAAs in the presence of backing reflector were discussed. Scanning properties of connected slots and dipoles were compared. It was concluded that performance of CAAs depend on the backing reflector, distance between radiator and ground plane and energy stored in the feeding points. It has been shown that the capacitive effect in the dipole feeding is an extra feature for the dipole as compared to the slot to make it suitable for wider scan angles.

Table 3.4 shows the comparison of the proposed design (details in chapter 5) with the previous work with respect to size and applications.

Table 3.4: Comparison between proposed and previous work based on connected array

| | Freq(GHz) | system size(mm) | Array Type | Applications |
|---|---|---|---|---|
| [14] | 3-5 | 216×153 | Dipoles | Wide-band Radar |
| [15] | 0.45-1.45 | | Dipoles | Wide-band Radar |
| [17] | 1.74, 2.55, 3.4 | 235×118 | Long slot | Cellular |
| [61] | 0.4-2 | 760×760×203 | Planar slot | Phased array |
| Pro. 4G/5G integrated Design | 12.5 | 60×100×0.8 | Planar slot | Mobile |

## 3.5 Summary

In this chapter, we have discussed the previous works on MIMO systems and CAA. We also discussed some of our proposed design features compared with the previous work and commented that our proposed designs give nice contribution in the literature since defected ground structures (DGS) as dual function ones (i.e. an isolation enhancement mechanism as well as a 5G radiating structure) has never been proposed before.

# CHAPTER 4

# 4G MIMO ANTENNA SYSTEMS

This chapter covers the results and discussion of 4G MIMO antenna systems. It presents three 4G MIMO antenna systems with 4 and 6 antenna elements. Moreover, a defected ground structure (DGS) is used to improve the isolation between various antenna elements of the MIMO antenna system.

## 4.1 Printed Inverted-F Antenna (PIFA) MIMO Antenna System

PIFAs are the most used antennas for mobile phones. These antennas consist of four main parts: 1) feed, 2) shorting pin, 3) radiating element, 4) ground plane. The geometry of single element PIFA antenna is shown in Figure 4.1.

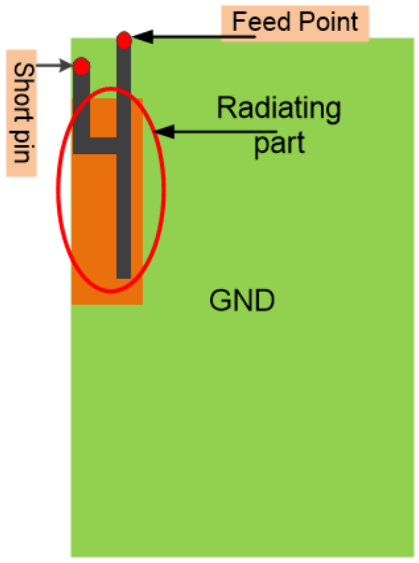


Figure 4.1: Geometry of PIFA Antenna.

The proposed modified PIFA based MIMO antenna system geometry is shown in Figure 4.2. The proposed MIMO antenna system consist of 4 antenna elements. All the radiating elements are short circuited with the GND plane using shorting pins to make antenna size compact. The dielectric constant ($\epsilon_r$) of the substrate used is 4.3 with the height of 0.8mm. The overall board dimensions are 100×60×0.8 $mm^3$ representing a standard cell phone size with single element dimensions of 26× 6 $mm^2$. The length of the single element antenna is around $\lambda/4$ (26mm). It is compact, low profile and suitable for mobile handsets.

All antennas are etched on the top 4 corners of the substrate as shown in Figure 4.2(a) while GND plane is on bottom side. A DGS (GND slots) is used to improve the isolation as shown in Figure 4.2(b). DGS is consisted of ground slots. The size of a single slot is 28.5×0.5 $mm^2$ with 0.5mm spacing between adjacent slots. At the resonance frequency, the slots were

a part of radiating structure and were acting like a band reject filter and hence improved the isolation. A fabricated prototypes of the proposed MIMO antenna system with DGS is shown in Figure 4.3.

### 4.1.1 Current Distributions

The current distributions on the PIFA MIMO antenna system are shown in Figure 4.4(a) and 4.4(b). Without DGS, it can be seen that when Ant-1 (Figure 4.2) is excited and other are terminated with matched load. A high current is coupled through adjacent ports due to sharing the same ground plane. When we apply a DGS, the current is trapped and minimized through the ground slots. A significant change is observed at Ant-2 and Ant-3 (10dB to 15dB as shown in Figure 4.5(a) and Figure 4.5(b)). Although, DGS is introduced between Ant-1 and Ant-3 but coupling current is also reduced between Ant-2 and Ant-4 when Ant-2 is excited and others are terminated with match loads as shown in Figure 4.4(c).

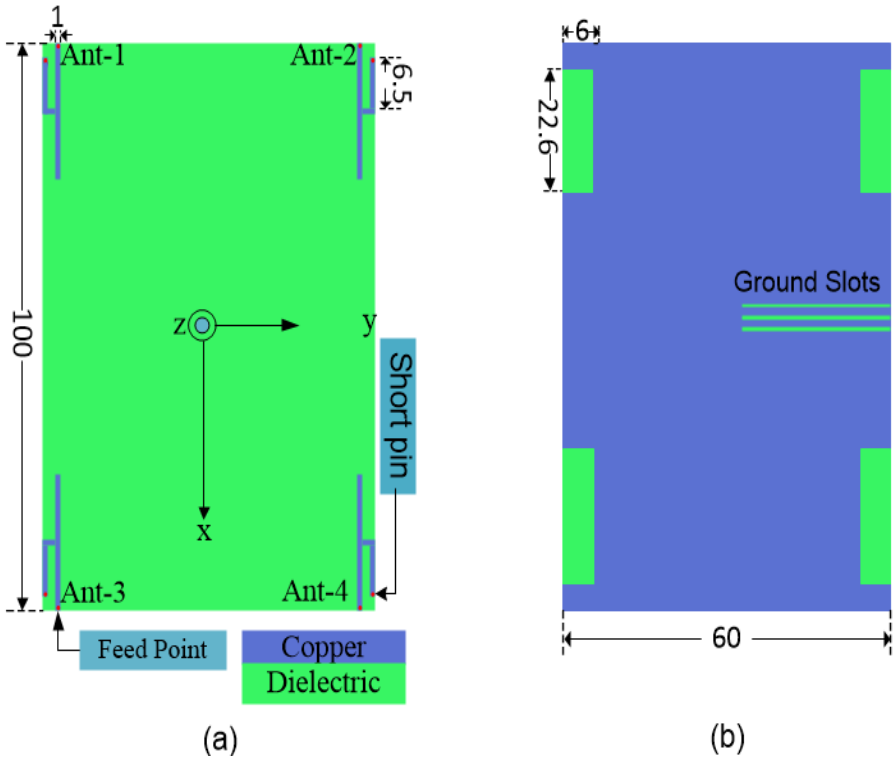


Figure 4.2: Proposed 4-element PIFA based MIMO antenna system (a) Top view (b) Bottom view- all dimensions are in mm.

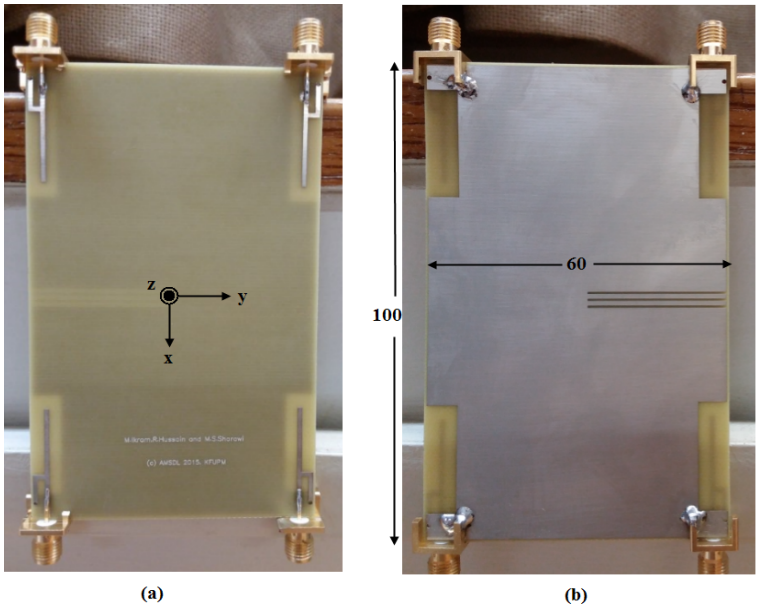


Figure 4.3: Proposed 4 element PIFA based MIMO antenna with DGS: Fabricated Model (a) Top view (b) Bottom view - All dimensions are in millimeters (mm).

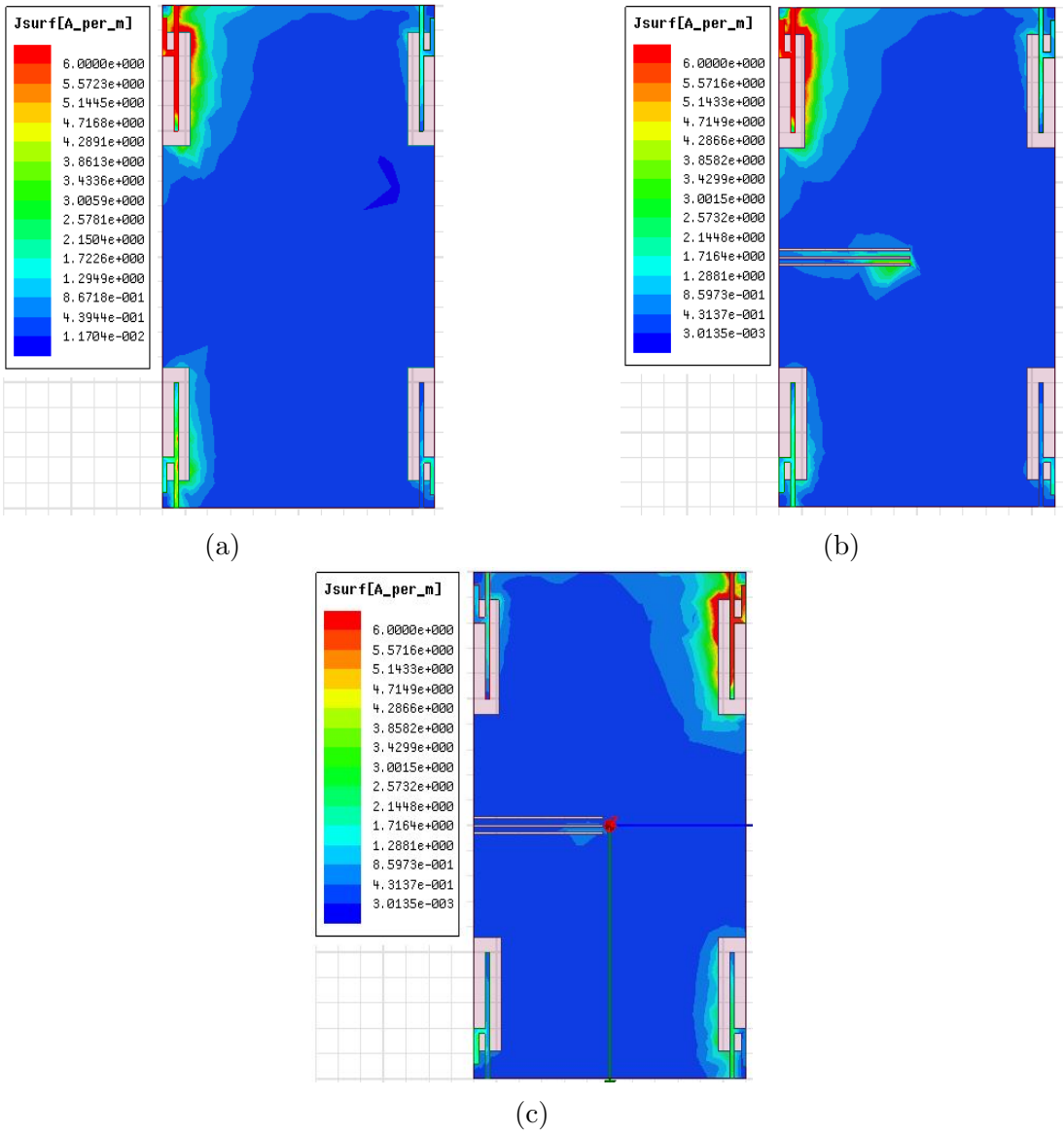


Figure 4.4: Current distributions: (a) P1 is activated at 2.1 Without DGS (b) P1 is activated at 2.1 GHz With DGS (c) P2 is activated at 2.1 GHz With DGS.

### 4.1.2 S-Parameters

The proposed MIMO antenna system was modeled and simulated using HFSS$^{TM}$. The S-parameters of the fabricated design were measured using an Agilent N9918A vector network

analyzer at the antennas and microwave structure design laboratory (AMSDL), KFUPM. The simulated and measured reflection coefficient curves of the antenna without DGS are shown in Figure 4.5(a) while Figure 4.5(b) shows the simulated reflection coefficient curves with DGS. All the curves show that the 4-elements of MIMO system were resonating at 2.1 GHz. The -10dB bandwidth was 218 MHz from 2048 to 2266 MHz.

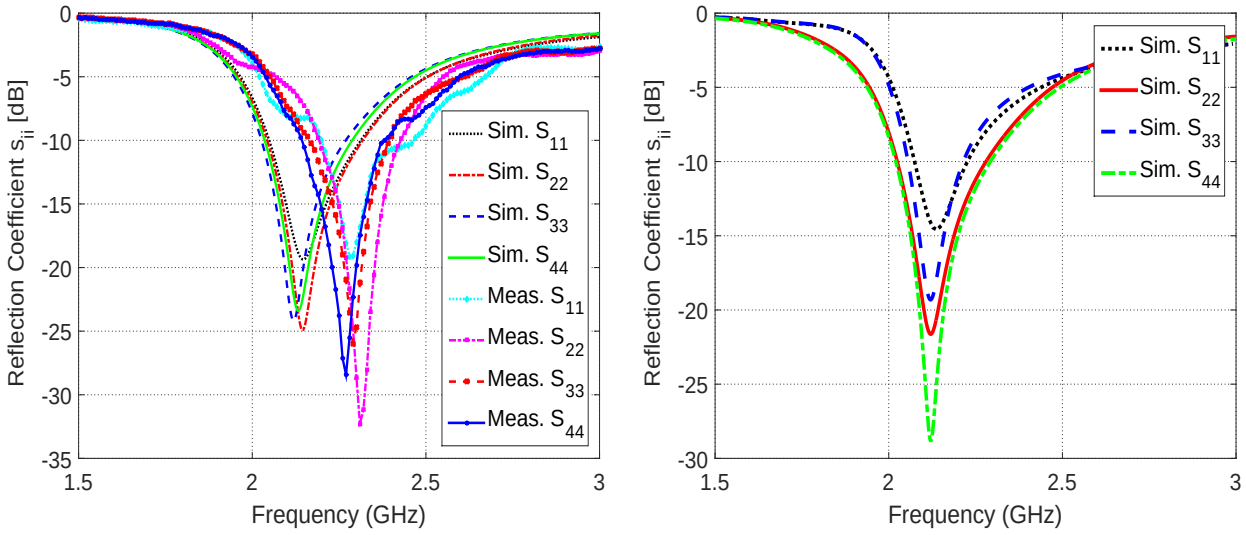


(a) (b)

Figure 4.5: S-parameters curves (a) $|s_{ii}|$-Simulated and measured without DGS (b) $|s_{ii}|$-Simulated with DGS.

The simulated isolation curves of the proposed MIMO antenna system are shown in Figure 4.6. Figure 4.6(a) shows the simulated isolation curves for the MIMO antenna without DGS while Figure 4.6(b) shows the simulated isolation curves with DGS. The minimum isolation between Ant-1 and Ant-3 was -10 dB as shown in Figure 4.6(a). 5 dB improvement in isolation was achieved as shown in Figure 4.6(b). A decrease in the bandwidth to 149 MHz from 2072 to 2210 MHz using the DGS was obtained. The measured reflection coefficient curves of the MIMO system with DGS are shown in Figure 4.7(a) while Figure 4.7(b) shows

the measured isolation curves with DGS.

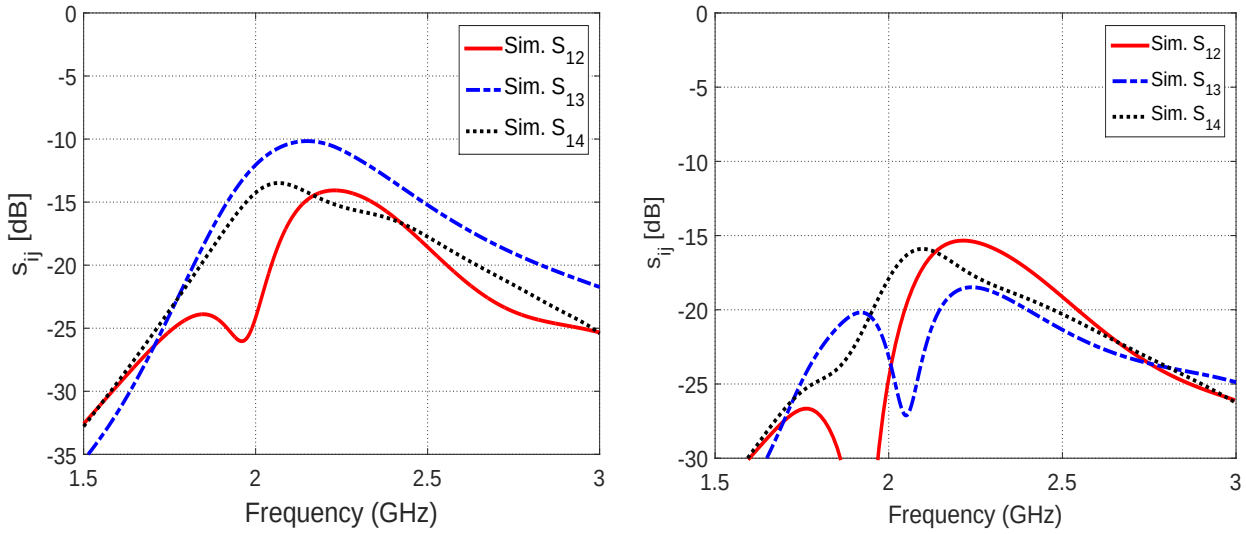


Figure 4.6: Isolation curves (a) $|s_{ij}|$-Simulated without DGS (b) $|s_{ij}|$-Simulated with DGS.

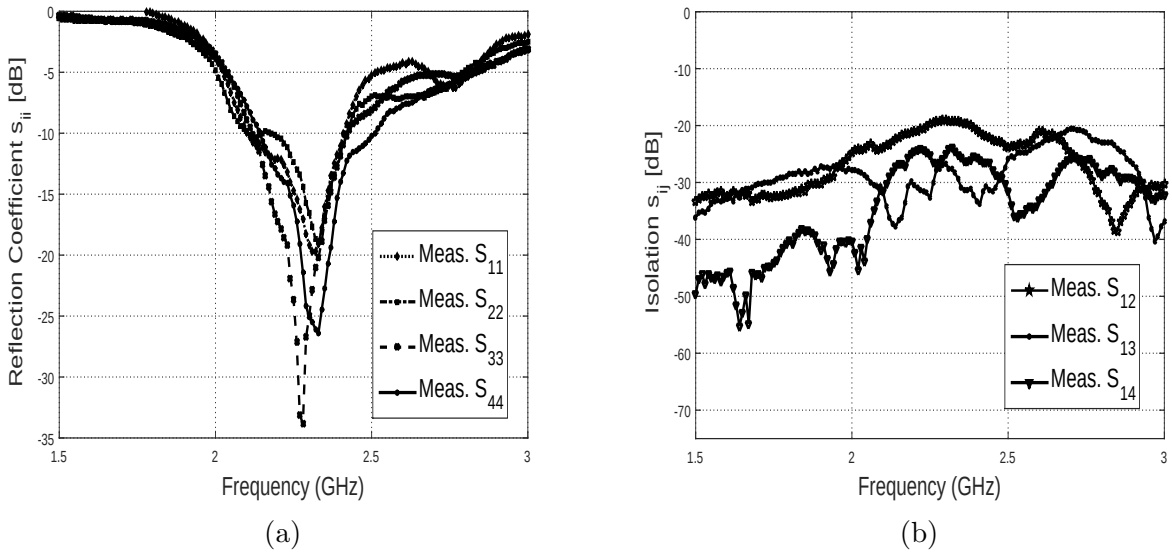


Figure 4.7: S-parameters curves (a) $|s_{ii}|$-Measured with DGS (b) $|s_{ij}|$-measured with DGS.

### 4.1.3 Radiation Patterns

The simulated maximum gain of all MIMO antenna elements is 4dBi. The 2D radiation patterns in terms of $E_{total}$ are shown in Figure 4.8. It can be seen from the 2-D patterns that the simulated patterns are tilted which will lead to low correlation between the MIMO channels. The envelop correlation coefficient ($\rho_e$) values were computed based on radiation pattern and were 0.0842, 0.1518, 0.0125, between antenna elements (Ant-1, Ant-2), (Ant-1, Ant-3) and (Ant-1, Ant-4), respectively. The $\rho_e$ values show good MIMO performance.

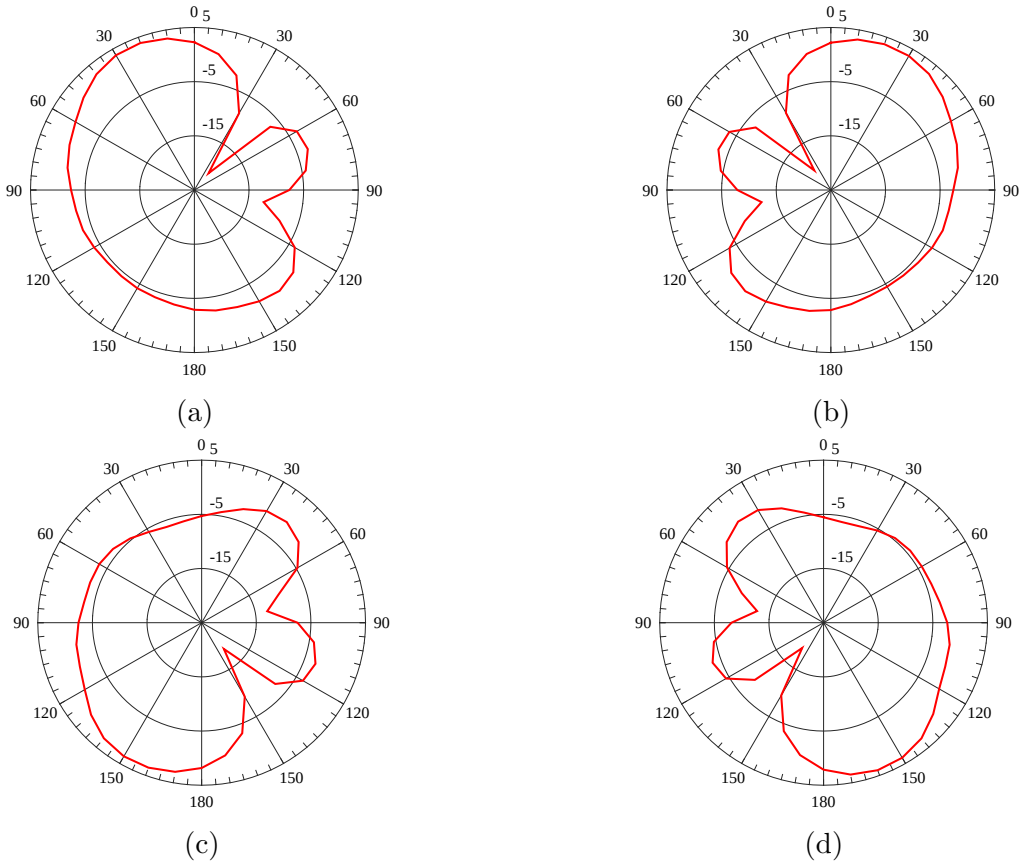


Figure 4.8: Simulated 2-D Radiation patterns of $E_{total}$, $\phi - cuts$ at $\theta = 90^o$ (a) Ant-1 (b) Ant-2 (c) Ant-3 (d) Ant-4.

## 4.2 4-Element L-Shaped Monopole MIMO antenna System

Monopole antenna is also famous for mobile phones because of their compact size and easy fabrication. It consist of three main parts: 1) feed, 2) radiating element, 3) ground plane. Sometimes it needs matching structure to match with 50Ω. we use short circuit stub for matching. The geometry of single L-shaped monople antenna is shown in Figure 4.9.

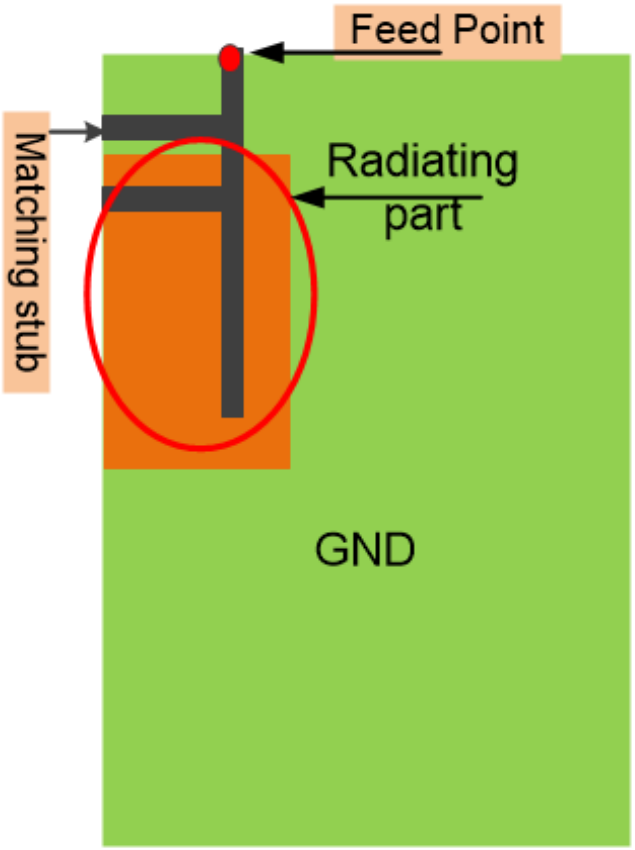


Figure 4.9: Geometry of monopole Antenna.

The proposed modified monopole based MIMO antenna system geometry is shown in

Figure 4.10. The proposed MIMO antenna system consists of 4 antenna elements. All the radiating elements were short circuited with the GND plane using metallic plate to resonate at the lower frequency band. The dielectric constant ($\epsilon_r$) of the substrate used is 4.3 with height 0.8mm. The overall board dimensions are $100\times60\times0.8$ mm$^3$ with single element dimensions of $23\times$ 9 mm$^2$. The length of the single element antenna was around $\lambda/4$ (23mm).

All antennas are etched on the top 4 corners of the substrate as shown in Figure 4.10(a) while GND plane is on bottom side. A deflected GND structure (DGS) was used to improve the isolation as shown in Figure 4.10(b). The DGS consisted of an array of GND slots and a ring. The size of a single slot is $35\times1.5$ mm$^2$ with 3 mm spacing between adjacent slots. At the resonance frequency, the slots and ground ring were a part of radiating structure and were acting like a band reject filters and hence improved the isolation. The size of a ring was $\lambda/2$. A fabricated prototype of the two MIMO antenna systems without and with DGS are shown in Figures 4.11(a) and 4.11(b).

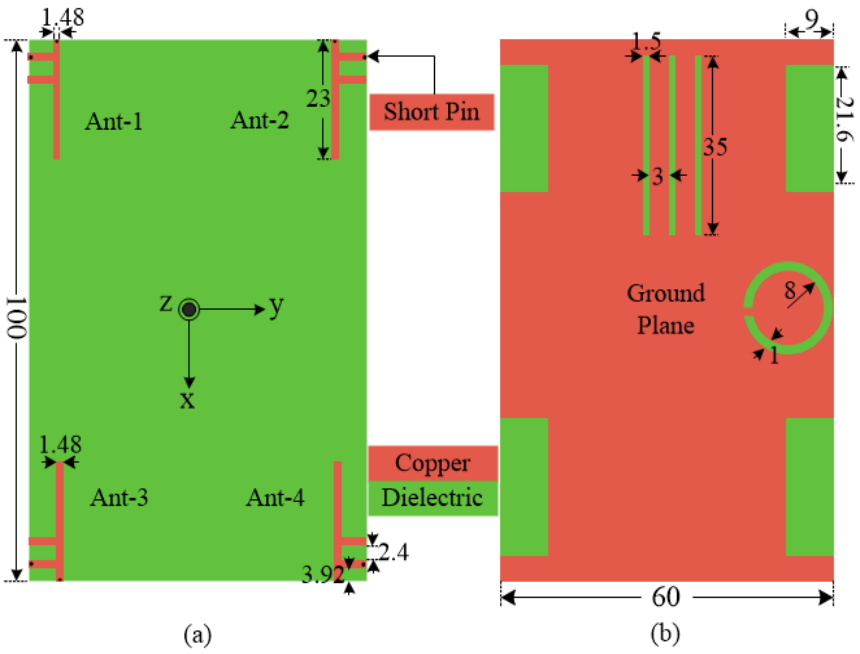


Figure 4.10: Propsed L-shaped MIMO antenna (a) Top view (b) Bottom view- All dimensions are in millimeters (mm).

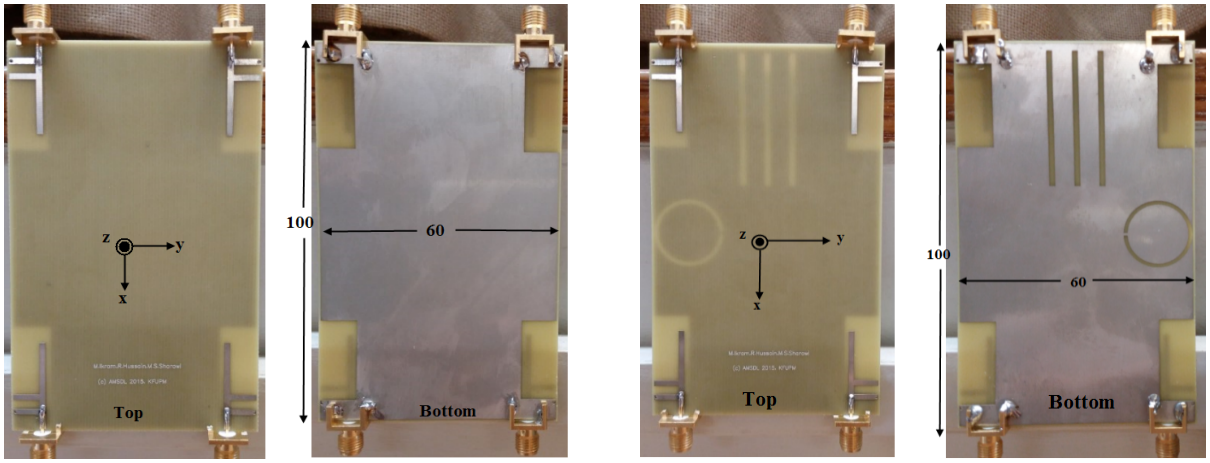


Figure 4.11: Fabricated models: (a) Without DGS (b) With DGS- all dimensions are in mm.

### 4.2.1 S-Parameters

The proposed MIMO antenna system was modeled and simulated using HFSS$^{TM}$. The S-parameters of the fabricated design were measured using an Agilent N9918A vector network analyzer. The radiation pattern and efficiency were measured in a SATIMO star-lab chamber at MVG-Italy. The measurement setup is shown in Figure 4.12.

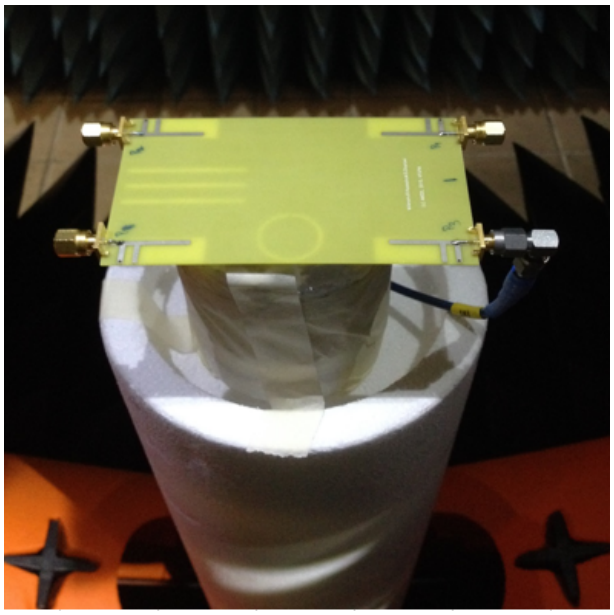

Figure 4.12: Measurement setup in a Satimo star Lab chamber.

The simulated and measured reflection coefficient and isolation curves of the MIMO antenna system without DGS are shown in Figure 4.13(a) and Figure 4.13(b). The simulated and measured reflection coefficient and port isolation with incorporation of DGS are shown in Figures 4.14(a) and 4.14(b), respectively. All simulation curves show that all antenna elements are resonating at 2.1GHz with -10dB bandwidth of 193 MHz covering 1997 to 2190 MHz for a design with DGS. The measured reflection coefficient show a bandwidth of 128

MHz with a center frequency around 2.168 GHz.

Isolation is improved within the band, as can be seen from the Figure 4.14(b). There is a notch at -17dB showing a noticeable improvement in the isolation. The array of slots take care of improving isolation between Ant-1 and Ant-2, the simulated value of isolation at 2.1 GHz without DGS is 14dB and with DGS is 16dB, while the circular slot improves isolation between Ant-1 and Ant-3, the simulated value of isolation at 2.1 GHz without DGS is 11dB and with DGS is 17dB. The small frequency chnage in measured results is due to the fabrication tolerance in the material properties and attaching the connector.

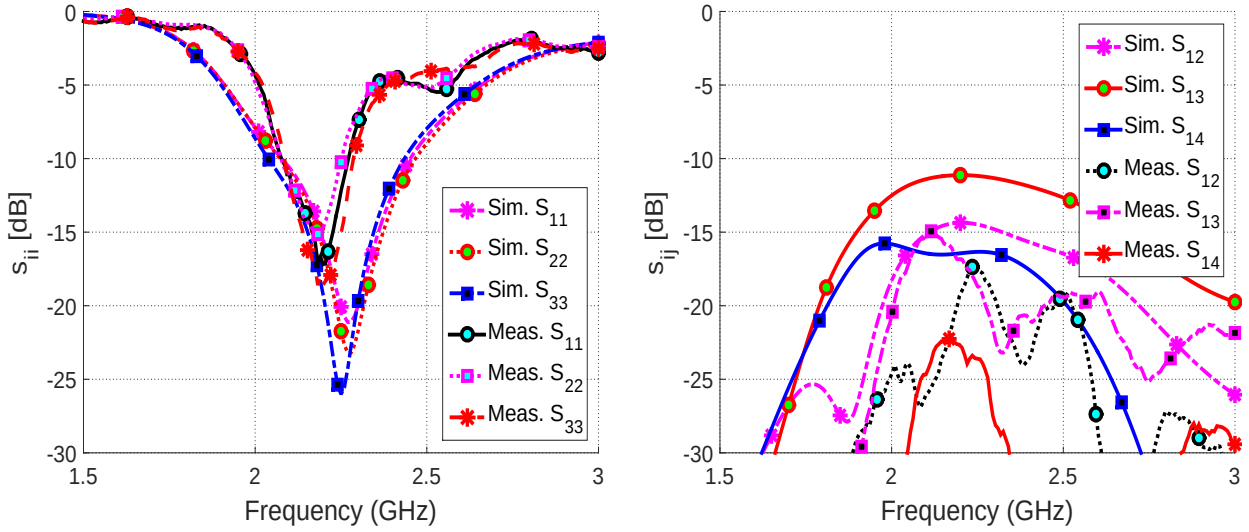


(a) (b)

Figure 4.13: S-parameters curves (a) $|\mathbf{s}_{ii}|$-Simulated and measured without DGS (b) $|\mathbf{s}_{ij}|$-Simulated and measured without DGS.

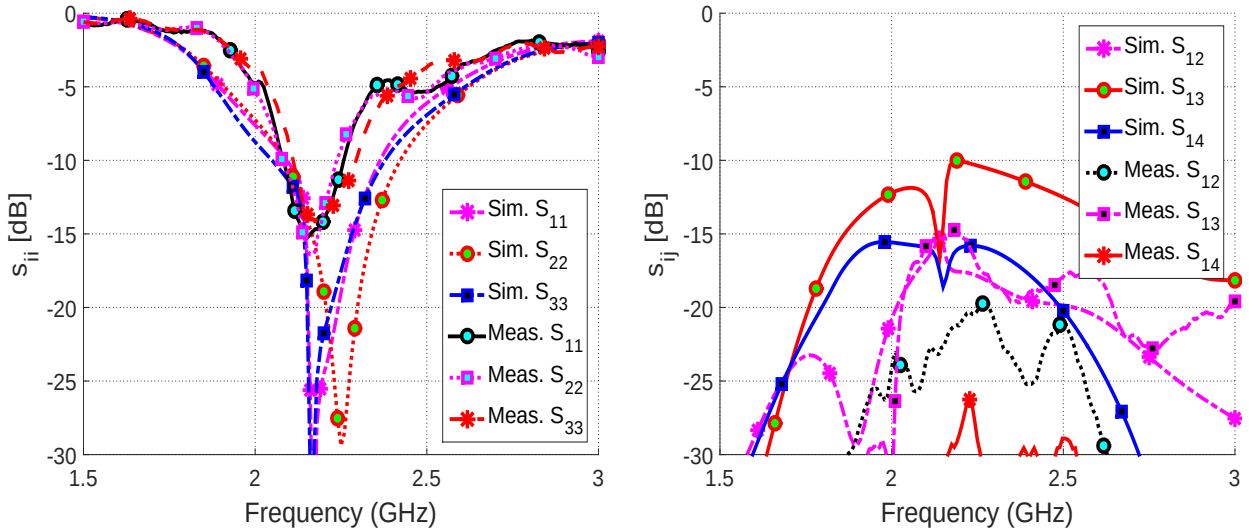


(a) (b)

Figure 4.14: S-parameters curves (a) $|\mathbf{s}_{ii}|$-Simulated and measured with DGS (b) $|\mathbf{s}_{ij}|$-Simulated and measured with DGS.

### 4.2.2 Current Distributions

The current distributions on the monopole MIMO antenna system are shown in Figure 4.15(a) and 4.15(b) at the center frequency of 2.1 GHz. Without DGS, It can be seen that when Ant-1 (Figure 4.10) is excited and other are terminated with matched load. A high current is coupled through the adjacent ports due to sharing same ground plane. When we apply a DGS, the current is trapped and minimized through ground slots. A significant change is observed between Ant-2 and Ant-3 (Figure 4.15(b)). Isolation before DGS was 11dB and after applying DGS, it became 17dB at 2.1 GHz between Ant1 and Ant-3.

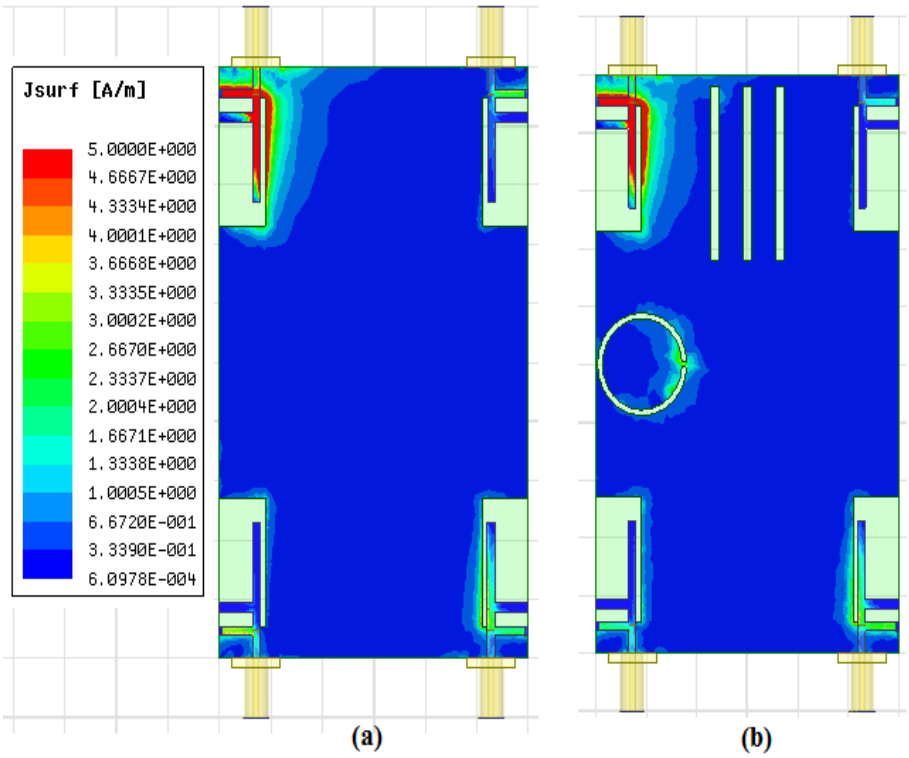


Figure 4.15: Current distributions on proposed 4 element monopole MIMO antenna system at 2.1 GHz (a) Without DGS (b) With DGS.

### 4.2.3 Radiation patterns

For the evaluation of the MIMO system on the basis of its radiation patterns were measured using a SATIMO star lab chamber (Figure 4.12), the normalized measured radiation patterns in terms of Etotal at 2.1 GHz are illustrated in Figure 4.16 for the x-z and x-y planes (referred to Figure 4.10). The maximum values of Etotal for Ant-1 to Ant-4 are 2.44dB at ($\theta = -152^o$, $\phi = 154^o$), 2.19dB at ($148^o$, $133^o$), 2.75dB at ($-160^o$, $26^o$), and 2.74dB at ($108^o$, $74^o$), respectively. In Figure 4.16(a) and Figure 4.16(c) 2-D $\theta$ cuts are ploted for maximum values of $E_{total}$ of each antenna at their respective $\phi$. In Figure 4.16(b) and Figure 4.16(d)

2-D cuts are plotted at $\theta = 90^o$ for $\phi - cuts$. It can be seen from the 2-D patterns that the measured patterns are tilted in the x-z and x-y planes which will lead to low correlation between the MIMO channels.

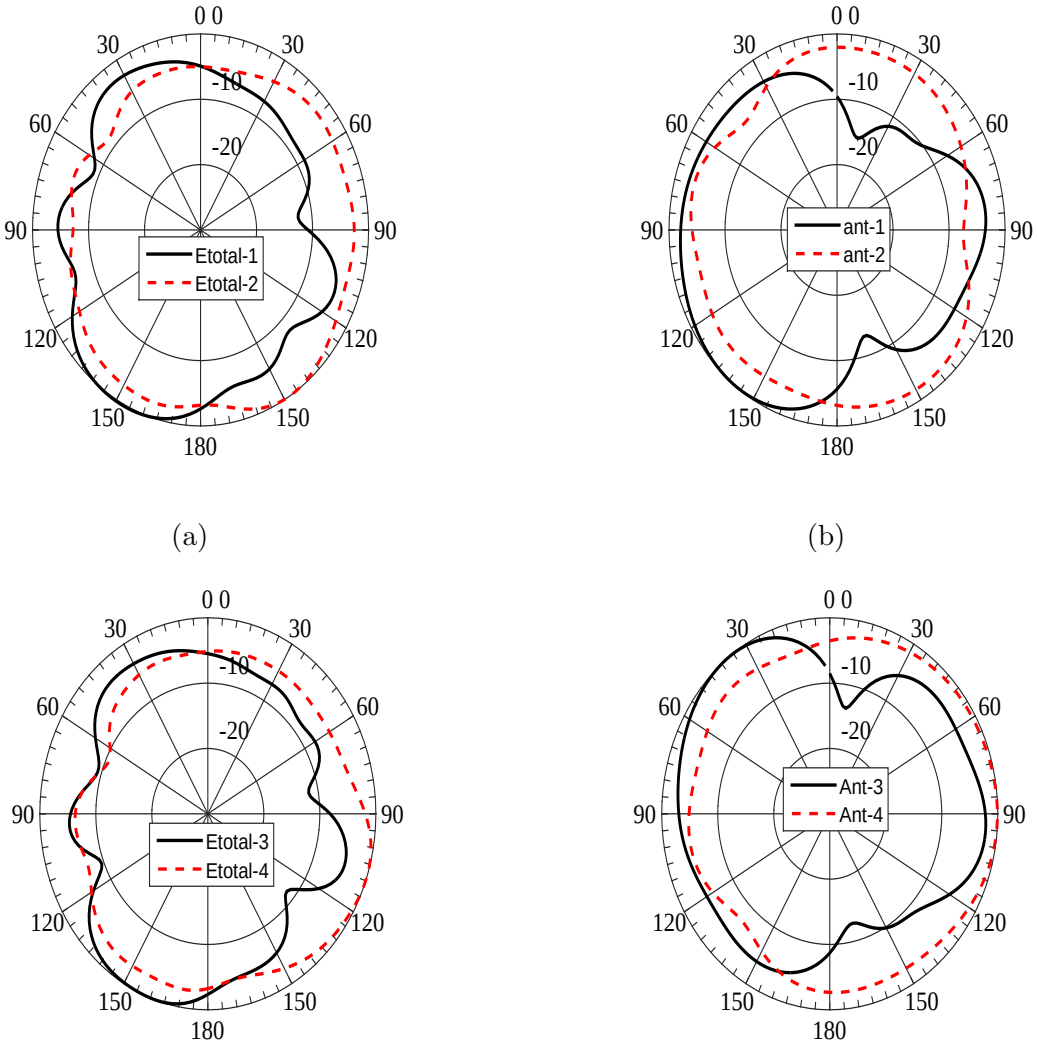


(a) (b)

(c) (d)

Figure 4.16: Measured 2-D Radiation patterns of $E_{total}$ (a) $\theta - cuts$ for Ant-1 at $\phi = 154^o$ and Ant-2 at $\phi = 133^o$ (b) $\phi - cuts$ for Ant-1 and Ant-2 at $\theta = 90^o$ (c) $\theta - cuts$ for Ant-3 at $\phi = 26^o$ and Ant-4 at $\phi = 74^o$ (d) $\phi - cuts$ for Ant-3 and Ant-4 at $\theta = 90^o$.

The simulated maximum gain observed for the proposed MIMO antennas was 4.27 dBi.

The measured gain and efficiency of all 4-elements are shown in Figure 4.17 . The values of the gain and efficiency were found to be 3.1dBi and 70%, 2.7dBi and 70%, 3.45dBi and 70%, 3.5dBi and 70% for Ant-1 to Ant-4, respectively, at 2.168 GHz.

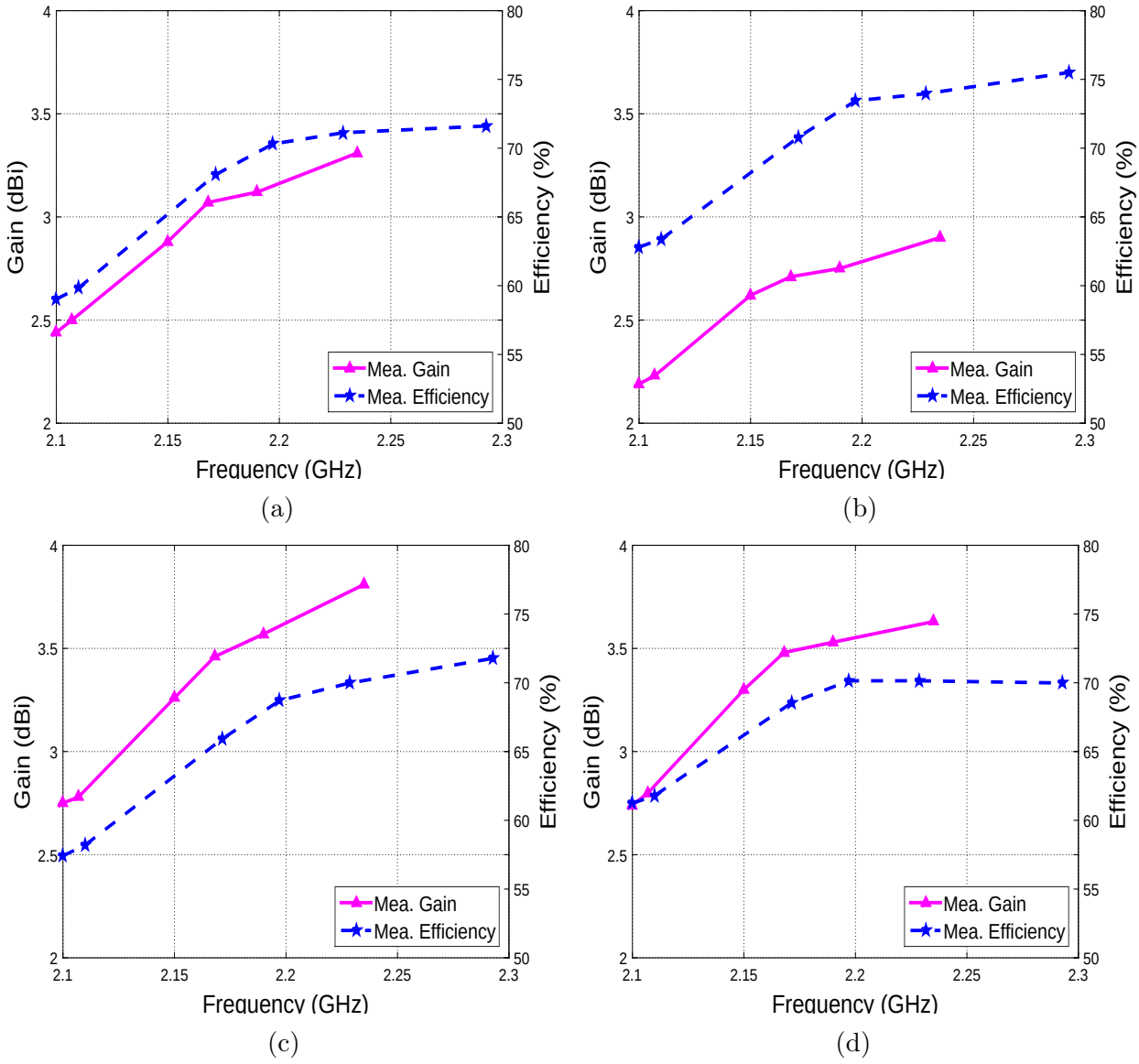


Figure 4.17: Measured gain and efficiency curves (a) Ant-1 (b) Ant-2 (c) Ant-3(d) Ant-4

The ECC values were computed based on the 3D radiation patterns using the equation in [2] with maximum values of 0.1889, 0.0132, 0.0045, between antenna elements (Ant-1, Ant-

2), (Ant-1, Ant-3), and (Ant-1, Ant-4), respectively, at 2.168 GHz. At other frequencies, values of ECC are given in Table 4.1, which shows that there is acceptable agreement between simulated and measured values of the ECC. All values are below 0.5 that shows that this proposed design can fulfill the requirements of a 4G MIMO system.

Table 4.1: Measured envelop correlation coefficient (ECC).

| Freq (GHz) | ECC12 | ECC13 | ECC14 | ECC24 |
|---|---|---|---|---|
| 2 | 0.1830 | 0.0515 | 0.0038 | 0.0134 |
| 2.1 | 0.1827 | 0.0100 | 0.0031 | 0.0138 |
| 2.107 | 0.1808 | 0.0038 | 0.0032 | 0.0230 |
| 2.168 | 0.1989 | 0.0132 | 0.0045 | 0.0314 |

## 4.3 6-Element Monopole based MIMO antenna System

Monopole antenna is also famous for mobile phones because of their compact size and easy fabrication. It consist of three main parts: 1) feed, 2) radiating element, 3) ground plane. Sometimes it needs matching structure to match with 50Ω. we use short circuit stub for matching. The geometry of single loop-shaped monople antenna is shown in Figure 4.18. This shape was chosen to minimize the size of the radiating part so that we can have more antenna elements.

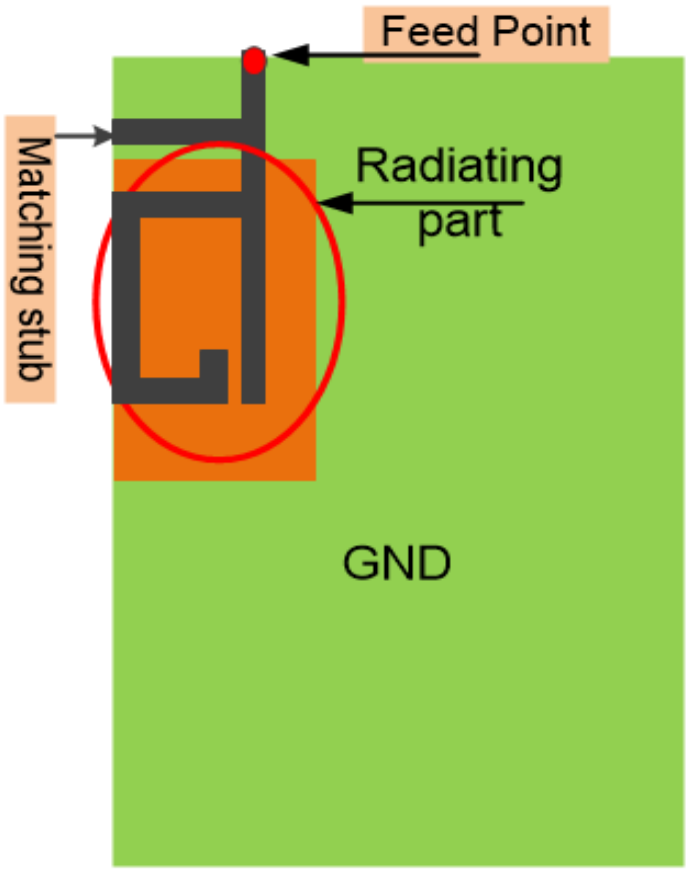


Figure 4.18: Geometry of loop shaped monopole Antenna.

The proposed modified-monopole 6-element MIMO antenna system geometry is shown in Figure 4.19. The dielectric constant ($\epsilon_r$) of the substrate used is 4.3 with height of 0.8mm. The overall board dimensions are 115×65 mm$^2$ with single antenna element dimensions of 11.1×9 mm$^2$. The length of the single antenna element is around $\lambda/4$ which is usually used for a monopole antenna. The matching of printed monopole with 50 ohm SMA connector was improved using short circuit stub as shown in Figure 4.19(a). Please notice that all the radiating elements are etched at top layer of substrate and Ground plane is in the bottom

layer.

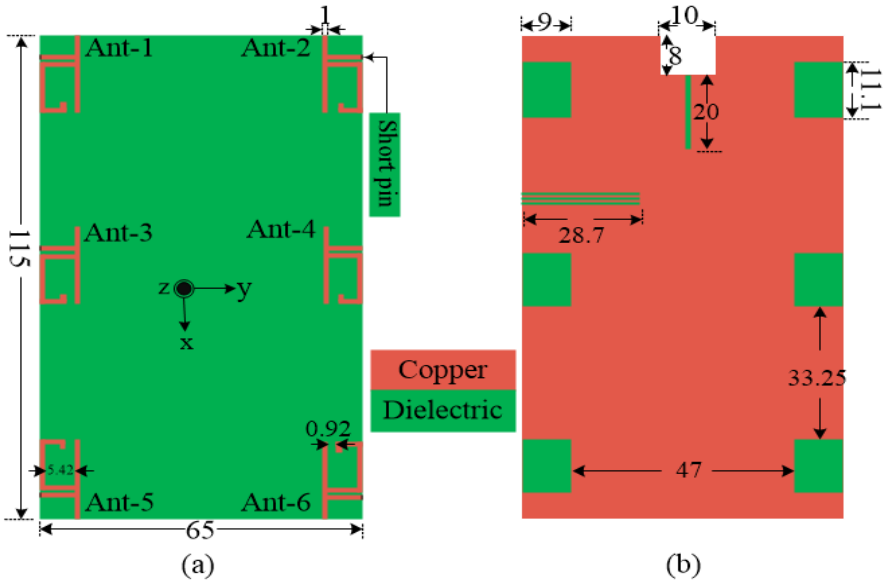


Figure 4.19: Propsed 6-element MIMO antenna system (a) Top view (b) Bottom view - All dimensions are in millimeter (mm).

All 6 elements are etched at the corners of the substrate to enhance the distance between them. The minimum spacing between the antennas is 34 mm which is less than $\lambda/2$. Due to sharing same ground plane and having small distance among them as compared to wavelength, there is low isolation among the different antennas which degrade the port efficiency of the MIMO system because some power can go to the adjacent antenna element.

To improve the isolation, a DGS is used in the ground plan which consists of a combination of 3 horizontal and one vertical slots. The size of horizontal slots is $28.7 \times 0.5$ mm$^2$ and spacing between them is 0.5 mm. The size of the vertical slot is 20 mm . These slots act like a band reject filter and improves isolation at the required band. A $8 \times 10$ mm$^2$ mm cut in the board also shown in the Figure 4.19. This cut is for the placement of the camera in the

mobile phones. The fabricated prototype of the proposed MIMO antenna system is shown in Figure 4.20. Figures 4.20(a) and 4.20(b) show the top and bottom view of the fabricated model, respectively.

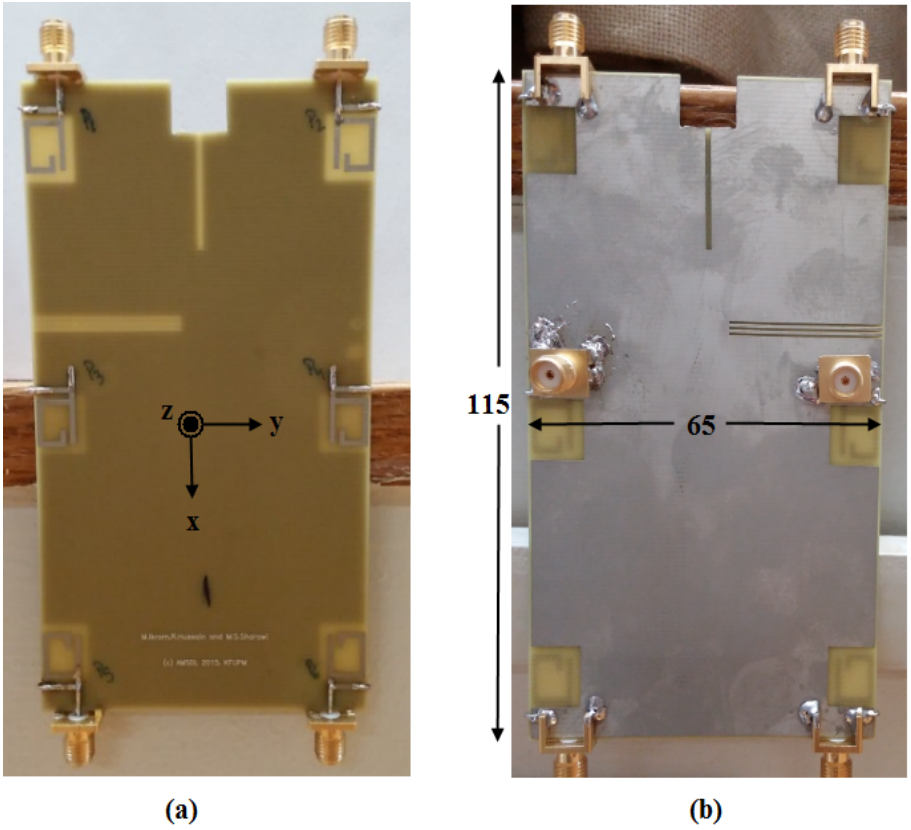


Figure 4.20: Proposed Fabricated model of MIMO antenna system (a) Top view (b) Bottom view - All dimensions are in millimeter (mm).

### 4.3.1 S-Parameters

The proposed MIMO antenna system was modeled and simulated using HFSS$^{TM}$. The S-parameters of the fabricated design were measured using an Agilent N9918A vector network analyzer. The radiation pattern and efficiency were measured using a SATIMO star lab

chamber at MVG-Italy. The measurement setup is shown in Figure 4.21.

The simulated reflection coefficient curves of the antenna without DGS are shown in Figure 4.22(a) while Figure 4.22(b) shows the measured reflection coefficient curves. All the resonance curves show that all the 6-elements of MIMO system were resonating at 2 GHz. The minimum -10 dB bandwidht achieved was 61 MHz from 1999 to 2060 MHz. Small shift in the band is due to fabrication tolerance. The simulated and measured results are in good agreement.

The simulated and measured isolation curves without DGS of the proposed MIMO antenna system are shown in Figures 4.23(a) and 4.23(b), respectively. The worst case simulated isolation value of 8 dB was observed between Ant-1 and Ant-2 without DGS.

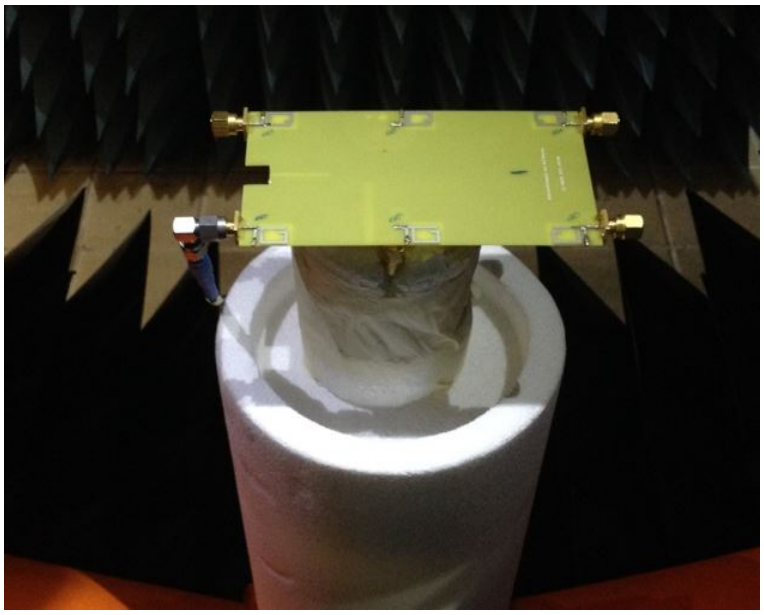

Figure 4.21: Measurement setup in a Satimo star Lab chamber.

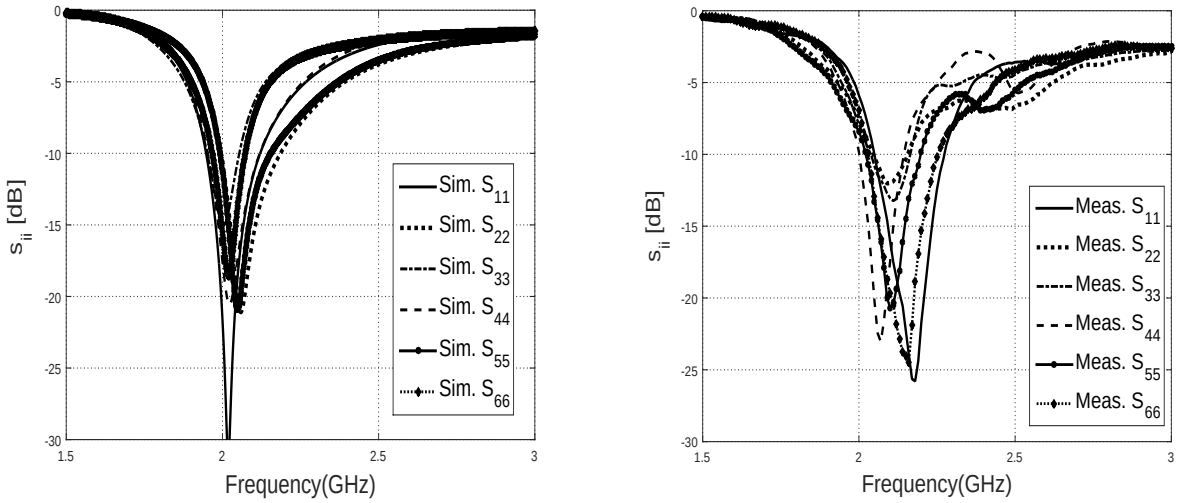


Figure 4.22: S-parameters curves (a) $|s_{ii}|$-Simulated without DGS (b) $|s_{ii}|$-Measured without DGS.

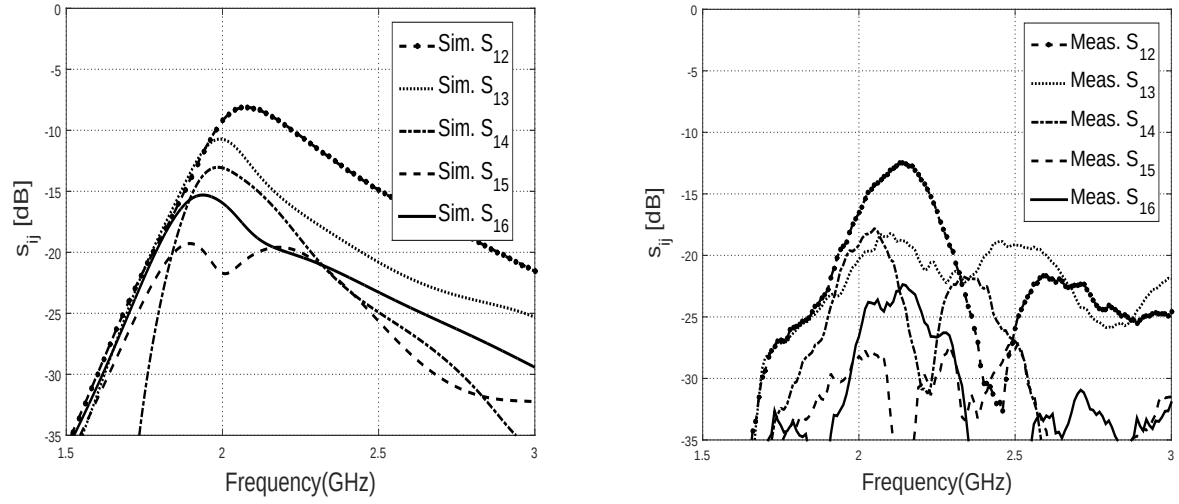


Figure 4.23: Isolation curves (a) $|s_{ij}|$-Simulated without DGS (b) $|s_{ij}|$-Measured without DGS.

The simulated reflection coefficient curves of the antenna with DGS are shown in Figure 4.24(a) while Figure 4.24(b) shows the measured reflection coefficient curves. All the reso-

nance curves show that all the 6-elements of MIMO system were resonating around 2 GHz. The isolation curves are shown in figures 4.25(a) and 4.25(b). By using DGS the worst case isolation was 14dB as shown in Figure 4.25(a). 6dB improvement is observed between Ant-1 and Ant-2 and also for the other antennas as well.

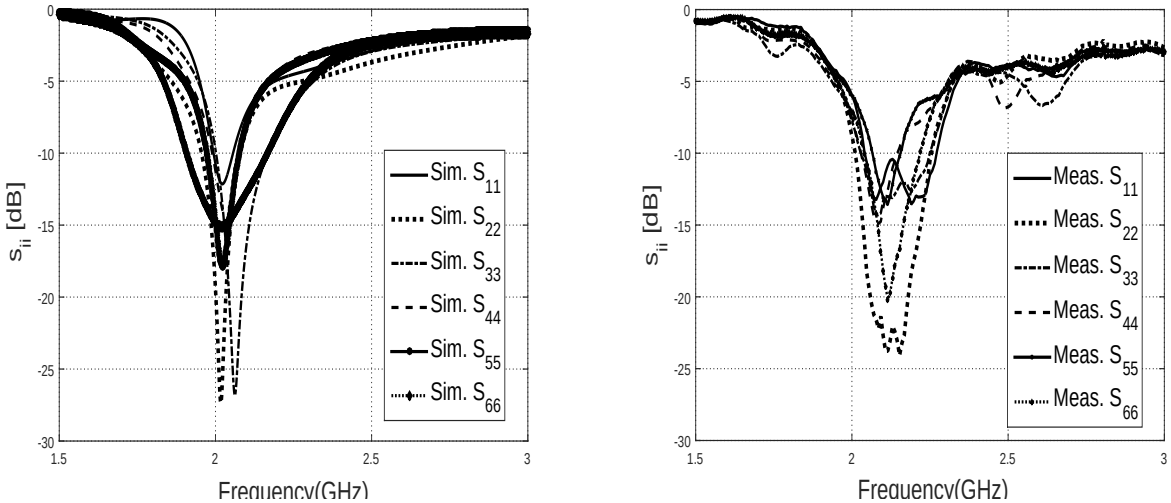


(a) (b)

Figure 4.24: S-parameters curves (a) $|s_{ii}|$-Simulated with DGS (b) $|s_{ii}|$-Measured with DGS.

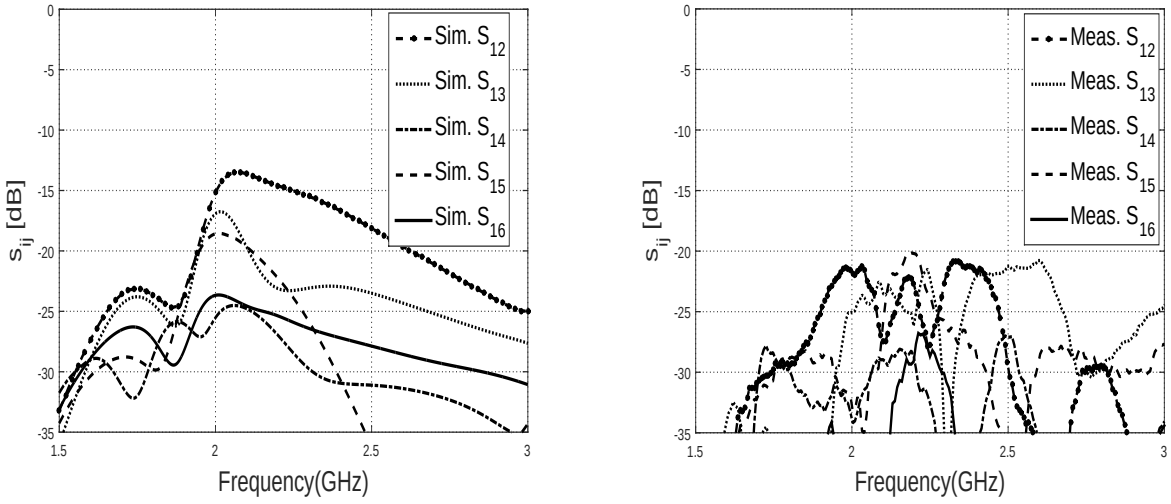


(a) (b)

Figure 4.25: Isolation curves (a) $|s_{ij}|$-Simulated with DGS (b) $|s_{ij}|$-Measured with DGS.

### 4.3.2 Current Distributions

The current distributions on the monopole MIMO antenna system are shown in Figure 4.26 at the center frequency of 2GHz. Without a DGS, It can be seen that when Ant-1 is excited and other are terminated with matched load, a high current is coupled through the adjacent ports due to sharing same ground plane as shown in Figure 4.26(a). Also, same result is observed in Figures 4.26(b) and 4.26(c) when Ant-2 and Ant-6 are activated at 2GHz, respectively. After applying a DGS, current is trapped and minimized through ground slots. A significant change is observed at Ant-2, Ant-3 and Ant-5 (Figure 4.26(d)) when Ant-1 is activated. Since, DGS have been applied between Ant-1-Ant-2 and Ant-1-Ant-3, a major improvement in isolation is achieved among those elements only. However, there was some minor improvement observed among other elements as shown in Figure 4.26(e) when Ant-2 is activated and others are terminated with matched load.

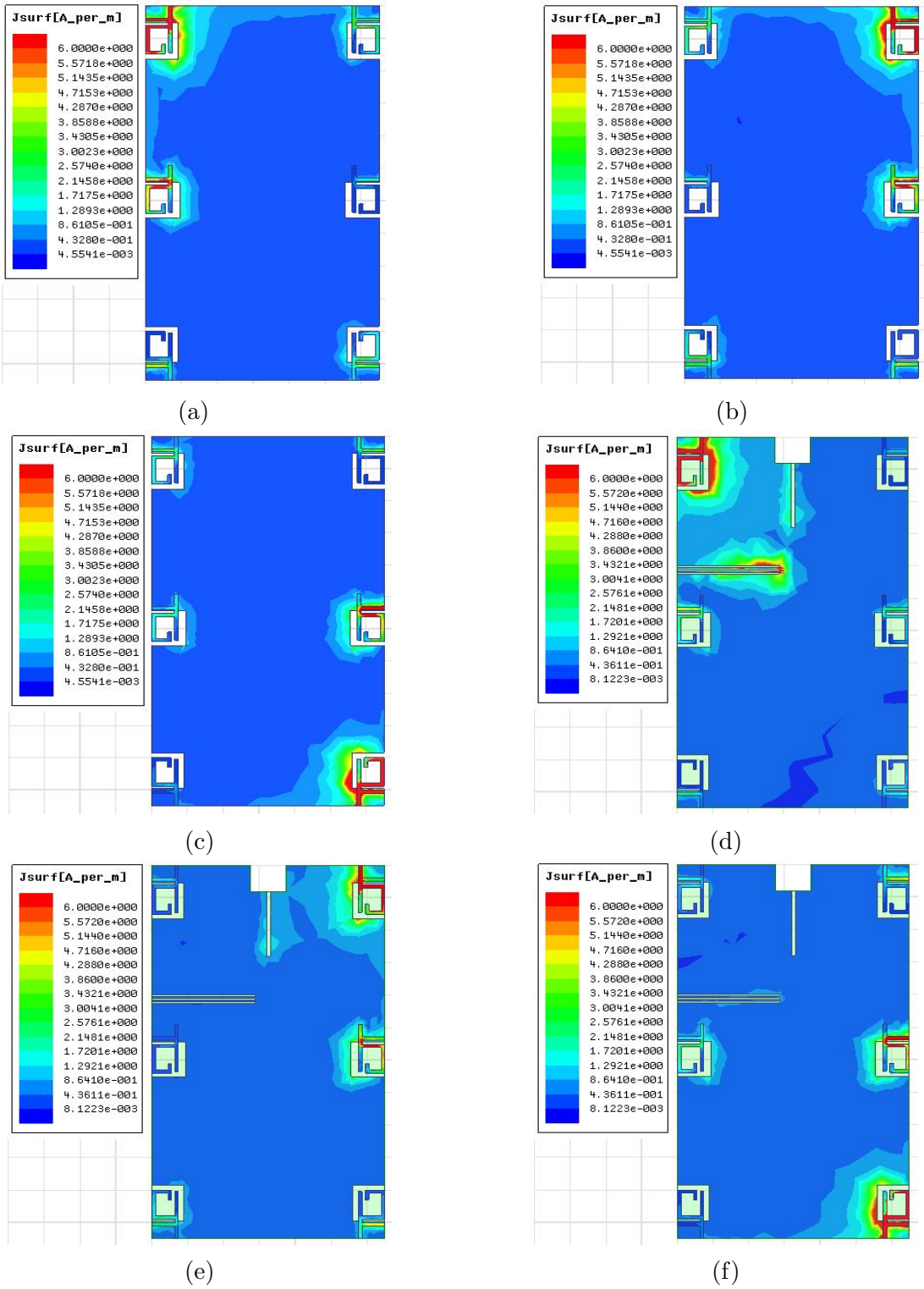


Figure 4.26: Current distribution on proposed 6 element monopole MIMO antenna at 2GHz (a) P1 is activated Without DGS (b) P2 is activated without DGS (c) P6 is activated without DGS (d) P1 is activated with DGS (e) P2 is activated with DGS (f) P6 is activated with DGS.

### 4.3.3 Radiation Patterns

The normalized measured radiation patterns in terms of Etotal at 2070 MHz are illustrated in Figure 4.27 for the x-z and x-y planes (referred to Figure 4.19). The maximum values of Etotal for Ant-1 to Ant-6 are 3.56 dB at ($\theta = 174^o$ and $\phi = 10^o$), 3.54dB at ($\theta = 116^o$, $\phi = 110^o$), 3.78dB at ($\theta = -164^o$, $\phi = 166^o$), 3.14dB at ($\theta = 162^o$, $\phi = 4^o$), 3.37dB at ($\theta = -172^o$, $\phi = 4^o$), 3.37dB at ($\theta = 130^o$, $\phi = 78^o$), respectively. In Figures 4.27(a), 4.27(c) and 4.27(e), 2-D $\theta - cuts$ are ploted for maximum value of each antenna at their respective $\phi$. In 4.27(b), 4.27(d) and 4.27(f), 2-D $\phi - cuts$ at $\theta = 90^o$ for all antennas are shown. It can be seen from the patterns that the measured patterns are tilted in the x-z and x-y planes which will lead to low correlation between the MIMO channels.

The simulated maximum gains observed for the proposed MIMO antenna system were 3.8 dBi, 3.3 dBi, 3.67 dBi, 3.67 dBi, 3.32 dBi and 2.52 for Ant-1-Ant-6, respectively at 2070 MHz. The measured gain and efficiency of all 6-elements are shown in Figure 4.28. The value of the maximum gain and efficiency were found to be 3.6 dB and 72%, 3.55 dB and 62%, 3.78 dB and 55%, 3.2 dB and 55%, 3.4 and 58% and 2.2 and 56% for Ant-1 to Ant-6, respectively, at 2070 MHz. Good agreement is observed.

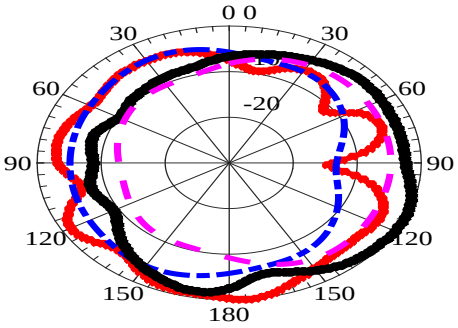


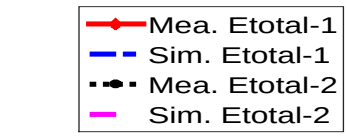


(a)

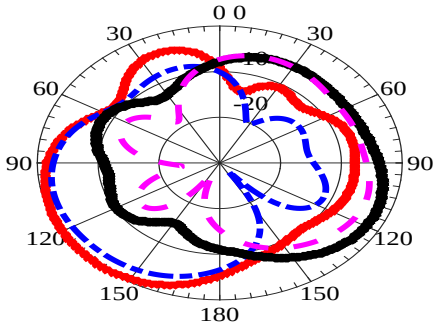


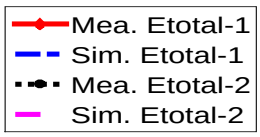


(b)

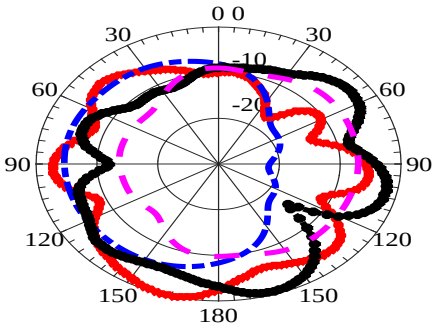


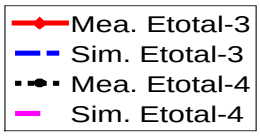


(c)

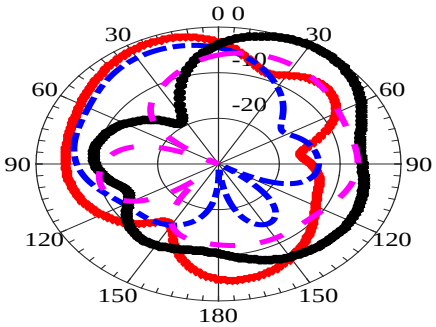


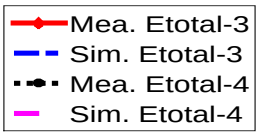


(d)

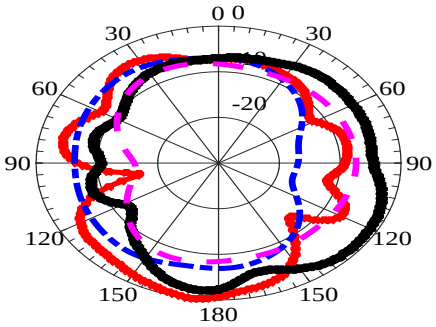


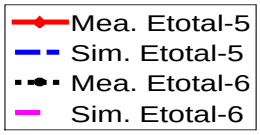


(e)

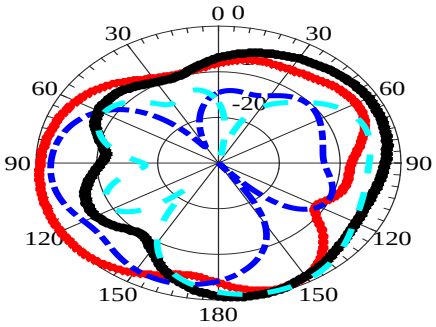


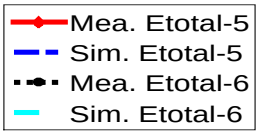


(f)

Figure 4.27: Measured and simulated 2-D radiation patterns (a) $(\theta - cuts)$ Ant-1 at $\phi = 10^o$ and Ant-2 at $\phi = 110^o$ (b) $(\phi - cuts)$ Ant-1 and Ant-2 at $\theta = 90^o$ (c) $(\theta - cuts)$ Ant-3 at $\phi = 166$ and Ant-4 at $\phi = 4$ (d) $(\phi - cuts)$ Ant-3 and Ant-4 at $\theta = 90^o$ (e) $(\theta - cuts)$ Ant-5 at $\phi = 4$ and Ant-6 $\phi = 78$ (f) $(\phi - cuts)$ Ant-5 and Ant-6 at $\theta = 90^o$.

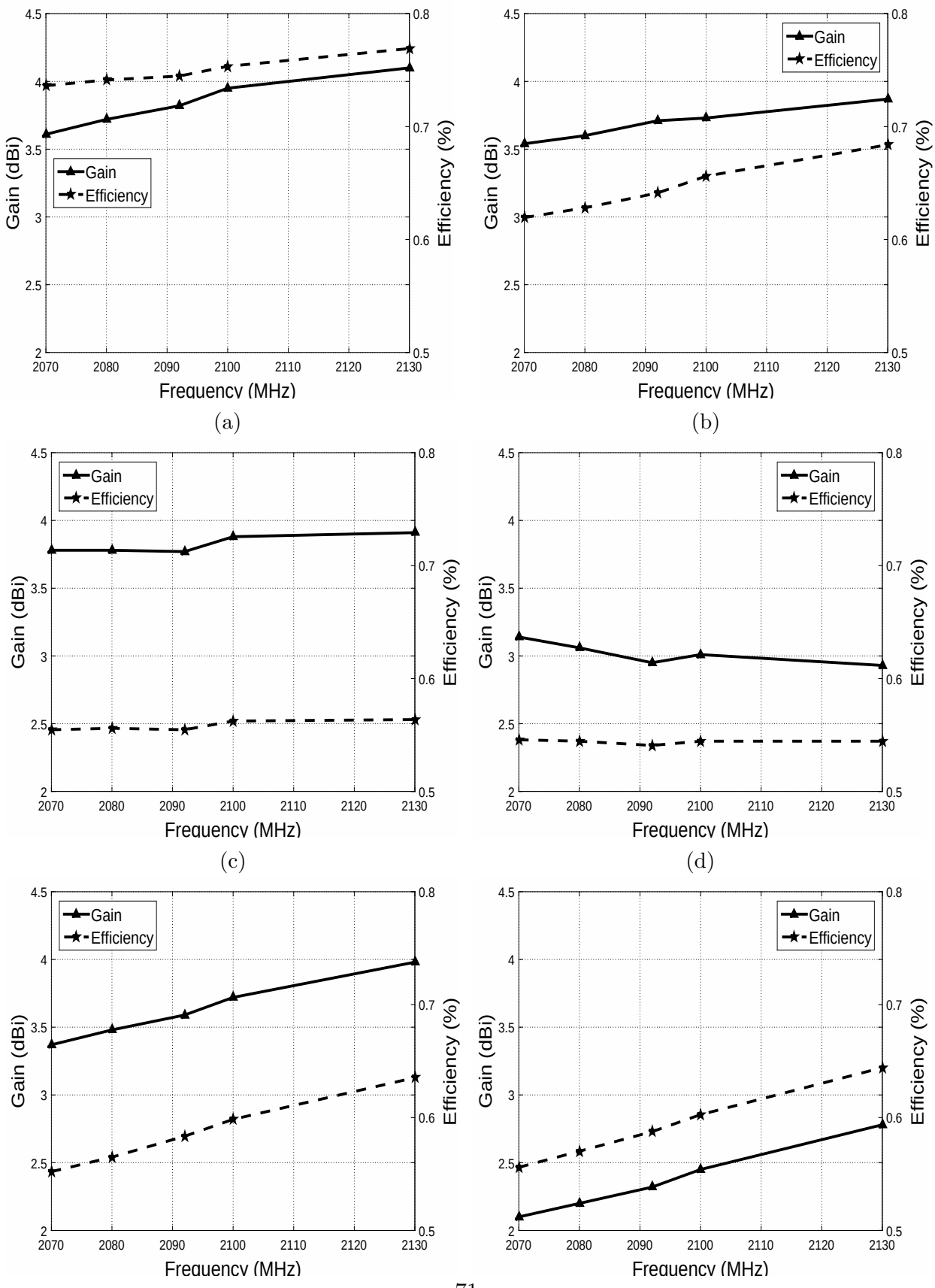




Figure 4.28: Measured gain and efficiency (a) Ant-1 (b) Ant-2 (c) Ant-3 (d) Ant-4 (e) Ant-5 (f) Ant-6.

### 4.3.4 Envelope Correlation coefficient (ECC) Values

The envelop correlation coefficient (ECC) values were computed based on the 3D measured patterns in an isotropic environment using the Eq. in [2] with maximum values of 0.2092, 0.0849, 0.0432, 0.0189 and 0.0091 between antenna elements (Ant-1, Ant-2), (Ant-1, Ant-3), (Ant-1, Ant-4), (Ant-1, Ant-5) and (Ant-1, Ant-6), respectively, at 2070 MHz. At other frequencies the values of ECC are given in Table 4.2 which shows that they are acceptable measured values. All values are below 0.5 showing that this proposed design can fulfill the requirements of a 4G MIMO antenna system.

Table 4.2: Measured envelop correlation coefficient (ECC)

| Freq (GHz) | ECC12 | ECC13 | ECC14 | ECC15 | ECC16 |
|---|---|---|---|---|---|
| 2.07 | 0.2092 | 0.0849 | 0.0432 | 0.0189 | 0.0091 |
| 2.08 | 0.2096 | 0.0876 | 0.0430 | 0.0179 | 0.0092 |
| 2.1 | 0.2103 | 0.0933 | 0.0419 | 0.0165 | 0.0094 |
| 2.13 | 0.2049 | 0.0995 | 0.0383 | 0.0135 | 0.0099 |

### 4.3.5 Summary

This chapter covered the design of three 4G MIMO antenna systems with 4 and 6 antenna element configurations. Moreover, a defected ground structure (DGS) was used to improve the isolation between various antenna elements of the MIMO antenna system. The simulated and measured results were compared and good agreement was observed. A PIFA based

MIMO antenna system provided 4 dBi gain at 2.1 GHz with improved isolation whereas 4-element monopole based MIMO system provided 3 dBi gain and 70% efficiency. Finally, a 6-element MIMO antenna system gave 3 dBi gain and 55% efficiency at 2 GHz with improved isolation. A comparison is shown in the Table 4.3 for aforementioned three 4G MIMO designs.

Table 4.3: Comparison between proposed 4G designs.

| Ant type | No. of Ants. | Freq(GHz) | board size(mm) | Min. Isolation | BW (MHz) | Effi (%) | Gain (dBi) |
|---|---|---|---|---|---|---|---|
| PIFA | 4 | 2.072-2.210 | 60×100×0.8 | 15 | 138 | 75 | 4 |
| Monopole | 4 | 1.997-2.190 | 60×100×0.8 | 15 | 193 | 70 | 3 |
| Monopole | 6 | 1.999-2.060 | 65×115×0.8 | 15 | 61 | 55 | 2.5 |

# CHAPTER 5

# 4G/5G INTEGRATED ANTENNA SYSTEMS WITH CONNECTED ANTENNA ARRAYS

In this chapter, we will discuss the L-shaped MIMO antenna system along with connected antenna array (CAA) to prove the concept that CAA can be used as a radiator and an isolation enhancement structure. Subsequently, we will design the new MIMO antenna system with 4 PIFA elements along with the CAA. This CAA will be used for dual functions, as a radiator for 5G band and an isolation enhancement structure for 4G band. Finally, comparison of the results will be discussed based on simulations and measurements.

## 5.1 L-shaped Monopole with Connected antenna array

The proposed modified monopole based MIMO antenna system geometry is shown in Figure 5.1. The proposed MIMO antenna system consists of 4 antenna elements. All the radiating elements were short circuited with the GND plane using metallic plate to resonate at the lower frequency band. The dielectric constant ($\epsilon_r$) of the substrate used was 4.3 with height 0.8mm. The overall board dimensions were $100\times60\times0.8$ mm$^3$ with single element dimensions of $23\times$ 9 mm$^2$. The length of the single antenna element was around $\lambda/4$.

All antennas were etched on the top 4 corners of the substrate as shown in Figure 5.1(a) while GND plane is on bottom side. A deflected GND structure (DGS) was used to improve the isolation as shown in Figure 5.1(b). The DGS consisted of GND slots and a ring. The size of a single slot was $35\times1.5$ mm$^2$ with 3 mm spacing between adjacent slots. At the resonance frequency, the slots and ground ring were a part of radiating structure and were acting like a band reject filter and hence improved the isolation.

Another feature of GND slots was to act as CAA. This CAA was periodically fed through 50 ohm microstrip line on the top layer as shown Figure 5.1(a). Only two feeding lines are introduced to apply the concept. It is resonating at 4 GHz. We can increase the frequency by increasing the feeding lines. CAA frequency depends on spacing between feeding lines. If we increase the number of feeding lines it will decrease spacing between feed lines and ultimately shift the frequency at higher bands.

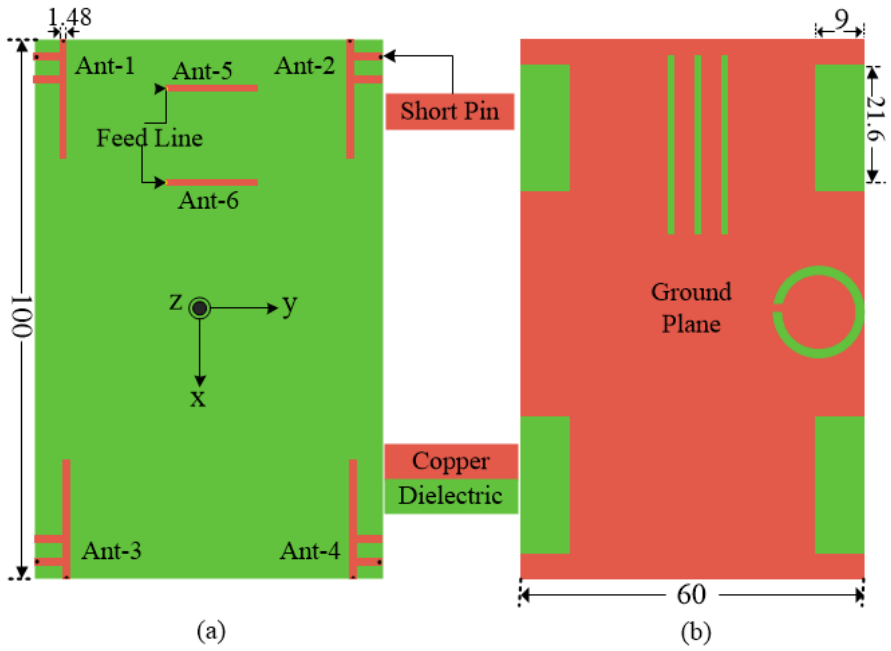


Figure 5.1: Integrated MIMO antenna system (a) Top view (b) Bottom view - All dimensions are in millimeter (mm).

### 5.1.1 S-parameters

The proposed MIMO antenna system is modeled and simulated using HFSS$^{TM}$. The simulated reflection coefficients of PCA are shown in Figure 5.2(a). The $3 \times 2$ CAA is resonating at center frequency of 4090 MHz. The -10dB bandwidth was 240 MHz from 3990 to 4230 MHz. Simulated isolation curves are shown in Figure 5.2(b), showing good isolation between MIMO antennas and CAA. The worse case isolation observed was -27dB. The simulated and measured reflection coefficient and isolation curves for the 4G MIMO antennas were the same as Figure 4.13 and Figure 4.14 which shows the dual function of ground slots. They are acting like a band reject filter as well as CAA.

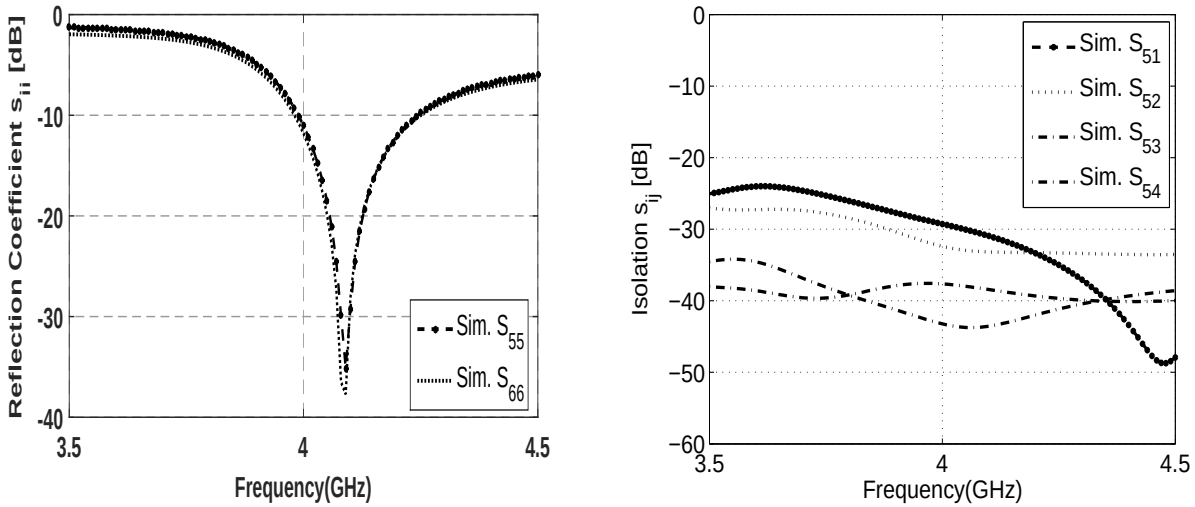


(a) (b)

Figure 5.2: S-parameters curves (a) $|s_{ii}|$-Simulated (only for CAA) with DGS (b) $|s_{ij}|$-Simulated with DGS.

### 5.1.2 Current Distributions

The current distributions on the monopole MIMO system are shown in Figure 5.3(a) and 5.3(b) at 2.1 GHz frequency. Without DGS, It can be seen that when Ant-1 is excited and others are terminated with matched load. A high current is coupled through the adjacent ports due to sharing same ground plane. When we apply a DGS and make it as CAA, the current is trapped and minimized through ground slots. A significant change is observed between Ant-2 and Ant-3 (Figure 5.3(b)). The current distribution at 4 GHz are shown in Figure 5.4 which shows that at 4 GHz only CAA will resonate and no coupling current on MIMO antennas.

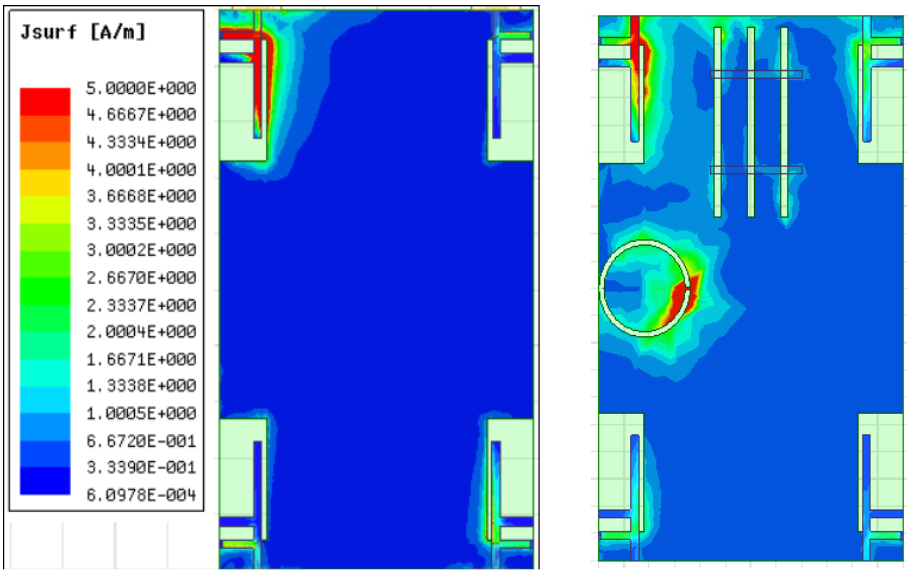


Figure 5.3: Current distributions on proposed MIMO antenna (a) Without DGS (b) With DGS and CAA at 2.1 GHz.

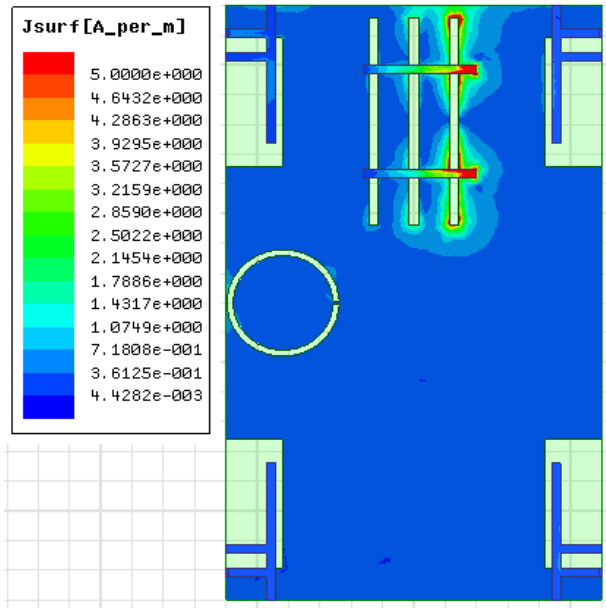


Figure 5.4: Current distributions on CAA at 4GHz.

### 5.1.3 Radiation Patterns

The maximum gain observed for 4G MIMO antennas was 4.27 dBi as shown in Figures 5.5(a), 5.5(b) and 5.5(c) are the gain patterns for Ant-1, Ant-2 and Ant-3. Figure 5.5(d) shows the maximum gain of the CAA equal to be 5.42 dBi. The envelop correlation coefficient ($\rho_e$) values are computed based on the radiation patterns and are 0.0498, 0.0356, 0.0759, between antenna elements (Ant-1, Ant-2), (Ant-1, Ant-3) and (Ant-1, Ant-4), respectively. The $\rho_e$ values show good MIMO performance.

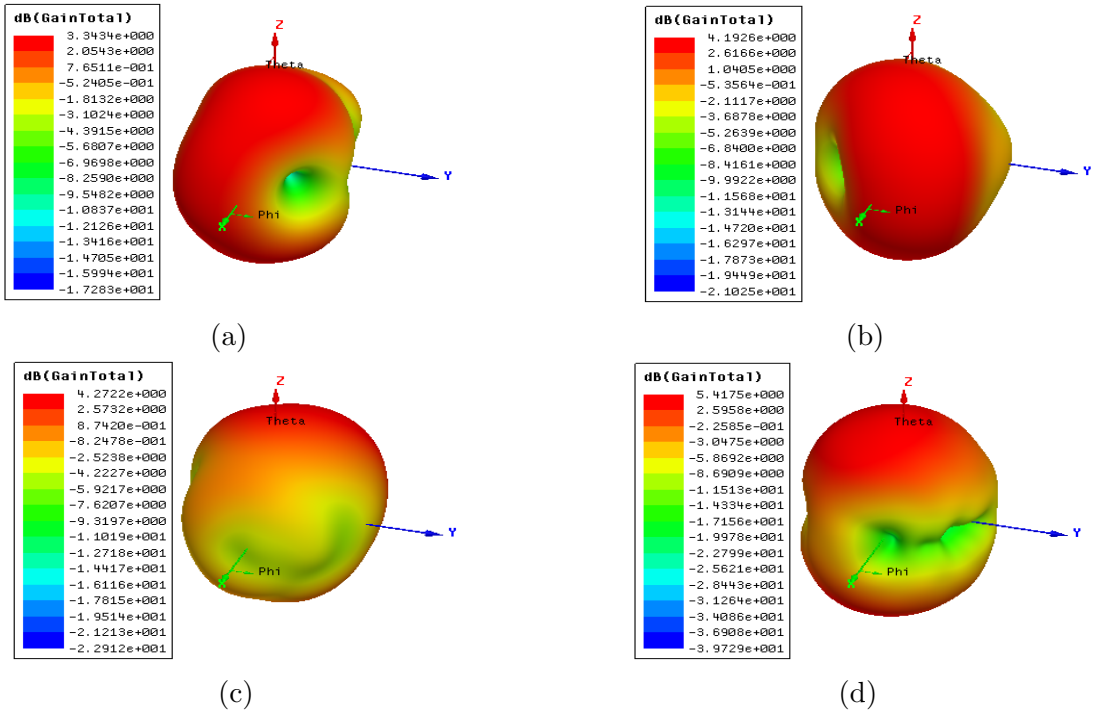


Figure 5.5: Simulated 3-D gain patterns (a) Ant-1 (b) Ant-2(c) Ant-3 at 2.1 GHz (d) CAA at 4 GHz.

## 5.2 A 4G/5G Antenna System with Dual Function Connected Antenna Array (CAA)

In this work, an integrated design of PIFA based MIMO antenna system for 4G bands with a planar CAA for potential 5G bands is presented. The unique feature of the proposed design is in its planar structure (fabricated on a two layer PCB), low profile, compact and accommodating 4-elements along with a CAA in an area of a typical smart phone backplane size. Moreover, the proposed design is the first to present a dual function slot array that behaves as a defected ground structure (DGS) for isolation enhancement within the MIMO antenna system band at 2.1 GHz and as a radiator (CAA) for 5G applications at 12.5 GHz. The integrated antenna system is analyzed and good agreement between simulation and measured results is achieved.

### 5.2.1 Design of the integrated 4G/5G antenna system

The geometry of the proposed modified PIFA based 4-element MIMO antenna system with the CAA is shown in Figure 5.6. It is modeled and simulated using HFSS$^{TM}$ 2015. An RO4350 material is used as a substrate. The dielectric constant ($\epsilon_r$) of the substrate used is 3.5 with the height of 0.76mm. The overall board dimensions are $100\times60\times0.76$ mm$^3$.

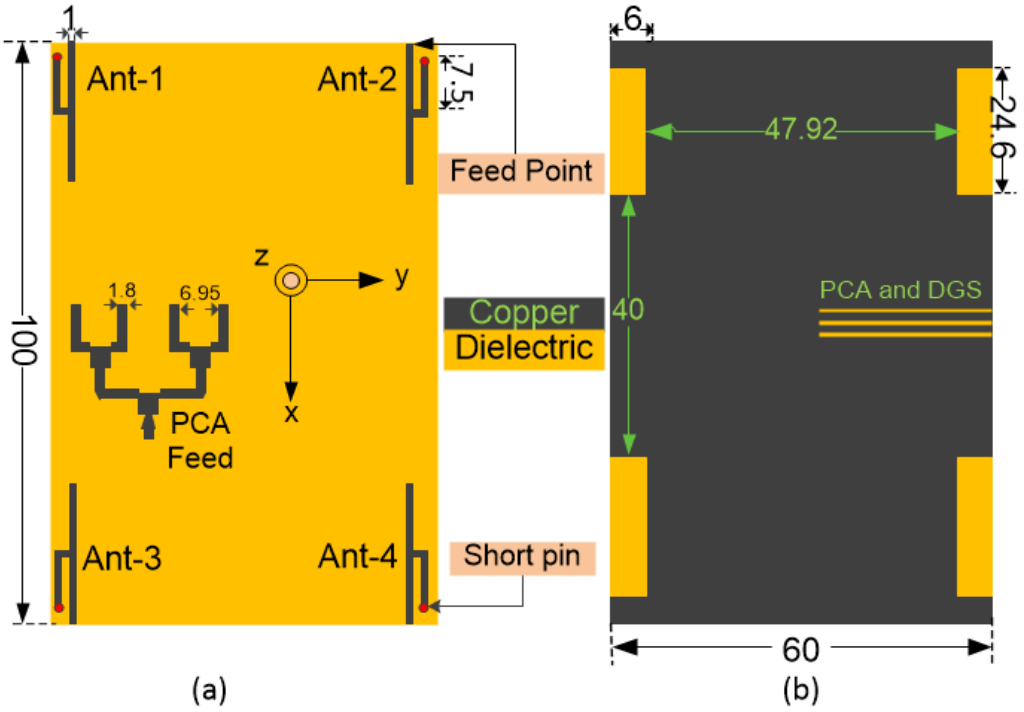


Figure 5.6: Proposed integrated design (a) Top view (b) Bottom view - All dimensions are in millimeters (mm).

### 5.2.2 MIMO Antenna System

As shown in Figure 5.6(a), all the 4G MIMO antenna elements (Ant-1-Ant-4) are etched on the 4 corners of the top side of the substrate while the GND plane is on the bottom side (Figure 5.6(b)). They are short circuited with the GND plane using shorting pins. Their geometry is chosen to occupy a small area. The size of the single antenna element is 27×6 $mm^2$ which is around $\lambda/4$ at 2.1 GHz. The spacing between Ant-1 and Ant-2 is 47.92mm while between Ant-1 and Ant-3 is 40mm. This spacing is less than $\lambda/2$ which yields low isolation between them.

### 5.2.3 DGS and CAA

To improve MIMO port efficiency, isolation enhancement via a DGS is used. Slots in the GND plane are used as a DGS. These slots are optimized by their length and number to enhance the isolation at 2.1GHz. The best results were obtained using 3 slots. The size of each slot was $35\times0.5$ mm$^2$ and the spacing between them was 0.5mm. The DGS was placed between Ant-1 and Ant-3 due to the low isolation between them.

After the study of the isolation enhancement on the MIMO antenna system, the concept of CAA is applied. A 1-to-4 line feed network (power combiner/divider) is designed on the top layer of the substrate to excite the slots and make them radiate at 12.5 GHz as shown in Figure 5.6(a) with detailed geometry in Figure 5.7. The feeding network is optimized to provide constant phase and equal magnitude at its four output ports (F1-F4). The magnitude and phase curves of the transmission coefficient between F5 (PCA input) to F1-F4 (Figure 5.7) are shown in Figure 5.8(a) and Figure 5.8(b), respectively. Note that there is less than 1dB amplitude difference between inner and outer branches at 12.5 GHz due to slight path length differences. The phases are almost same.

The effect of spacing on the frequency is shown in Table 5.1 which shows that 5G frequency can be tuned to any desired frequency by changing spacing between feed lines. We compare two designs monopole and PIFA. In monopole case, we used 2 feed lines as discussed in previous section and it covered lower frequency band of 4 GHz. But for the PIFA one we used 4 feeding lines to reduce spacing between feed lines so that we can have higher frequency band of 12.5 GHz

Table 5.1: Comparison of 4G/5G integrated designs based on spacing between feed lines of 5G bands.

| Ant. type | Spacing b/w Feeds | Spacing in $\lambda$ | Freq(GHz) |
|---|---|---|---|
| Monopole | 17.5mm | 0.24 | 4.2 |
| PIFA | 6.95mm | 0.28 | 12.5 |

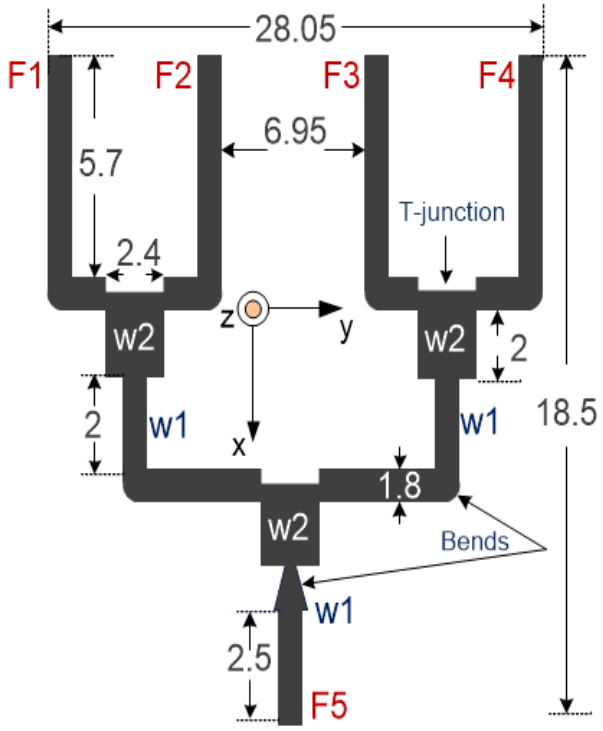


Figure 5.7: Feed network geometry of CAA. All dimensions are in mm.

The widths of F1-F5 and $w1$ microstrip-lines are 1.8mm to give 50 Ω lines while $w2$ ones are set to 2.4mm to provide 35 Ω, $\lambda/4$ transformers. These transformers are used to convert 25 Ω to 50 Ω. The location of the feeding network is also optimized along the slots (y-axis)

to match for 50 Ω on the PCA as well as to maintain isolation improvement. To excite the slots periodically, the F1-F4 feeding lines are equally spaced (6.95mm which is around $\lambda/4$ at 12.5 GHz) from each other to make them excite the slots as a CAA, as discussed in [11]. Transmission matching techniques (bends and T junctions) are applied in the feeding network to improve the matching.

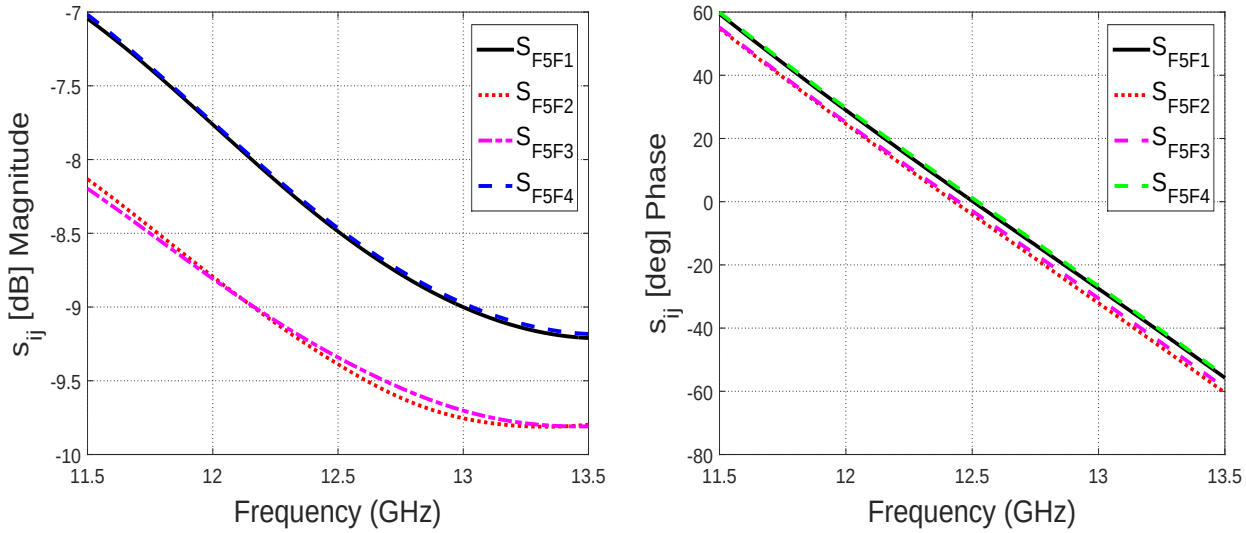


(a) (b)

Figure 5.8: Transmission coefficient curves of the PCA feed network alone (a) $|s_{ij}|$-Simulated magnitude (b) $|s_{ij}|$-Simulated phase.

The current distributions of the proposed design are shown in Figure 5.9. When P1 (Ant-1 of the MIMO antenna system) is excited and others are terminated with matched loads, a noticeable coupling current can be seen on P2 and P3, indicating low isolation. After applying the DGS (or CAA), a noticeable improvement in the coupling current is observed at P2 and P3 at 2.1 GHz, showing improved isolation (Figure 5.9(b)). The DGS is thus minimizing the currents on the ground. Isolation is also improved between P2 and P4 when P2 is excited as shown in Figure 5.9(c) due to the presence of the DGS, as it affects the

current distribution slightly between them. This slight improvement is not as much as that between P1 and P3, because the DGS is placed directly between them. It should be noted that our goal is to improve isolation among all elements as much as possible via the dual functionality of the DGS acting as a CAA. If higher frequency bands are required for the 5G CAA, two of them can be easily placed between the 4-MIMO antennas. This DGS is thus minimizing the coupling currents on the ground. A current distribution is shown in Figure 5.9(d) for the CAA at 12.5 GHz when P5 is activated and others are terminated with match loads. It is showing very low coupling currents between the MIMO system and the CAA.

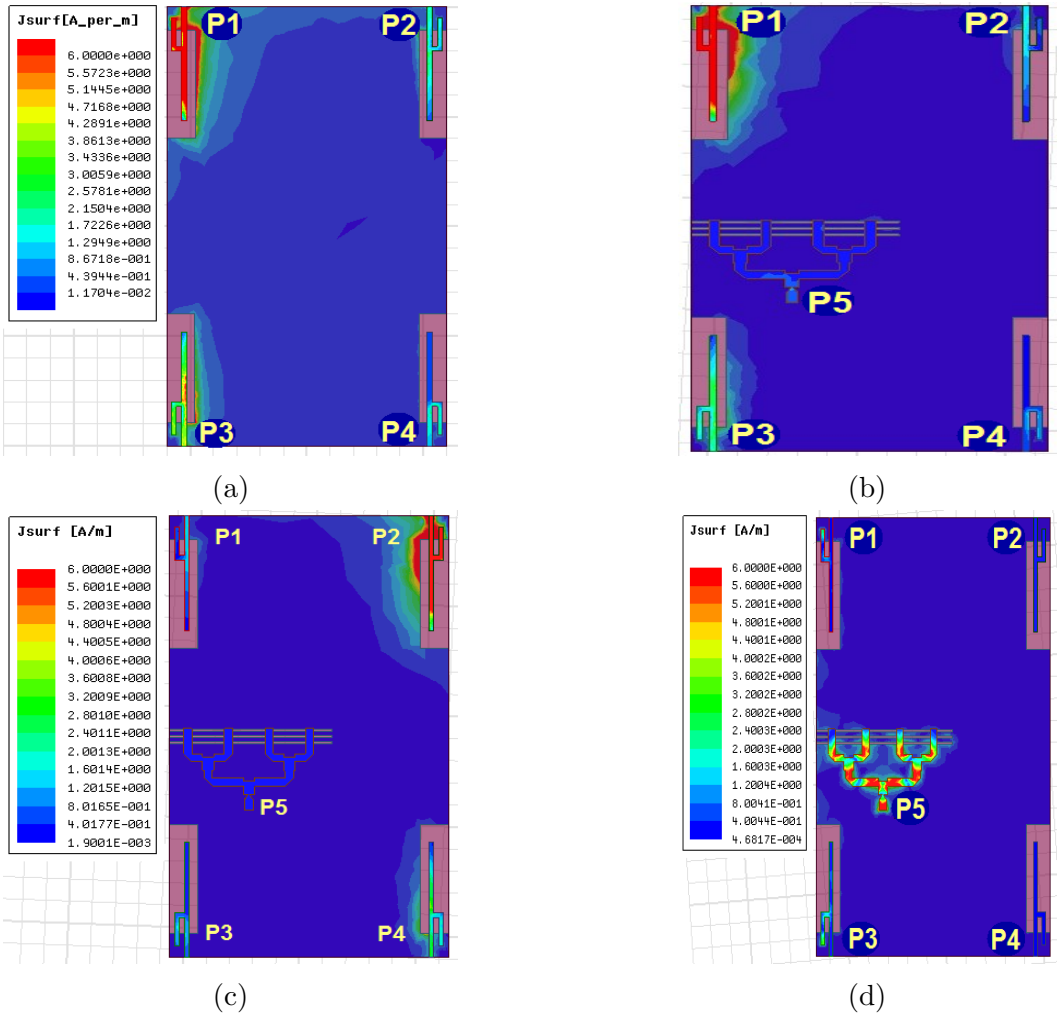


Figure 5.9: Current distributions on the proposed 4G/5G integrated design (a) P1 of MIMO antenna system at 2.1 GHz is activated (b) P1 of MIMO antenna system is activated with a CAA at 2.1 GHz (d) P2 of MIMO antenna system is activated with a CAA at 2.1 GHz (e) CAA (P5) is activated at 12.5 GHz.

### 5.2.4 Port Parameters

The fabricated prototype was made using an LPKF S103 milling machine at AMSDL at KFUPM. The S-parameters of the fabricated design were measured using an Agilent N9918A vector network analyzer. The radiation patterns and efficiency were measured using a

SATIMO star-lab chamber at MVG-Italy. The radiation pattern measurement setup is shown in Figure 5.10. The fabricated model without and with the CAA are shown in Figure 5.11 and Figure 5.12, respectively.

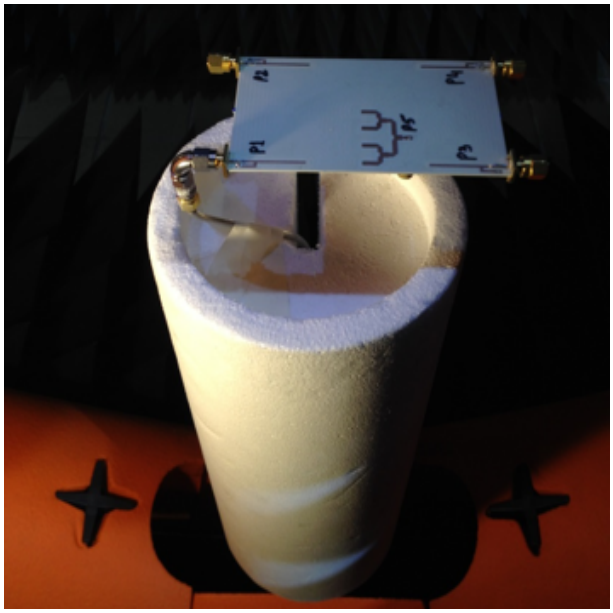

Figure 5.10: The Proposed 4G/5G Integrated antenna design in the measurement setup in a Satimo star Lab.

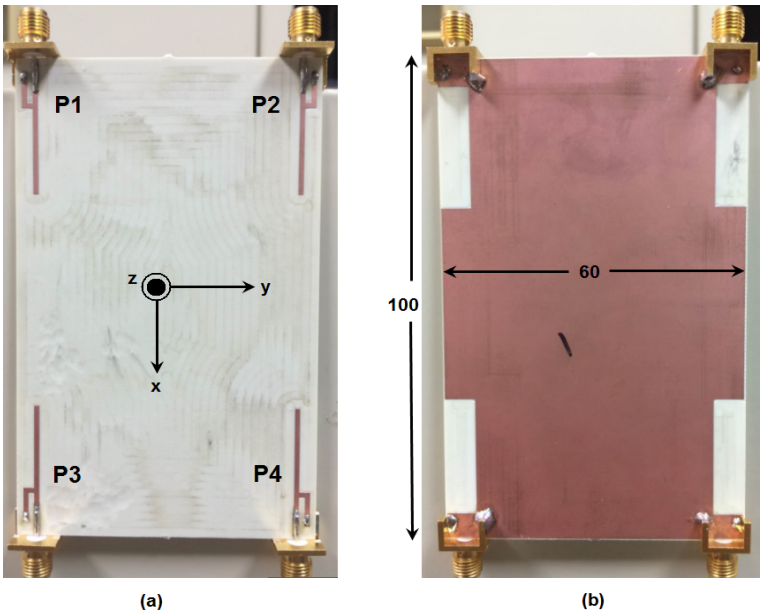


Figure 5.11: Fabricated model of the MIMO antenna system without CAA (a) Top view (b) Bottom view - All dimensions are in millimeters (mm).

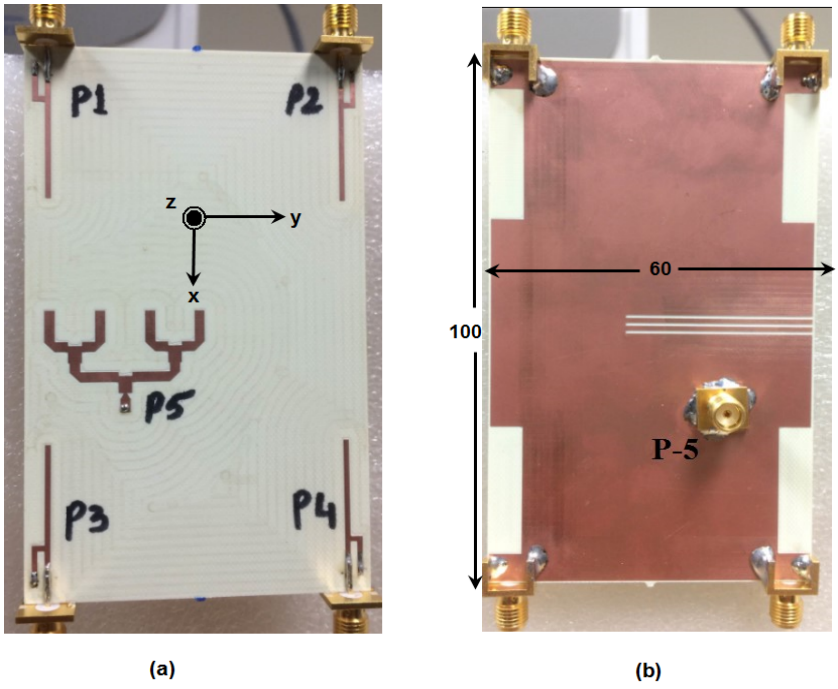


Figure 5.12: Fabricated model of the integrated 4G/5G antenna design (a) Top view (b) Bottom view - All dimensions are in millimeters (mm).

The simulated reflection coefficient curves of the antenna without CAA are shown in Figure 5.13(a) while Figure 5.13(b) shows the measured reflection coefficient curves. All the resonance curves show that the 4-elements of the MIMO antenna system are resonating at 2.1 GHz. The measured minimum -10 dB bandwidth was 217 MHz from 2040 to 2257 MHz. The simulated and measured isolation curves without the CAA of the proposed MIMO antenna system are shown in Figure 5.13(c) and Figure 5.13(d), respectively. The worst case simulated isolation value of 9.5 dB was observed between Ant-1 (P1) and Ant-3 (P3) while it was 13 dB between Ant-1 (P1) and Ant-2 (P2).

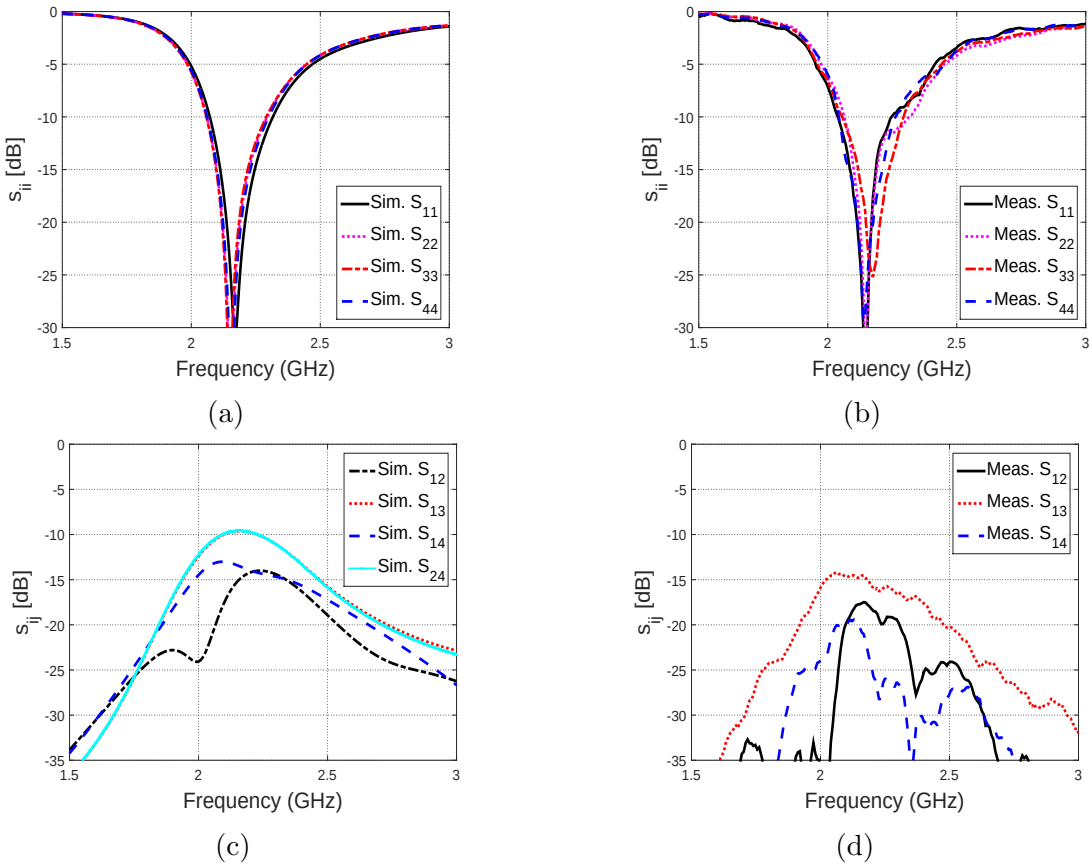


Figure 5.13: S-parameters curves without DGS (a) $|s_{ii}|$-Simulated (b) $|s_{ii}|$-Measured (c) $|s_{ij}|$-Simulated (d) $|s_{ij}|$-Measured, {simulated (sim.), measured(meas.)}.

The simulated reflection coefficient curves of the integrated antenna design are shown in Figure 5.14(a) while Figure 5.14(b) shows the measured reflection coefficient curves. The simulated and measured isolation curves of the proposed integrated design are shown in Figures 5.14(c) and 5.14(d), respectively. The measured bandwidth covered was 205 MHz from 2058 to 2263 MHz. The worst case simulated isolation value of 13.5 dB was observed between Ant-1 (P1) and Ant-3 (P3) while it was 17 dB between Ant-1 (P1) and Ant-2 (P2). A 4dB extra isolation was achieved using the DGS (PCA). The improvement in isolation can also be observed in the measured curves in Figure 5.13(d) and Figure 5.14(d).

The simulated and measured reflection coefficients of the CAA are shown in Figure 5.15(a). The resonance curves show that the CAA is resonating at 12.5 GHz. The measured minimum -10dB bandwidht achieved was 580 MHz from 12.17 to 12.75 GHz. A good agreement between simulated and measured results is observed. The measured isolation curves between the CAA and MIMO antenna system are shown in Figure 5.15(b) showing high isolation (more than 16dB) between them.

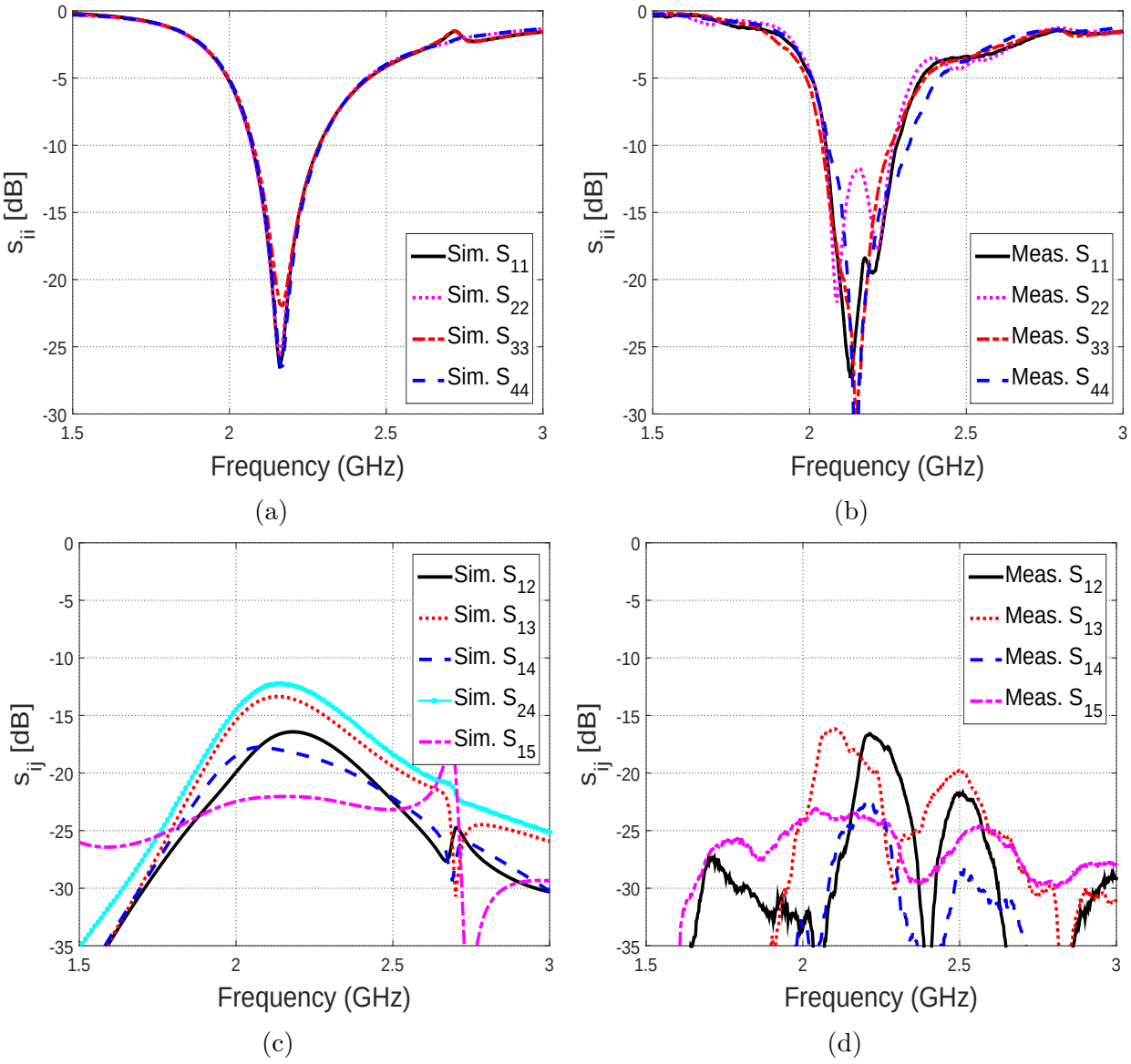


Figure 5.14: S-parameters curves of the integrated 4G/5G design only for the MIMO antenna system (a) $|s_{ii}|$-Simulated (b) $|s_{ii}|$-Measured (c) $|s_{ij}|$-Simulated (d) $|s_{ij}|$-Measured, {simulated (sim.), measured(meas.)}.

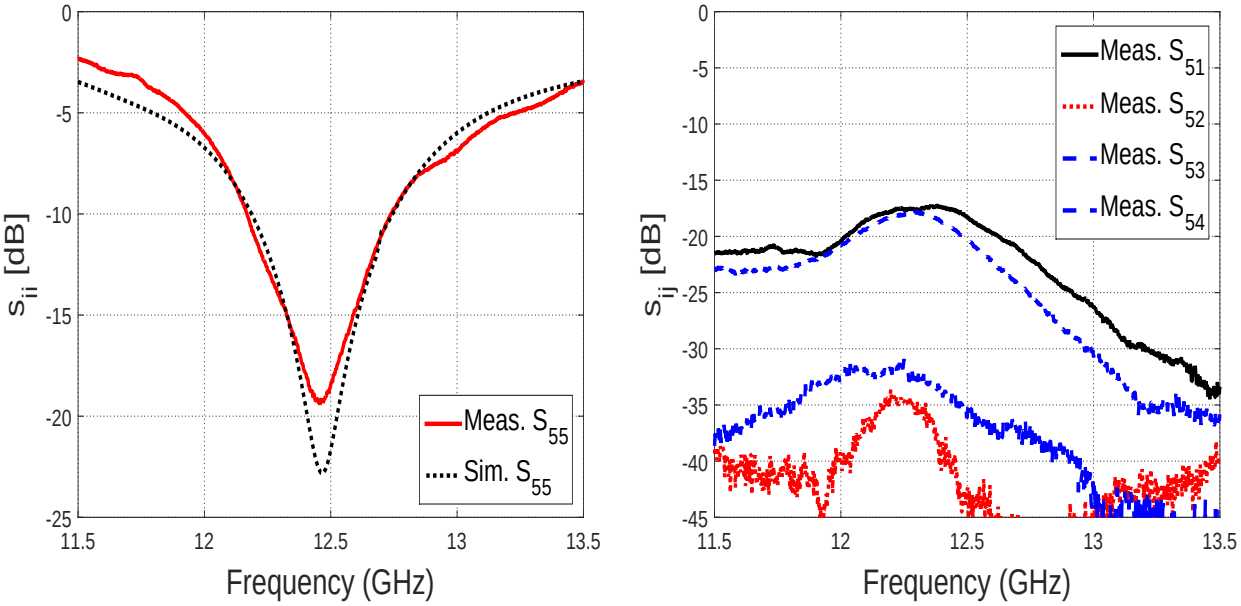


(a) (b)

Figure 5.15: S-parameters curves of the integrated 4G/5G design only for the CAA (a) $|s_{ii}|$-Simulated and measured (b) $|s_{ij}|$-Measured, {simulated (sim.), measured(meas.)}.

### 5.2.5 Radiation Patterns

The normalized simulated and measured 2D radiation patterns in terms of Etotal for the MIMO antenna system at 2.1 GHz are illustrated in Figure 5.16 for the x-y and y-z planes (referred to Figure 5.6). The maximum measured values of Etotal for Ant-1 to Ant-4 were 3.71 dB, 3.16dB, 3.31dB and 3.43dB, respectively. The Figure shows that the beam maxims are tilted due to the presence of the GND that acts as a reflector. This is of advantage as it will lower the ECC values. The maximum value of Etotal for the CAA was 8.3 dB. The slightly titled beam of the array is due to the asymmetry end termination of the slot array. In Figure 5.16(a) and Figure 5.16(c), 2-D $\theta - cuts$ are plotted for each antenna at $\phi = 90^o$. In Figures 5.16(b) and 5.16(d), 2-D $\phi - cuts$ at $\theta = 60^o$ for all MIMO antennas are shown.

The beam tilts are clear. The 2D patterns in terms of Etotal for the CAA at 12.5 GHz are shown in Figure 5.16(e) and Figure 5.16(f). Figure 5.16(e) shows the $\theta - cuts$ at $\phi = 0^o$ while Figure 5.16(f) shows $\phi - cuts$ at $\theta = 90^o$. The beam tilt as well as the radiation maximas are opposite to the location of the feed network.

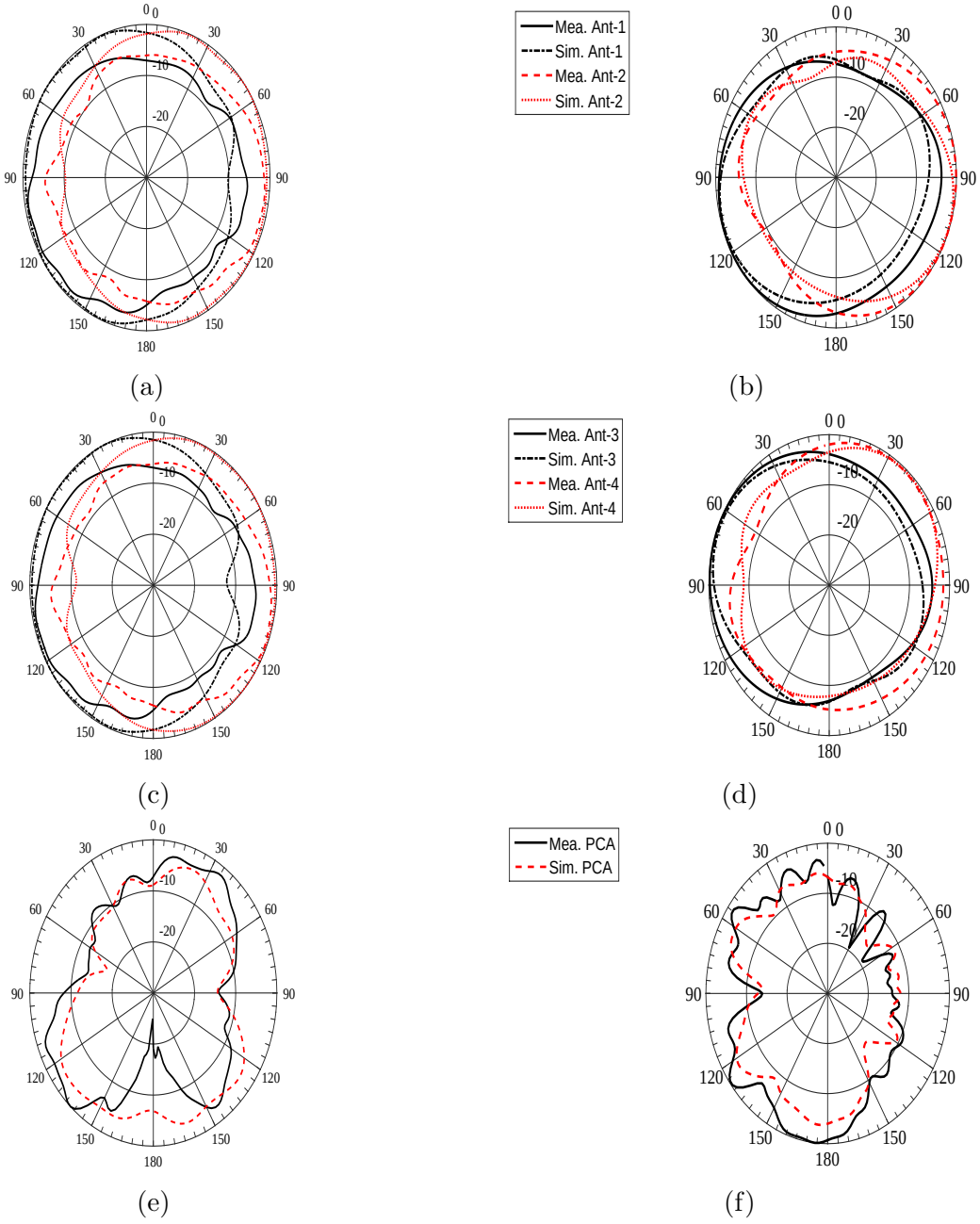


Figure 5.16: Normalized measured and simulated radiation patterns ($E_{total}$) (a) ($\theta - cuts$) Ant-1 and Ant-2 at $\phi = 90^o$ (b) ($\phi - cuts$) Ant-1 and Ant-2 at $\theta = 60^o$ (c) ($\theta - cuts$) Ant-3 and Ant-4 at $\phi = 90^o$ (d) ($\phi - cuts$) Ant-3 and Ant-4 at $\theta = 60^o$ (e) ($\theta - cuts$) CAA at $\phi = 0^o$ (f) ($\phi - cuts$) CAA at $\theta = 90^o$.

The simulated maximum gains observed for the proposed integrated design were 3.45 dBi,

3.76 dBi, 3.6 dBi, 3.2 dBi and 7.3 dBi for Ant-1-Ant-4 and the CAA, at 2.15 GHz and 12.5 GHz, respectively as shown in Figure 5.17. The measured and simulated maximum gain and efficiency values of all MIMO elements are shown in Figure 5.18. The minimum efficiency at 2.1 GHz was 74%. Differences between measured and simulated gains did not exceed 1.5 dBi across the complete band of operation for all antennas. The curves of maximum gain and efficiency versus frequency for the CAA are shown in Figure 5.19 and were 8.5 dBi and 83% at 12.5 GHz, respectively. Differences between measurements and simulation did not exceed 1dB across the complete band covered.

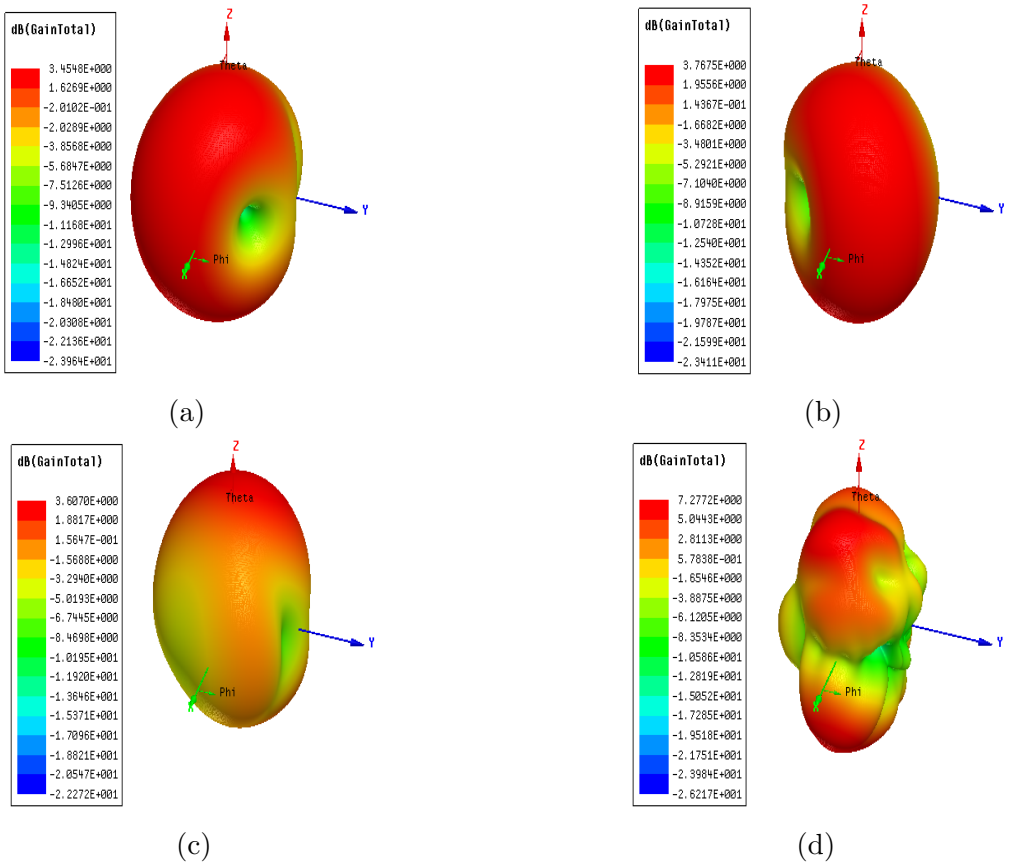


Figure 5.17: 3-D simulated gain patterns (a) Ant-1 (b) Ant-2 (c) Ant-3 (d) CAA.

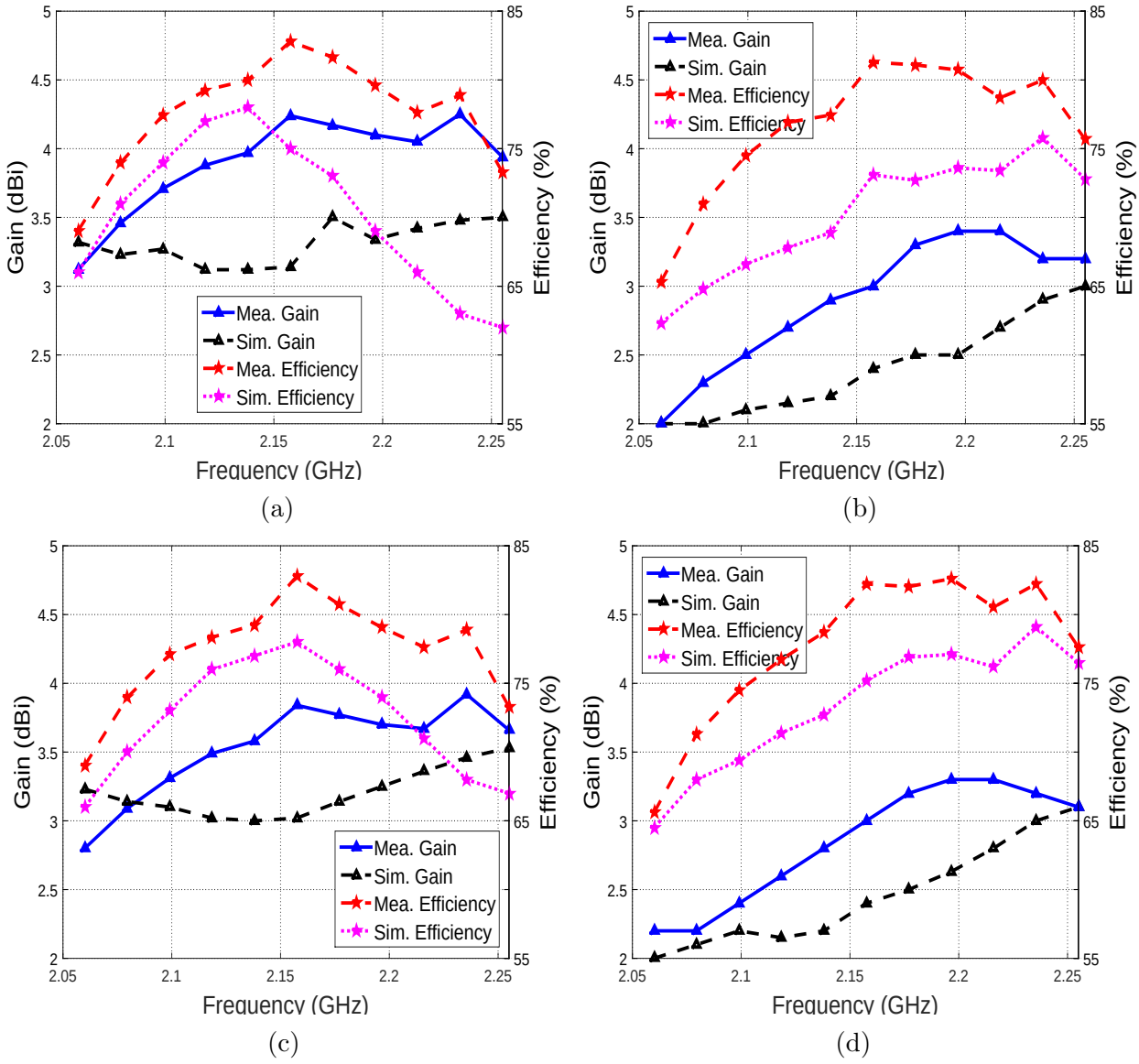


Figure 5.18: Measured maximum gain and efficiency curves (a) Ant-1 (b) Ant-2 (c) Ant-3 (d) Ant-4.

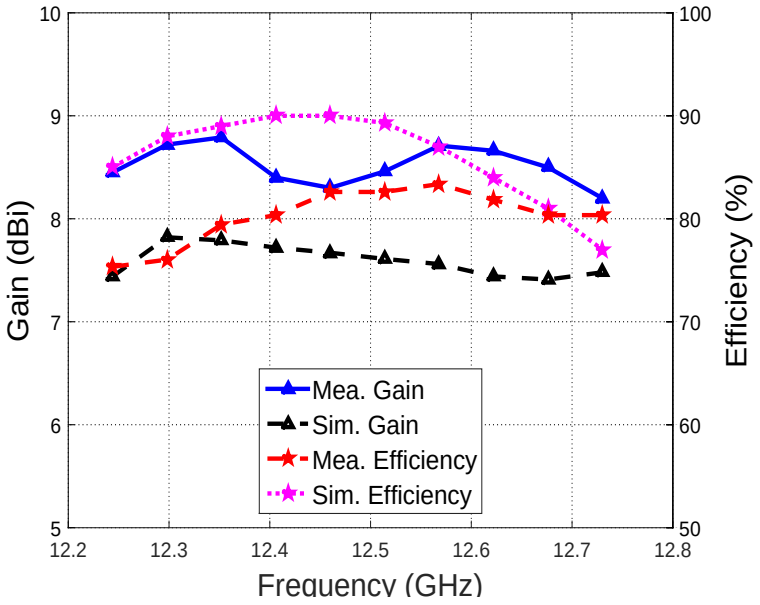


Figure 5.19: Measured and simulated maximum gain and efficiency curves for CAA.

### 5.2.6 MIMO Performance

The envelope correlation coefficient (ECC) values were computed based on the measured 3D radiation patterns using the Eq. in [2] with maximum obtained values of 0.2005, 0.2495 and 0.0623 between antenna elements (Ant-1, Ant-2), (Ant-1, Ant-3) and (Ant-1, Ant-4), respectively, at 2.1 GHz. At other frequencies the values of the measured ECC are given in Table 5.2 which shows that they are acceptable values. All values are below 0.5 that shows that this proposed design can fulfill the requirements of a 4G MIMO antenna system.

Table 5.2: Measured envelope correlation coefficient (ECC) values

| Freq (GHz) | $ECC_{12}$ | $ECC_{13}$ | $ECC_{14}$ | $ECC_{24}$ |
|---|---|---|---|---|
| 2.08 | 0.1819 | 0.2333 | 0.0560 | 0.2271 |
| 2.1 | 0.2005 | 0.2495 | 0.0623 | 0.2457 |
| 2.12 | 0.2073 | 0.2615 | 0.0643 | 0.2669 |
| 2.14 | 0.2106 | 0.2824 | 0.0678 | 0.2929 |

## 5.3 Summary

This chapter covered the designing procedure of 4G/5G MIMO antenna systems with two different configurations. Moreover, a defected ground structure (DGS) was used as a connected antenna arrays (CAA) to improve the isolation between various antenna elements of the MIMO antenna system as well as a radiator at 5G bands. Finaly, 4G/5G integrated MIMO antenna system is tested at Satimo Star-Lab MVG-Italy. Measured results were compared with simulation and good agreement was observed. The integrated antenna system covered 2.1 and 12.5 GHz bands. MIMO performance metrics were calculated with high gain of 8 dBi and efficiency of 80%. A 4dB improved isolation was achieved within 4G MIMO antenna systems.

# CHAPTER 6

# CONCLUSIONS & FUTURE WORK

## 6.1 Conclusions

Two types of 4-element MIMO antenna systems (i.e. PIFA and monopole) for LTE mobile applications were successfully simulated and fabricated. Isolation enhancement structures were introduced based on defected ground structures(DGS) in both designs to improve the port isolation. The size of a substrate was $100\times60\times0.8$ mm$^3$ for both MIMO antenna systems and operated at 2.1 GHz with at least 150 MHz bandwidth. A gain of 4 dBi was observed in PIFA MIMO antenna system, whereas It was 3 dBi for monopole MIMO antenna system. Another MIMO antenna system based on 6-element monopole antennas was also presented at 2 GHz with 60 MHz bandwidth. The size of a substrate was $110\times65\times0.8$ mm$^3$. The measured efficiency was above 55% for all antenna elements with the gain of 3 dBi.

All aforementioned designs were fabricated on FR4 material with dielectric constant of 4.3 and they were low profile and compact in size.

The MIMO performance matrices (i-e ECC and isolation) were calculated. ECC values were below 0.5 and isolation was above 10dB in all designs which are acceptable values for 4G applications. Moreover, there was good agreement between simulated and measured values. The dual function of ground slots was introduced on 4-element monopole and PIFA MIMO antenna systems, as an isolation enhancement structure as well as connected antenna array. This dual function was operated at two frequencies. The first for the 4G MIMO antenna system as an isolation enhancement structure at 2.1 GHz and the second at 12.5 GHz, new 5G band as an CAA. The integrated antenna system was fabricated on a substrate RO-4350 with dimensions of $100\times60\times0.76$ mm$^3$. It covered two bands of 2.1 and 12.5 GHz with 205 and 580 MHz bandwidths, respectively. Gains of 8 dBi and 3.2 dBi were observed for CAA and 4G MIMO antenna system, respectively. The efficiency was 80% for CAA while it was 74% for MIMO antenna system. A 4dB improved isolation was also achieved within 4G MIMO antenna system.

## 6.2 Future Work

This thesis was mainly focused on 4G/5G integrated MIMO antenna systems along with connected antenna arrays. This work can be extend into following projects:

- Multiband 4G MIMO antenna system with higher than 6 number of antennas to cover more 4G bands such as 1.9, 2.6, 3.6 GHz.
- 5G MIMO antenna system at mm-Wave range up-to 30 GHz to get more bandwidth for 5G applications.

By these configurations, we will be able to meet the requirements of rapidly increasing data rates in the mobile communications.

# REFERENCES


[1] *X. Zhou, X. Quan, and R. Li, A Dual-Broadband MIMO Antenna System for GSM/UMTS/LTE and WLAN Handsets,"IEEE Antennas and Wireless Propagation Letters, vol. 11, pp. 551-554, 2012.*

[2] *M. S. Sharawi, Printed MIMO Antenna Engineering, Norwood, MA: Artech House, 2014.*

[3] *Ericsson, Ericsson Mobility Report," Nov. 2015. http://ericsson.com/res/docs/2015/mobility-report/ericsson-mobility-report-nov-2015.pdf*

[4] *IWPC, Evolutionary & Disruptive Visions Towards Ultra High Capacity Networks,"International Wireless Industry Consoritum (IWPC), April 2014.*

[5] *Y. Wang, J. Li, L. Huang, Y. Jing, A. Georgakopoulos, and P. Demestichas, 5G Mobile: Spectrum Broadening to Higher-Frequency Bands to Support High Data Rates,"IEEE Vehicular Technology Magazine, vol. 9, no. 3, pp. 39–46, 2014.*

[6] *J. Gozalves, Fifth-Generation Technologies Trials [Mobile Radio]," IEEE Vehicular Technology Magazine, vol. 11, no. 2, pp. 5–13, June 2016.*

[7] *Ericsson, Ericsson 5G Radio access," April 2016. https://www.ericsson.com/res/docs/whitepapers /wp-5g.pdf*

[8] *D. Cavallo, Connected Array antennas: Analysis and design, PhD thesis, TNO, The Haguue, The Netherlands 2011.*

[9] *Z. N. Chen and Dr. Michael Y. W. Chia, Broadband Planar Antennas: Design and Applications, John Wiley & sons, 2006.*

[10] *R. C. Hansen, Phased Array Antennas, John Wiley & sons, 2009.*

[11] *A. Neto and J. J. Lee,"Ultrawide-Band Properties of Long Slot Arrays,"IEEE Transaction on Antenna and Propagation, vol. 54, no. 2, pp. 534543, Feb. 2006.*

[12] *R. C. Hansen, Linear Connected Arrays, IEEE Antenna and Wireless Propagation Letters, vol. 3, pp. 154-156, 2004.*

[13] *I. Tzanidis, Ultrawideband Low-Profile Arrays of Tightly Coupled Antenna Elements: Excitation, Termination and Feeding Methods, PhD thesis, Electrical and Computer Engineering, The Ohio State University, 2011.*

[14] *D. Cavallo, A. Neto, G. Gerini, A. Micco, and V. Galdi,"A 3-to 5-GHz Wideband Array of Connected Dipoles With Low Cross Polarization and Wide-Scan Capabilities,"IEEE Transaction on Antennas and Propagation, vol. 61, no. 3, pp. 1148–1154, March 2013.*

[15] *J. Gilmore and D. B. Davidson,"Suppressing Undesired Common-Mode Resonances in Connected Antenna Arrays,"IEEE Transactions on Antennas and Propagation, vol. 53, pp. 5245-5250, 2015.*

[16] *J. Lee, S. Livingston, R. Koenig, D. Nagata, and L. Lai,"Long slot arrays - part2: ultra wideband test results,"IEEE International Symposium on Antennas and Propagation Society, vol. 1A, pp. 586589, 2005.*

[17] *H. B. Molina and J. Hesselbarth,"Reactively Matched Long Slot Linear Connected Array Antenna,"IEEE 9th European Conference on Antennas and Propagation (EuCAP), pp. 15, 2015.*

[18] *H. Carrasco, H.D. Hristov, R.Feick, and D. Cofre, Mutual coupling between planar inverted-F antennas,"Microwave and optical Technology Letters, vol. 42, no.3, pp. 224-227, Aug. 2014.*

[19] *M.K.T. Al-Nuamani and W. G. Whittow, Performance investigation of a dual element IFA array at 3 GHz for MIMO terminals,IEEE Loughborough Antennas and Propagation conference, pp. 1-5, Nov. 2011.*

[20] *I. Yeom, J. Kim, and C. Jung, Compact dual band MIMO antenna with high isolation performance, Proceedings of Asia-pacific Microwave conference (APMC), pp. 766-769, Dec. 2010.*

[21] *S. -C. Chen, Y. -S. Wang, and S. -J. Chung, A Decoupling Technique for Increasing the port Isolation Between Two Strongly Coupled Antennas,"IEEE Transaction on Antenna and Propagation, vol. 56, no.12, pp. 3650-3658, Dec. 2008.*

[22] *R. A. Bhatti, S. Yi, and S. -O. Park, Compact Antenna Array With Port Decoupling for LTE-Standardized Mobile Phones,"IEEE Antenna and Wireless Propagation Letters, vol. 8, pp. 1430-1433, 2009.*

[23] *Z. Li, Z. Du, M. Takahashi, K. Saito, and K. Ito, Reducing Mutual Coupling of MIMO Antennas With Parasitic Elements for Mobile terminals,"IEEE Transaction on Antenna and Propagation, vol. 60, no. 2, pp. 473-481, Feb. 2012.*

[24] *K. -S. Min, D.-J. Kim, and Y. -M. Moon, Improved MIMO Antenna by Mutual Coupling Suppression Between Elements,IEEE The European Conference on Wireless Technology, pp. 135-138, 2005.*

[25] *C. -H. Lee, S. -Y. Chen, and P. Hsu, Integrated Dual Planar Inverted-F Antenna With Enhancement Isolation ,"IEEE Antenna and Wireless Propagation Letters, vol. 8, pp. 963-965, 2009.*

[26] *C. -Y. Chiu, C. -H Cheng, R. D. Murch, and C. R. Rowell, Reduction of Mutual Coupling Between Closely-Packed Antenna Elements,"IEEE Transaction on Antennas and Propagation, vol. 55, no. 6, pp. 1732-1738, Jun. 2007.*

[27] *C. -H. Lee, S. -Y. Chen, and P. Hsu, A Compact Planar MIMO antenna System of Four Elements with Similar Radiation Characteristics and Isolation Structure,"IEEE Antenna and Wireless Propagation Letters, vol. 8, pp. 1107-1110, 2009.*

[28] *A. Habashi, J. Nourinia, and C. Ghobadi, A Rectangular defected ground structure (DGS) for reduction of Mutual Coupling Between closely spaced microstrip antennas,IEEE Iranian Conference on Electrical Engineering(ICEE2012), pp. 1347-1350, May 2012.*

[29] *J. -F. Li, Q. -X. Chu, and T. -G. Huang, A Compact Wideband MIMO antenna with Two Novel Bent Slits,"IEEE Transaction on Antennas and Propagation, vol. 60, no. 2, pp. 482-489, Feb. 2012.*

[30] *J.-F. Li, Q. -X. Chu, and T. -G. Huang, Printed MIMO antennas System Using Neutralization line Technique for Wireless USB-Dongle Applications ,"IEEE Transaction on Antennas and Propagation, vol. 60, no. 2, pp. 456-463, Feb. 2012.*

[31] *S. Ranvier, C. Luxey, P. Suvikunnas, R. Staraj, and P. Vainikainen, Capacity enhancement by Increasing both mutual Coupling and Efficiency: A Novel Approach ,"IEEE Antenna and Propagation International Symposiaum (APS/URSI), pp. 3632-3635, Jun. 2007.*

[32] *Z. Li, M. -S. Han, X. Zhao, and J. Choi, MIMO antenna with isolation enhancement for wireless USB dongle Applications at WLAN band,Proceeding Asia-pacific Microwave conference (APMC), pp. 758-761, 2010.*

[33] *Y. Lee, H. Chung, J. Ha, and j. Choi, Design of a MIMO antenna with Improved isolation using Metamaterials, IEEE International workshop on Antennas, pp. 231-234, Mar. 2011.*

[34] *H. S. Lee and H. M. Lee, Isolation Improvement Between Loop Antennas with absorber Cell, IEEE International Symposium on Antennas and Propagation (APS/URSI), pp. 1735-1738, Jul 2011.*

[35] *J. B. Andersen and H. H. Rasmussen, Decoupling and De scattering Networks for Antennas,"IEEE Transaction on Antennas and Propagation, pp. 841-846, Nov. 1976.*

[36] *Y. Chung, S. -S. Jeon, D. Ahn, J. -I. Choi, and T. Itoh, High Isolation Dual Polarized Patch Antenna Using Integrated Defected Ground Structure,"IEEE Microwave and Wireless Components Letters, vol. 14, no. 1, pp. 4-6,, Jan. 2004.*

[37] *T.-W. Kang and K. -L.Wong, Isolation Improvement of WLAN internal Laptop computer Antennas Using dual-band strip Resonator,IEEE Asia-pacific Microwave conference (APMC), pp. 2478-2481 , Dec. 2010.*

[38] *M. S. Sharawi, A. B. Numan, M. U. Khan, and D. N. Aloi, A Dual-Element Dual-band MIMO Antenna System With Enhanced Isolation For Mobile Terminals,"IEEE Antenna and Wireless Propagation Letters, vol. 11, pp. 1006-1009, 2012.*

[39] *M. S. Sharawi, A. B. Numan, M. U. Khan, and D. N. Aloi, A CSRR Loaded MIMO Antenna System for ISM Band Operation ,"IEEE Transaction on Antennas and Propagation, vol. 61, no. 8, pp. 4265-4274, Aug. 2013.*

[40] *M. S. Sharawi, A. B. Numan, and D. N. Aloi, Isolation Improvement in a Dual-band Dual-Element Antenna System Using Capacitively Loaded Loops,"Progress In Electromagnetic Research, vol. 134, pp. 247-266, 2013.*

[41] *L. Yang and T. Li, "Box-folded four-element MIMO antenna system for LTE handsets," IEEE Electronics Letters, vol. 51, no. 6, pp. 440–441, March 2015.*

[42] *Ghosh, T. N. Tran, and T. L. Ngoc, "Miniaturized Four-Element Diversity PIFA," IEEE Antennas and Wireless Propagation Letters, vol. 12, pp. 396–400, March 2013.*

[43] *S. Zhang, J. Xiong, and S. He, "MIMO antenna system of two closely-positioned PIFAs with high isolation," IEEE Electronics Letters, vol. 45, no. 15, July 2009.*

[44] *S. Zhang, B. K. Lau, Y. Tan, Z. Ying, and S. He,"Mutual Coupling Reduction of Two PIFAs With a T-Shape Slot Impedance Transformer for MIMO Mobile Terminals," IEEE Antennas and Wireless Propagation Letters, vol. 60, no. 3, pp. 1521-1530, March 2012.*

[45] *G. Li, H. Zhai, Z. Ma, C. Liang, R. Yu, and S. Liu,"Isolation-Improved Dual-Band MIMO Antenna Array for LTE/WiMAX Mobile Terminals,"IEEE Antennas and Wireless Propagation Letters, vol. 13, pp. 1128–1131, 2014.*

[46] *A. Jain, P.K. Verma, and V.K. Singh,"Performance analysis of PIFA based 4×4 MIMO antenna," IEEE Antennas and Wireless Propagation Letters, vol. 48, no. 9, April 2012.*

[47] *T. Hall and S. K. Sharma,"S- and C-Band Omni-Directional Antennas in MIMO Arrangement on Bent Ground Plane for a Conducting Cylinderical Surface," IEEE Antennas and Wireless Propagation symposium (APS/URSI), 2015.*

[48] *S. Ghosh,T. N. Tran, and T. Le-Ngoc,"Miniaturized MIMO-PIFA with Pattern and Polarization Diversity,"IEEE Electronics Letters, 2012.*

[49] *M. K.T. Al-Nuaimi,"Mutual Coupling Evaluation of Dual-Miniaturized PIFA Antenna Array for MIMO Terminals,"European Wireless, pp. 618–621, April 2011.*

[50] *R. Addaci, F. Ferrero, D. Seetharamdoo, T. Le Huy, R. Staraj, and M. Berbineau,"Multi-band Multi-Antenna System with New Approach of PIFA Bandwidth Enhancement,"European Conference on Antennas and Propagation (EUCAP), pp. 2880–2883, 2014.*

[51] *A. A. H. Azremi, M. Kyro, J. Ilvonen, J. Holopainen, S. Ranvier, C. Icheln, and P. Vainikainen,"Five-Element Inverted-F Antenna Array for MIMO Communications and Radio Direction Finding on Mobile Terminal," Loughborough Antennas and Propagation Conference, pp. 557–560, Nov 2009.*

[52] *A. A. H. Azremi, M. Costa, V. Koivunen, and P. Vainikainen,"Ambiguity Analysis of Isolation Based Multi-antenna Structures on Mobile Terminal,"5th European Conference on Antennas and Propagation (EUCAP), pp. 552–556, 2011.*

[53] *J. M. Lee, K. B. Kim, H. K. Ryu, and J. M. Woo,"A Compact Ultrawideband MIMO Antenna With WLAN Band-Rejected Operation for Mobile Devices,"IEEE Antennas and Wireless Propagation Letters, vol. 11, pp. 990–993, 2012.*

[54] *M. Karaboikis, C. Soras, G. Tsachtsiris, and V. Makios,"Four-element Printed Monopole Antenna Systems for Diversity and MIMO Terminal Devices,"IEEE 17th In-*

*ternational Conference on Applied Electromagnetics and Communications (ICECom), pp 193-156, Nov. 2003.*

[55] *F. Malek, N. A. Zainuddin, M. Z. A. Abd Aziz, H. Nornikman, B. H. Ahmad, M. F. A. Malek, and M. A. Othman,"Double C-Shaped Monopole Antenna Array for Dual Band WLAN Application,"IEEE Symposium on Wireless Technology, pp. 274–279, Sep. 2013.*

[56] *Q. Rao and K. Wilson,"Design, Modeling, and Evaluation of a Multiband MIMO/Diversity Antenna System for Small Wireless Mobile Terminals,"IEEE Transaction On Components, Packing, And Manufacturing Technology, vol. 1, no. 3, March 2011.*

[57] *S. W. Su, C.-T. Lee, and F.-S. Chang,"Printed MIMO-Antenna System Using Neutralization-Line Technique for Wireless USB-Dongle Applications,"IEEE Transaction on Antenna and Propagation, vol. 60, no. 2, Feb. 2012.*

[58] *Y. Ding, Z. Du, K. Gong, and Z. Feng,"A Four-Element Antenna System for Mobile Phones,"IEEE Antennas and Wireless Propagation Letters, vol. 6, pp. 655–658, 2007.*

[59] *D. Sarkar, A. Singh, K. Saurav, and K. V. Srivastava,"Four-element quad-band multiple-inputmultiple-output antenna employing split-ring resonator and inter-digital capacitor,"IET Microwaves, Antennas and Propagation, vol. 9, pp. 14531460, 2015.*

[60] *S. C. Fernandez, and S. K. Sharma,Multiband Printed Meandered Loop Antennas With MIMO Implementations for Wireless Routers, IEEE Antennas and Wireless Propagation Letters, vol. 12, pp. 9699, 2013.*

[61] *J. J. Lee, S. Livingston, and R. Koenig,"Wide Band Long Slot Array Antennas,"IEEE international symposium on Antennas and Propagation Society (APS/URSI), pp. 452455, 2003.*

[62] *A. Neto, D. Cavallo, G. Gerini, and G. Toso,"Scanning Performances of Wideband Connected Arrays in the Presence of a Backing Reflector,"IEEE Transaction on Antenna and Propagation, vol. 57, no. 10, pp. 30923102, Oct. 2009.*

# Vitae

- Name: Muhammad Ikram
- Nationality: Pakistani
- Date of Birth: 01-04-1989
- Email: *ikram439@gmail.com*
- Permenant Address: Street No. 1, Taj colony Depalpur, Dist. Okara, Punjab, Pakistan.

# Publications

## Patents:

1. Mohammad S. Sharawi and ***Muhammad Ikram*** , A Multi-Port Multi-Band Single Connected MIMO Antenna, Filed in USPO, June 2016.

2. Mohammad S. Sharawi, ***Muhammad Ikram*** and Rifaqat Hussain An Integrated multi-standard Antenna System with Dual Function Connected Array, Filed in USPO, July 2016.

3. Mohammad S. Sharawi, ***Muhammad Ikram*** and Rifaqat Hussain Low Profile Printed Monopole based MIMO Antenna System for Smart Phone Applications, Filed in KFUPM for USPO, Oct 2016.

## Journals:

1. ***Muhammad Ikram***, Rifaqat Hussain, Oalid Hammi and Mohammad S. Sharawi, An L-shaped 4-element Monopole Antenna system with Enhanced Isolation for Mobile Applications, Mircowaves and Optical Technology Letters, Wiley, vol. 58, no. 11, pp. 2587–2591, Nov. 2016.

2. Mohammad S. Sharawi, ***Muhammad Ikram*** and Atif Shammim, A two concentric loop based connected array MIMO antenna system for 4G/5G terminals

under 2nd revision in IEEE Transaction on antenna and Propagation, Jan. 2017.

3. ***Muhammad Ikram***, Rifaqat Hussain and Mohammad S. Sharawi, A 4-element MIMO Antenna System with A Dual Function Connected Array, submitted in IEEE Antenna and Wireless Propagation Letters, Nov. 2016.

# Conferences:

1. ***Muhammad Ikram***, Rifaqat Hussain and Mohammad S. Sharawi, Compact 4-Element MIMO Antenna with Isolation Enhancement for 4G LTE Terminals, IEEE International Symposium on Antenna and Propagation (APS/URSI 2016), Fajardo, Puerto Rico, USA, July 2016.

2. ***Muhammad Ikram***, Rifaqat Hussain and Mohammad S. Sharawi, Low profile 6-Element Modified-Monopole MIMO Antenna System for Mobile Applications, IEEE International Symposium on Antenna and Propagation (APS/URSI 2016), Fajardo, Puerto Rico, USA, July 2016.

3. Rifaqat Hussain, ***Muhammad Ikram*** and Mohammad S. Sharawi, Indoor Channel Capacity Measurement of Wide-Band MIMO Antenna with Isolation Enhancement, IEEE International Symposium on Antenna and Propagation (APS/URSI 2016), Fajardo, Puerto Rico, USA, July 2016.

4. ***Muhammad Ikram***, Rifaqat Hussain and Mohammad S. Sharawi, A 4G MIMO Antenna System with Dual Function Ground Slots, IEEE Asia-Pacific Conference on

Antennas and Propagation (APCAP 2016), Kaohsiung, Taiwan, July 2016.

5. ***Muhammad Ikram*** and Mohammad S. Sharawi, Compact 10-element monopole based MIMO Antenna System for 4G Mobile Phones, IEEE 16th Mediterranean Microwave Symposium (MMS 2016), UAE, Nov. 2016.